UNIVERSIDADE ESTADUAL PAULISTA
"JÚLIO DE MESQUITA FILHO"

EZEQUIEL JOSÉ PÉREZ MONTERROZA

Encapsulação de carotenoides em matrizes de amilose por diferentes processos: Formação de criogéis, ultrassom e precipitação em meio ácido

São José do Rio Preto
2018

Ezequiel José Pérez Monterroza

Encapsulação de carotenoides em matrizes de amilose por diferentes processos: Formação de criogéis, ultrassom e precipitação em meio ácido

Tese apresentada como parte dos requisitos para obtenção do título Doutor em Engenharia Ciência de Alimentos, junto ao Programa de Pós-Graduação em Engenharia e Ciência de Alimentos, Área de Concentração - Engenharia de Alimentos, do Instituto de Biociências, Letras e Ciências Exatas da Universidade Estadual Paulista "Júlio de Mesquita Filho" Campus de São José do Rio Preto.

Financiadora: Coordenação de Aperfeiçoamento de Pessoal de Nível Superior (CAPES)

Orientadora: Prof.ª Drª. Vânia Regina Nicoletti

Co-Orientadora: Prof.ª Drª. Célia Maria Landi Franco

São José do Rio Preto
2018

Pérez Monterroza, Ezequiel José.
Encapsulação de carotenoides em matrizes de amilose por diferentes processos : formação de criogéis, ultrassom e precipitação em meio ácido / Ezequiel José Pérez Monterroza. -- São José do Rio Preto, 2018
143 f. : il., tabs.

Orientador: Vânia Regina Nicoletti Telis
Coorientador: Célia Maria Landi Franco
Tese (doutorado) – Universidade Estadual Paulista "Júlio de Mesquita Filho", Instituto de Biociências, Letras e Ciências Exatas

1. Tecnologia de alimentos. 2. Microencapsulação. 3. Carotenoides. 4. Amilose. 5. Precipitação (Química) 6. Abacate. I. Universidade Estadual Paulista "Júlio de Mesquita Filho". Instituto de Biociências, Letras e Ciências Exatas. II. Título.

CDU – 664.09

Ficha catalográfica elaborada pela Biblioteca do IBILCE
UNESP - Câmpus de São José do Rio Preto

Ezequiel José Pérez Monterroza

Encapsulação de carotenoides em matrizes de amilose por diferentes processos: Formação de criogéis, ultrassom e precipitação em meio ácido

Tese apresentada como parte dos requisitos para obtenção do título Doutor em Engenharia Ciência de Alimentos, junto ao Programa de Pós-Graduação em Engenharia e Ciência de Alimentos, Área de Concentração - Engenharia de Alimentos, do Instituto de Biociências, Letras e Ciências Exatas da Universidade Estadual Paulista "Júlio de Mesquita Filho" Campus de São José do Rio Preto.

Financiadora: Coordenação de Aperfeiçoamento de Pessoal de Nível Superior (CAPES)

Comissão Examinadora

Profª. Drª. Vânia Regina Nicoletti
Presidente e Orientadora-IBILCE
UNESP-São José do Rio Preto

Profª. Drª. Maria Aparecida Mauro
Membro Titular-IBILCE
UNESP-São José do Rio Preto

Prof. Dr. Marinônio Lopes Cornélio
Membro Titular-IBILCE
UNESP-São José do Rio Preto

Profª. Drª. Izabel Cristina Freitas Moraes
Membro Titular- USP-Pirassununga

Prof. Dr. Carlos Raimundo Ferreria Grosso
Membro Titular-UTFPR- Londrina

São José do Rio Preto, 26 de fevereiro de 2018

Dedico este trabalho a Ezequiel C, Amira, Lilia, Sofia e Ana María Chaux pelo apoio e fortalecimento do meu espírito para vencer minhas lutas diárias.

AGRADECIMENTOS

À minha orientadora, Profª. Drª. Vânia Regina Nicoletti, pelos ensinamentos, orientação, dedicação e paciência, por estar sempre disposta a me ajudar na elaboração deste trabalho.

À Profa.Dra Célia Maria Landi Franco por suas sugestões, disponibilidade e ajuda na utilização do difractômetro de Raios X.

Aos membros da banca examinadora, por terem participado da minha defesa, pelas suas sugestões para o desenvolvimento deste trabalho.

Aos professores Dr. João Claudio Thomeo, Dra. Vânia Nicoletti, Dr. Javier Telis, e Dr. Vanildo Luiz Del Bianchi, pelas disciplinas ministradas que ajudaram na minha formação profissional.

Ao o Prof. Dr. Vanildo Luiz Del Bianchi, pela confiança e apoio em meu processo para começar o caminho ao doutorado.

À Coordenação de Aperfeiçoamento de Pessoal de Nível Superior (CAPES) pela bolsa de estudos.

RESUMO

O amido é ideal como material de parede na preparação de sistemas de liberação controlada, é barato e considerado GRAS. O amido está constituído por dois biopolímeros de D-glicose, a amilose e a amilopectina, as quais representam 99 % da matéria seca do grânulo. A amilose tem a capacidade de formar complexos com algumas moléculas hidrofóbicas como *flavors* e ácidos graxos, os quais são capazes de resistir a variações de pH e temperaturas elevadas, tornando-se interessante para a formulação de sistemas de liberação controlada de nutrientes. O objetivo inicial deste projeto foi a utilização de amilose extraída da mandioca e do amido de milho com alto teor de amilose comercial (Hylon VII, 72% de amilose) com o intuito de encapsular bixina e avaliar a formação de complexos de inclusão de V-amilose, bem como a sua caracterização usando difração de raios X (DRX), calorimetria exploratória de varredura, espectroscopia de infravermelho, microscopia eletrônica de varredura (MEV), cor, teor de bixina encapsulado, ensaios reológicos oscilatórios e capacidade de liberação. Foram estudados os efeitos das condições de processo de encapsulação por precipitação em solução ácida e através do tratamento com ultrassom sobre as interações entre a bixina e o amido. O efeito da proteína de soro de leite sobre o processo de encapsulação por precipitação em solução ácida também foi estudado. Finalmente, foi realizado um estudo de otimização usando a metodologia de superfície de resposta para selecionar as melhores condições em ambos os métodos, maximizando a capacidade de carga interior da matriz de amido. Além disso, pelo fato de que os xerogéis e criogéis de amido têm ganhado interesse na indústria como sistemas para a microencapsulação de compostos bioativos, este trabalho também explora a capacidade da amilose de mandioca para encapsular carotenoides usando essas metodologias. Nesse caso foram usados como moléculas-hóspedes os carotenoides presentes no óleo de abacate, luteína e neoxantina. Os resultados da encapsulação da bixina usando Hylon VII e proteína por precipitação de uma solução ácida mostraram que existe interação entre a proteína de soro de leite, o Hylon VII e a bixina, como foi observado na análise por FT-IR, no entanto, os padrões de difração e a análise por DSC

não confirmaram a formação de complexos de inclusão do tipo V-amilose com a bixina. Porém, transições endotérmicas com ponto de fusão em 117,2, 105 e 104 °C foram observadas nas amostras preparadas a 90 °C com 0%, 10% e 20% de proteína, respectivamente. Cabe ressaltar que um aumento no conteúdo de proteína causou uma diminuição na entalpia de fusão desta estrutura, assim como um decréscimo em sua cristalinidade relativa, o qual foi causado provavelmente pela interação entre a bixina e a proteína. No grupo das amostras preparadas a 90 °C, o aumento no conteúdo de proteína resultou em uma tendência a aumentar o conteúdo e bixina encapsulado. Os resultados de FT-IR mostraram que as bandas de absorção associadas com as vibrações do grupo -C=C- desaparecem, indicando restrição da cadeia da bixina na matriz, assim como o aumento da disponibilidade para interagir com a proteína, embora, essas interações pareçam ser poucas a altas temperaturas. Os padrões de liberação da bixina foram afetados pelo conteúdo de proteína e a temperatura usada no processo de encapsulação, resultando em diferentes porcentagens de liberação. Nos ensaios de encapsulação da bixina com ultrassom foi avaliado o efeito do tratamento sobre as interações amido-bixina. Os resultados por DSC e DRX não confirmaram a formação de complexos de inclusão tipo V-amilose, no entanto, a análise por FT-IR indicou que as bandas de absorção do grupo funcional -C=O da bixina desapareceram depois do processo de encapsulação, o que sugere a existência de interação entre a bixina e o amido. Aparentemente esta não foi encapsulada eficientemente dentro da cavidade de amilose, provavelmente pelo seu tamanho molecular. Os espectros mecânicos dos géis formados durante o processo de encapsulação por ultrassom mostraram uma leve variação dos módulos de armazenamento (G') e de perda (G''), com G'>G'', indicando tratar-se de géis fracos. O maior teor de bixina encapsulado no interior da matriz foi obtido com potência de ultrassom de 150 W por 60 minutos de tratamento. As amostras submetidas ao ultrassom foram menos susceptíveis à ação do fluido intestinal simulado, provavelmente devido ao aumento das interações entre a bixina e o amido em comparação à amostra controle. Em ambos os métodos de encapsulação a morfologia das partículas apresentou superfície irregular e erodida, com protrusões provocadas pela agregação de amilose. Através da análise estatística, observou-se que nos dois métodos de preparação todos os fatores tiveram efeito significativo ($p<0,05$) sobre o teor de bixina, tanto na superfície como no interior da matriz de amido. Na encapsulação por precipitação em meio ácido, o maior teor de bixina na matriz foi encontrado com o tratamento a 90 °C usando amilose de mandioca junto com proteína. De forma geral, com o uso de amilose de mandioca obteve-

se um maior teor de bixina encapsulado no interior da matriz e este sempre aumentou com o uso de proteína. Em relação ao tratamento com ultrassom, o maior teor de bixina encapsulado no interior da matriz foi alcançado com 2% de Hylon 150 W e 20 minutos de tratamento. A eficiência de encapsulação alcançada variou de 13,1% a 62,1% e de 17,3% a 94,5% usando tratamento com ultrassom e precipitação em meio ácido, respectivamente. As condições ótimas foram de 2% Hylon, 150 W e 20 minutos para o tratamento com ultrassom. Em relação ao método por precipitação em meio ácido foram 2% amilose de mandioca com proteína, a 68 °C. Os resultados obtidos no processo de encapsulação de luteína e neoxantina usando xerogéis e criogéis de amilose de mandioca indicaram que não houve formação de complexos de inclusão do tipo V-amilose. Entanto, os padrões de difração de raios X observados são característicos deste tipo de complexos. Foi observado um leve aumento na capacidade de encapsulação nas amostras retrodegradadas a -18°C e liofilizadas.

Palavras chaves: Amilose, bixina, luteína, neoxantina, avocado, xerogéis, criogéis, encapsulação.

ABSTRACT

The starch is considered safe and cheap, ideal as wall material in the formulation of delivery systems. Starch granule consists of two major types of α-glucans, amylose, and amylopectin, which represent about 99% of dry matter. Amylose and some hydrophobic molecules such as flavors and fatty acids, form amylose inclusion complexes. Amylose complexes resist to variations of pH and elevated temperature, being good candidates for the formulation of nutrient delivery systems. The initial objective of this thesis was to use high-amylose corn starch (Hylon VII, 72 % amylose) and amylose from cassava starch as wall material for the encapsulation of bixin, evaluating the formation of V-amylose inclusion complexes, and performing their characterization by using X-ray diffractometry, FT-IR spectrometry, scanning electron microscopy, oscillatory rheological tests, color, encapsulated bixin content, and release profile. The effects of process parametres used in the methods based on ultrasound treatment and precipitation in acid solution on the interaction between amylose and bixin were studied, as well as the effect of whey protein on the encapsulation process by precipitation in acid solution. The process conditions that would maximize the encapsulate bixin content inside of the starch matrix were determined by using desirability function. In addition, considering that xerogels and cryogels have gained interest as potential systems for microencapsulation of bioactive compounds and the use of silica aerogels as delivery systems has been demonstrated with success, this thesis explores the capacity of amylose from cassava starch to encapsulate carotenoids using these methodologies. In this case, the guest molecules were the carotenoids present in the avocado oil, lutein and neoxanthin. The results of FT-IR indicated that there was an interaction between protein, Hylon, and bixin in the encapsulation process by precipitation in acid medium. However, the diffraction patterns and the DSC analysis indicated no formation of V-amylose complexes. Nevertheless, although the set of samples prepared at 90°C with 0%, 10% e 20% of protein respectively, showed endothermal transitions with a melting point about 117,2º, 105º and 104°C The increase in protein content decreased the melting enthalpy and relative crystallinity, probably due to the interaction between bixin and protein. In the set

of samples prepared at 90°C, the increase in protein content led to a tendency to increase the encapsulate bixin content inside the matrix. The FT-IR analysis indicated that adsorption bands associated with the vibration of the group -C=C- disappeared due to the restriction of bixin chain into starch matrix and increase in the availability to interacting with the protein. However, these interactions seem to be fewer at the higher temperature. The bixin delivery patterns were affected by protein content and temperature used in the encapsulation process, resulting in different delivery amounts. In the encapsulation of bixin by ultrasound treatment, the effect of sonication power level on the interaction between starch and bixin was studied, nevertheless, the results of DSC and Xray diffraction indicated no formation of amylose inclusion complex. The FT-IR analysis showed that adsorption bands of the -C=O group in bixin disappeared after the encapsulation process, which confirms the interaction between starch and bixin, in spite of bixin having not be entrapped efficiently inside of the amylose cavity, probably due to its molecular size. Frequency sweep tests of gels formed during ultrasound encapsulation process showed a slight frequency dependence of G' and G'' moduli with G'>G'', with patterns correponding to weak gels. The highest bixin encapsulated content inside of matrix was reached using the combination of ultrasound power of 150 W and 60 min of treatment. The sonicated samples were less susceptible to action of simulated intestinal fluid, probably due to increases interaction between starch and bixin as compared to control sample. The particle morphology of samples prepared by both methods showed protrusions of aggregates of amylose, as well as irregular and eroded surfaces. Statistical analysis showed that in both methods, all factors had a significant effect ($p<0.05$) on bixin encapsulated content inside or on the surface of the matrix. In the encapsulation by precipitation in acid solution, the combination of 90 °C using amylose from cassava starch and protein leaded to the highest bixin encapsulated content. In general, amylose from cassava starch encapsulated a greater bixin content inside of matrix compared to Hylon, and the presence of protein increased this effect even more. Regarding ultrasound treatment, the combination of 2% of amylose from Hylon, and 20 min of treatment showed the highest bixin encapsulated content inside of matrix. Encapsulation efficiency ranged from 13.1% to 62.1% and 17.3% to 94.5% using ultrasound treatment and precipitation in acid solution respectively. The optimum conditions were 2% amylose, 150 W, and 20 min in the ultrasound treatment, whereas in the method by precipitation in acid solution the best conditions were 2% amylose from cassava starch with protein at 68 °C. The results obtained from DSC and FT-IR spectroscopy in the encapsulation using cryogels

and xerogels indicated no formation of inclusion complexes V-type of amylose. Nevertheless, the diffraction patterns were characteristic of this type of complexes. The samples retrograded at -18 °C and dried using freeze-drying had a slightly higher encapsulation degree than the samples retrograded at 8 °C.

Keywords: *Amylose, bixin, lutein, neoxanthin, avocado, xerogels, encapsulation, cryogels.*

ÍNDICE DE FIGURAS

FIGURAS CAPÍTULO 1

FIGURAS CAPÍTULO 2

FIGURAS CAPÍTULO 3

FIGURAS CAPÍTULO 4

FIGURAS CAPÍTULO 5

ÍNDICE DE TABELAS

SUMÁRIO

INTRODUÇÃO, OBJETIVOS E ESTRUTURA DA TESE

Introdução geral

Devido ao estilo de vida moderno têm-se produzido diversas mudanças nos hábitos alimentares e no modo de vida da população mundial, sendo que essas modificações têm trazido repercussões ao nível nutricional e de saúde pública. Em decorrência, observa-se o desenvolvimento das chamadas doenças não transmissíveis (DNT), entre as quais se destacam a obesidade, o diabetes mellitus, entre outras. Tais fatores influenciam no incremento das mortes prematuras e no alto custo dos serviços de saúde (ALVES; MAGALHÃES, 2006; HOYERT et al., 2012; SUBURU et al., 2013; BLOCH; VIERA, 2014).

Uma das propostas para abordar a problemática das DNT tem sido o uso de suplementos alimentícios e de ingredientes funcionais ou nutracêuticos. A incorporação desses compostos na dieta se converteu num importante desafio tecnológico, devido à sua baixa estabilidade nas condições de extração e processamento, além dos problemas inerentes à armazenagem e às condições próprias do trato gastrointestinal (TGI) (LESMES; BARCHECHATH; SHIMONI, 2008; BELITZ; GROSCH; SCHIEBER LE, 2009). A administração de compostos bioativos por via oral tem sido a mais aceita, uma vez que segue a mesma rota pelo TGI a que se submetem os alimentos. No entanto, a eficiência de sua liberação é limitada pela dieta, a qual pode aumentar ou diminuir a biodisponibilidade do composto ativo e, além disso, pode ser intensamente afetada pelas condições de baixo pH do estômago, pela ação enzimática, ou pelas condições alcalinas no intestino (ALVES-RODRIGUES; SHAO, 2004). Apesar disso, existe uma preferência muito alta dos consumidores por continuar com a ingestão oral desse tipo de compostos, o que motiva a busca pelo melhoramento contínuo das tecnologias de encapsulação e liberação controlada desse tipo de moléculas (MCCLEMENTS; LI, 2010; BRAITHWAITE et al., 2013). Entre os exemplos de nutracêuticos administrados através de sistemas de liberação controlda destacam-se glucosamina, condroitina, licopeno, resveratrol, coenzima-Q_{10}, creatina, melatonina, extratos vegetais, acetil-L-carnitina, S-adenosil metionina (SAME), ácido lipoico, dehidroepiandrosterona (DHEA) e algumas vitaminas hidro e lipossolúveis (BRAITHWAITE et al., 2013). Entre as metodologias para a preparação de sistemas de encapsulação estão as emulsões e nanoemulsões, as dispersões de lipídeos sólidos em solução aquosa (SCHUBERT; MÜLLER-GOYMANN, 2005; MCCLEMENTS; LI, 2010) e os lipossomas, os quais são afetados pela concentração do lipídeos e composição do nutracêutico (NACKA et al., 2001; GONNET;

LETHUAUT; BOURY, 2010). Alguns dos métodos mais utilizados na preparação desse tipo de sistemas incluem a coacervação simples e complexa e métodos de extrusão e moldagem, hidrogéis e complexos de ciclodextrinas (ANSARI et al., 2011; MATALANIS; JONES; MCCLEMENTS, 2011a; BRAITHWAITE et al., 2013).

O amido tem sido sugerido como uma solução tecnológica na proteção e liberação de ingredientes lipofílicos de valor nutricional. É considerado seguro e adequado para ser utilizado no desenvolvimento de matrizes de encapsulação e revestimento de compostos ativos (LALUSH et al., 2005a). O grânulo de amido é composto por dois tipos de alfa-glucanos, a amilose e a amilopectina, que representam 98% da sua massa seca. A quantidade de amilose varia dependendo da origem botânica: nos amidos denominados waxy ou cerosos esta se encontra em quantidades menores que 15%, enquanto nos catalogados como de alto conteúdo de amilose pode estar presente em teores acima de 40% (TESTER; KARKALAS; QI, 2004). Alguns trabalhos reportam a efetividade da amilose na geração de complexos de inclusão com algumas substâncias hidrofóbicas como álcoois, sabores e aromas (NUESSLI et al., 1997; LALUSH et al., 2005a; WULFF; AVGENAKI; GUZMANN, 2005b; ITTHISOPONKUL et al., 2007; PUTAUX et al., 2008). A amilose é um homopolímero linear de (1,4)-D-glucopiranose, que pode ser extraído do amido nativo ou sintetizado por sintetase como a amilosucrase ou fosforilase. Desse biopolímero se aproveita sua tendência a formar complexos moleculares denominados V-amilose, os quais podem ser usados para desenvolvimento de sistemas de liberação de compostos nutracêuticos (GODET; BIZOT; BULÉON, 1995; ZABAR et al., 2010). Modelos baseados em difração de raios-X mostram os complexos de V-amilose como hélices individuais de 6,7, ou 8 unidades de glicose por volta, similares aos encontrados nas configurações α-β-γ- das ciclodextrinas, as quais foram propostas para descrever a estrutura da V-amilose (OBIRO; SINHA RAY; EMMAMBUX, 2012a). A parte interior da hélice de amilose contém os grupos metileno e ligações glicosídicas que se alinham para formar uma cavidade hidrofóbica. Por outro lado, os grupos hidroxila localizam-se no exterior da hélice, convertendo-a numa superfície hidrofílica (LICHTENTHALER; IMMEL, 2000). A estrutura helicoidal se estabiliza pelas interações de ligações de hidrogênio e forças de Van der Waals entre a glicose presente na amilose, a água e a molécula a ser ligada. A interação hidrofóbica permite a acomodação do ligante dentro da cavidade hidrófoba da amilose; a força de união e as dimensões da hélice dependem da molécula hóspede.

Durante a preparação dos complexos de V-amilose, podem-se obter duas formas polimórficas, dependendo do solvente e das condições de pH e de temperatura. A primeira, denominada tipo I, tem uma estrutura amorfa com ponto de fusão menor de 100 °C. A segunda, do tipo II tem ponto de fusão maior que 100 °C e estrutura cristalina, o que converte os complexos de V-amilose em estruturas com grande capacidade de resistência ao calor (PUTAUX et al., 2008). A importância tecnológica de tais complexos encontra-se na sua estabilidade à hidrólise ácida, na grande capacidade de proteção às altas temperaturas e à oxidação, e na capacidade de liberar moléculas em sítios específicos do TGI, especificamente no cólon. Tudo isso faz da amilose uma matéria prima atrativa para produzir sistemas de liberação de compostos bioativos (GELDERS et al., 2004; BIAIS et al., 2006; PUTAUX et al., 2011). Em muitos dos estudos de inclusão tem-se usado amilose pura ou amido de batata, porém os lipídeos encontrados de forma natural neste último podem interferir na formação do complexo de inclusão. Os trabalhos relacionados com a formação de complexos de amilose a partir de amido de mandioca, tendo em conta que este possui uma percentagem de lipídeos menor que 0,1%, são escassos e se remetem ao estudo de complexos de inclusão de saborizantes (MOORTHY, 2002; ITTHISOPONKUL et al., 2007). Com base em estudos prévios de formação de complexos de inclusão entre a bixina e as ciclodextrinas (LYNG; PASSOS; FONTANA, 2005a; MARCOLINO et al., 2011), as quais tem uma cavidade hidrofóbica similar à encontrada na amilose, foi considerada a possibilidade de formação de complexos de inclusão tipo V entre a bixina e o amido com alto teor de amilose.

Por outro lado, os xerogéis, criogéis e aerogéis têm ganhado interesse na indústria como sistemas para a microencapsulação de compostos bioativos (GLENN; IRVING, 1995; GAUTHIER et al., 2004; JOB et al., 2006; HOEPFNER; RATKE; MILOW, 2008; COMIN; TEMELLI; SALDAÑA, 2012; DE MARCO et al., 2015). As propriedades dos xerogéis dependem do biopolímero usado e do processo de preparação. Xerogéis, criogéis e aerogéis têm sido preparados a partir de amilose pura ou amido de batata com alto teor de amilose, os quais têm sido usados na maioria dos estudos sobre complexos de inclusão. De acordo com Kapuśniak e Tomasik (2006a), na preparação de microcápsulas de amido de milho ceroso e de tapioca com lipídeos, a molécula hóspede não reage com o amido, mas a estrutura formada tem um alto potencial para ser usado na encapsulação.

Seguindo a estratégia de formulação de sistemas de liberação controlada, pretende-se estudar a encapsulação de carotenoides e explorar a possibilidade de

formação de complexos V-amilose, a partir dos carotenoides presentes no urucum (*Bixa orellana)* e no óleo de abacate, através de diferentes métodos: ultrassom, precipitação em meio ácido e preparação de xerogéis, criogéis. Sabe-se que os carotenoides são compostos de grande importância na dieta. A combinação das propriedades funcionais, sob o ponto de vista da proteção que proporciona o amido e o sinergismo com os carotenoides poderia ampliar o espectro de novas formulações de matrizes alimentares.

Objetivos

Objetivo geral

De forma ampla, este trabalho pretende avaliar e comparar a viabilidade da formação de complexos de inclusão do tipo V-amilose a partir de amido de mandioca e de amido de milho comercial com alto teor de amilose, para a encapsulação de bixina do extrato de urucum, utilizando os processos com ultrassom (termomecânico) e por precipitação em meio ácido das dispersões de amido (método clássico). O projeto também explora a capacidade da amilose de mandioca para encapsular carotenoides contidos no óleo de abacate - luteía e neoxantina - usando a formação de xerogéis e criogéis como metodologia de encapsulação.

Objetivos específicos

- Avaliar a formação de complexos de V-amilose com bixina, usando o método termomecânico baseado na aplicação de ultrassom.
- Avaliar a formação de complexos de V-amilose com bixina, usando o método clássico de preparação por precipitação em meio ácido.
- Avaliar os efeitos das condições operacionais dos métodos termomecânico e precipitação em meio ácido nas interações entre a matriz de amido e a bixina.
- Avaliar a capacidade de encapsulação e de liberação da matriz amido-bixina formada pelos métodos termomecânico e clássico.
- Selecionar as melhores condições para a produção de complexos através dos métodos termomecânico e clássico.
- Avaliar a encapsulação de luteína e neoxantina presentes no óleo de abacate e a formação de complexos de V-amilose a partir de amido de madioca, através da formação de xerogéis e criogéis.

ORGANIZAÇÃO DO TRABALHO EM CAPÍTULOS

A tese foi organizada em 5 capítulos como descrito a seguir:

Capítulo 1. É apresentada uma revisão bibliográfica que aborda os sistemas de encapsulação e liberação mais usados, assim como o papel do amido na formulação de sistemas de liberação controlada. Também é feita uma descrição da estrutura do grânulo de amido, e do potencial uso da amilose como material de parede, bem como na preparação de complexos de inclusão ou de xerogéis e criogéis. É feita uma descrição dos métodos de preparação dos complexos de amilose e a avaliação da microencapsulação com e sem complexação.

Capítulo 2. Nesse capítulo são estudados os efeitos do ultrassom sobre a capacidade de encapsulação e o perfil de liberação da matriz formada pelo amido com alto teor de amilose. São estudadas as interações entre o amido e a bixina, usando difração de raios X (DRX), calorimetria exploratória de varredura (DSC), espectroscopia de infravermelho (FT-IR), microscopia eletrônica de varredura (MEV). É avaliada a formação de complexos de amilose.

Capítulo 3. Nesse capítulo é avaliada a formação de complexos de inclusão da amilose usando a metodologia por precipitação em meio ácido. Também é avaliado o efeito da presença de proteína sobre o processo de encapsulação. São apresentados os resultados experimentais do perfil de liberação e a capacidade de encapsulação da matriz de amido e proteína.

Capítulo 4. São apresentados os resultados do processo de otimização usando a metodologia por superfície de resposta. São estudados os efeitos das variáveis dos processos de encapsulação usando ultrassom e precipitação em meio ácido.

Capítulo 5. É avaliada a capacidade de encapsulação dos géis de amilose na encapsulação do óleo de abacate através da formação de xerogéis e criogéis. Também é avaliada a formação de complexos de inclusão da amilose.

Referências bibliográficas

ALVES-RODRIGUES, A.; SHAO, A. The science behind lutein. **Toxicology letters**, v. 150, n. 1, p. 57–83, 15 abr. 2004.

ALVES, V.; MAGALHÃES, R. Obesidade no Brasil: tendências atuais. v. 24, p. 71–82, 2006.

ANSARI, K. A; VAVIA, P. R.; TROTTA, F.; CAVALLI, R. Cyclodextrin-based nanosponges for delivery of resveratrol: in vitro characterisation, stability, cytotoxicity and permeation study. **AAPS PharmSciTech**, v. 12, n. 1, p. 279–86, mar. 2011.

BELITZ, H.; GROSCH, W.; SCHIEBER LE, P. **Lipids. In Food Chemistry**. 4th ed ed. Berlin: Springer, 2009.

BIAIS, B.; LE BAIL, P.; ROBERT, P.; PONTOIRE, B.; BULÉON, A. Structural and stoichiometric studies of complexes between aroma compounds and amylose. Polymorphic transitions and quantification in amorphous and crystalline areas. **Carbohydrate Polymers**, v. 66, n. 3, p. 306–315, 2006.

BLOCH, M. J.; VIERA, A. J. Should patients with obesity and hypertension be treated differently from those who are not obese? **Current hypertension reports**, v. 16, n. 3, p. 418, mar. 2014.

BRAITHWAITE, M. C.; TYAGI, C.; TOMAR, L. K.; KUMAR, P.; CHOONARA, Y. E.; PILLAY, V. Nutraceutical-based therapeutics and formulation strategies augmenting their efficiency to complement modern medicine: An overview. **Journal of Functional Foods**, p. 1–18, out. 2013.

COMIN, L. M.; TEMELLI, F.; SALDAÑA, M. D. a. Barley beta-glucan aerogels via supercritical CO2 drying. **Food Research International**, v. 48, n. 2, p. 442–448, 2012.

DE MARCO, I.; BALDINO, L.; CARDEA, S.; REVERCHON, E. Supercritical Gel Drying for the Production of Starch Aerogels for Delivery Systems. **Chemical Engineering Transactions**, v. 43, p. 307–312, 2015.

GAUTHIER, B. M.; BAKRANIA, S. D.; ANDERSON, A. M.; CARROLL, M. K. A fast-supercritical extraction technique for aerogel fabrication. **Journal of Non-Crystalline Solids**, v. 350, p. 238–243, 2004.

GELDERS, G.; VANDERSTUKKEN, T.; GOESAERT, H.; DELCOUR, J. Amylose–lipid complexation: a new fractionation method. **Carbohydrate Polymers**, v. 56, n. 4, p. 447–458, jul. 2004.

GLENN, G. M.; IRVING, D. W. Starch-Based Microcellular Foams. **American Association of Cereal Chemists**, v. 72, n. 2, p. 155–161, 1995.

GODET, M. C.; BIZOT, H.; BULÉON, A. Crystallization of amylose-fatty acid complexes prepared with different amylose chain lengths. **Carbohydrate Polymer**, v. 1, n. 27, p. 47–52, 1995.

GONNET, M.; LETHUAUT, L.; BOURY, F. New trends in encapsulation of liposoluble vitamins. **Journal of controlled release: official journal of the Controlled Release Society**, v. 146, n. 3, p. 276–90, 15 set. 2010.

HOEPFNER, S.; RATKE, L.; MILOW, B. Synthesis and characterisation of nanofibrillar

cellulose aerogels. **Cellulose**, v. 15, n. 1, p. 121–129, 2008.

HOYERT, D. L.; PH, D.; XU, J.; STATISTICS, V. National Vital Statistics Reports Deaths: Preliminary Data for 2011. v. 61, n. 6, 2012.

ITTHISOPONKUL, T.; MITCHELL, J. R.; TAYLOR, A. J.; FARHAT, I. a. Inclusion complexes of tapioca starch with flavour compounds. **Carbohydrate Polymers**, v. 69, n. 1, p. 106–115, 1 maio 2007.

JOB, N.; PANARIELLO, F.; MARIEN, J.; CRINE, M.; PIRARD, J. P.; LÉONARD, A. Synthesis optimization of organic xerogels produced from convective air-drying of resorcinol-formaldehyde gels. **Journal of Non-Crystalline Solids**, v. 352, n. 1, p. 24–34, 2006.

KAPUŚNIAK, J.; TOMASIK, P. Lipid microencapsulation in starch. **Journal of microencapsulation**, v. 23, n. 3, p. 341–348, 2006.

LALUSH, I.; BAR, H.; ZAKARIA, I.; EICHLER, S.; SHIMONI, E. Utilization of amylose-lipid complexes as molecular nanocapsules for conjugated linoleic acid. **Biomacromolecules**, v. 6, n. 1, p. 121–130, 2005.

LESMES, U.; BARCHECHATH, J.; SHIMONI, E. Continuous dual feed homogenization for the production of starch inclusion complexes for controlled release of nutrients. **Innovative Food Science & Emerging Technologies**, v. 9, n. 4, p. 507–515, out. 2008.

LICHTENTHALER, F.; IMMEL, S. The Hydrophobic Topographies of Amylose and its Blue Iodine. **Starch/Stärke**, v. 52, n. 1, p. 1–8, 2000.

LYNG, S. M. O.; PASSOS, M.; FONTANA, J. D. Bixin and α-cyclodextrin inclusion complex and stability tests. **Process Biochemistry**, v. 40, n. 2, p. 865–872, 2005.

MARCOLINO, V. A.; ZANIN, G. M.; DURRANT, L. R.; BENASSI, M. D. T.; MATIOLI, G. Interaction of curcumin and bixin with β-cyclodextrin: Complexation methods, stability, and applications in food. **Journal of Agricultural and Food Chemistry**, v. 59, n. 7, p. 3348–3357, 2011.

MATALANIS, A.; JONES, O. G.; MCCLEMENTS, D. J. Structured biopolymer-based delivery systems for encapsulation, protection, and release of lipophilic compounds. **Food Hydrocolloids**, v. 25, n. 8, p. 1865–1880, 2011.

MCCLEMENTS, D. J.; LI, Y. Structured emulsion-based delivery systems: controlling the digestion and release of lipophilic food components. **Advances in colloid and interface science**, v. 159, n. 2, p. 213–28, 15 set. 2010.

MOORTHY, S. N. Physicochemical and Functional Properties of Tropical Tuber Starches: A Review. **Starch - Stärke**, v. 54, n. 12, p. 559–592, 2002.

NACKA, F.; CANSELL, M.; MÉLÉARD, P.; COMBE, N. Incorporation of alpha-tocopherol in marine lipid-based liposomes: in vitro and in vivo studies. **Lipids**, v. 36, n. 12, p. 1313–20, dez. 2001.

NUESSLI, J.; SIGG, B.; CONDE-PETIT, B.; ESCHER, F. Characterization of amylose—flavour complexes by DSC and X-ray diffraction. **Food Hydrocolloids**, v. 11, n. 1, p. 27–34, jan. 1997.

OBIRO, W. C.; SINHA RAY, S.; EMMAMBUX, M. N. V-amylose Structural Characteristics, Methods of Preparation, Significance, and Potential Applications. **Food Reviews International**, v. 28, n. 4, p. 412–438, 2012.

PUTAUX, J.-L.; CARDOSO, M. B.; DUPEYRE, D.; MORIN, M.; NULAC, A.; HU, Y. Single Crystals of V-Amylose Inclusion Complexes. **Macromolecular Symposia**, v. 273, n. 1, p. 1–8, nov. 2008.

PUTAUX, J.-L.; NISHIYAMA, Y.; MAZEAU, K.; MORIN, M.; CARDOSO, M. B.; CHANZY, H. Helical Conformation in Crystalline Inclusion Complexes of V-Amylose: A Historical Perspective. **Macromolecular Symposia**, v. 303, n. 1, p. 1–9, 17 maio 2011.

SCHUBERT, M; MÜLLER-GOYMANN, C . Characterisation of surface-modified solid lipid nanoparticles (SLN): influence of lecithin and nonionic emulsifier. **European journal of pharmaceutics and biopharmaceutics**, v. 61, n. 1–2, p. 77–86, set. 2005.

SUBURU, J.; GU, Z.; CHEN, H.; CHEN, W.; ZHANG, H.; CHEN, Y. Q. Fatty acid metabolism: Implications for diet, genetic variation, and disease. **Food Bioscience**, v. 4, p. 1–12, dez. 2013.

TESTER, R. F.; KARKALAS, J.; QI, X. Starch composition, fine structure and architecture. **Journal of Cereal Science**, v. 39, n. 2, p. 151–165, mar. 2004.

WULFF, G.; AVGENAKI, G.; GUZMANN, M. S. P. Molecular encapsulation of flavours as helical inclusion complexes of amylose. **Journal of Cereal Science**, v. 41, n. 3, p. 239–249, maio 2005.

ZABAR, S.; LESMES, U.; KATZ, I.; SHIMONI, E.; BIANCO-PELED, H. Structural characterization of amylose-long chain fatty acid complexes produced via the acidification method. **Food Hydrocolloids**, v. 24, n. 4, p. 347–357, jun. 2010.

CAPÍTULO 1. REVISÃO BIBLIOGRÁFICA

1.1 Sistemas de liberação de compostos bioativos

A microencapsulação de compostos bioativos é uma técnica usada em grande variedade de aplicações na indústria alimentícia (MCCLEMENTS; LI, 2010). Por exemplo, a encapsulação de isoflavonas aumenta sua biodisponibilidade; ou no caso dos carotenoides, os quais são compostos de importância nutricional, provê proteção contra a luz, calor e umidade (COHEN et al., 2011). A microencapsulação também melhora a solubilidade e fornece proteção contra ambientes adversos como os presentes no trato gastrointestinal (TGI). Por essa razão, a incorporação desses compostos na dieta converteu-se em um importante desafio devido à sua baixa estabilidade nas condições de extração e processamento, além dos problemas inerentes à armazenagem e às condições próprias do TGI (LESMES; BARCHECHATH; SHIMONI, 2008; BELITZ; GROSCH; SCHIEBER LE, 2009). Nesse sentido, os sistemas baseados em matrizes de amido e outros polissacarídeos têm ganhado interesse, uma vez que são considerados GRAS (geralmente reconhecido como seguro), melhoram a biodisponibilidade e solubilidade em água de moléculas bioativas e as protegem em sua passagem pelo sistema digestivo, o que transforma essas matrizes em material de parede ideais para a microencapsulação e proteção de compostos de valor nutricional (LALUSH et al., 2005a; COHEN et al., 2011).

Entre os nutracêuticos microencapsulados e administrados por via oral se incluem glucosamina, condroitina, licopeno, resveratrol, coenzima-Q10, creatina, melatonina, extratos vegetais, acetil-L-carnitina, S-adenosil metionina (SAME), ácido lipoico, dehidroepiandrosterona (DHEA) e algumas vitaminas hidro e lipossolúveis, flavors, carotenoides, óleos, ácidos graxos entre outros (WULFF; AVGENAKI; GUZMANN, 2005a; ABU-HARDAN; HILL; FARHAT, 2007; ITTHISOPONKUL et al., 2007; RADHIKA; SHANAVAS; MOORTHY, 2008; ZABAR et al., 2010; BRAITHWAITE et al., 2013).

Diversos sistemas de encapsulação e liberação têm sido propostos, sendo os mais utilizados apresentados a seguir. Em uma primeira categoria estão as emulsões e as nanoemulsões, as quais se distinguem pelo tamanho das gotas em suspensão: as primeiras apresentam gotas de diâmetro entre 100 nm a 100 μm, enquanto que, nas nanoemulsões os tamanhos estão entre 10 nm a 100 nm. Da mesma forma, tem-se desenvolvido dispersões de lipídeos sólidos em solução aquosa, muito similar às emulsões acima descritas, sendo sua cristalização controlada a fim de obter atributos específicos

(SCHUBERT; MÜLLER-GOYMANN, 2005; LI et al., 2010). Outro sistema de liberação são os lipossomas ou vesículas lipídicas microscópicas esféricas. Suas características se vêem afetadas pelo tamanho da vesícula, pela concentração de lipídeos e composição de nutracêuticos no interior do lipossoma (NACKA et al., 2001; GONNET; LETHUAUT; BOURY, 2010). Outros investigadores têm desenvolvido emulsões multicamada, as quais consistem de partículas de óleo dispersas em um meio aquoso e cobertas por nano camadas que estão localizadas ao redor destas, as quais podem ser produzidas a partir de um ou mais biopolímeros, tal como os fosfolipídios, polissacarídeos ou proteínas. (AOKI; DECKER; MCCLEMENTS, 2005). Outra alternativa para o desenvolvimento de agentes de liberação são os hidrogéis, os quais adsorvem o lipídeo que se encontra disperso em um meio aquoso. Tipicamente tais sistemas são produzidos a partir de uma emulsão dupla do tipo O/W1/W2 que lhes confere propriedades físico-químicas diferentes das apresentadas pelas emulsões convencionais. Alguns dos métodos mais utilizados na preparação desse tipo de sistemas incluem a coacervação simples e complexa e métodos de extrusão e moldagem (MATALANIS; JONES; MCCLEMENTS, 2011b; BRAITHWAITE et al., 2013). Da mesma forma, os complexos de ciclodextrina e seus derivados têm sido usados para melhorar a solubilidade, estabilidade e biodisponibilidade de compostos nutracêuticos (TONNESEN; MÁSSON; LOFTSSON, 2002; YUAN; JIN; XU, 2012). Tem sido reportado o desenvolvimento de micro e nano esponjas a partir de ciclodextrinas, sistema que contém microporos com uma grande área de superfície interna e boa capacidade de carga, o que melhora a eficiência de liberação (ANSARI et al., 2011)

Uma técnica comumente usada na proteção de carotenoides é a secagem por atomização, em que o betacaroteno pode ser encapsulado usando amido de mandioca nativo e ácido-modificado, assim como maltodextrina como material de parede na encapsulação. Esta tecnologia leva a altas retenções de betacaroteno (LOKSUWAN, 2007; SPADA et al., 2012; JANISZEWSKA-TURAK, 2017). Sharif et al. (2017) reportaram eficiências de encapsulação maiores de 90 %, na preparação de microcápsulas de betacaroteno e eugenol por spray drying depois de sua emulsificação, utilizando amido modificado com anidrido octenilsuccínico (OSA). Ahmed et al. (2015) alcançaram eficiências de encapsulação de 96 %, encapsulando astaxantina de biomassa de *H. pluvialis* usando goma arábica e maltodextrina como material de parede. Licopeno foi encapsulado com amido modificado com eficiências entre 21 a 30 % (ROCHA; FÁVARO-TRINDADE; GROSSO, 2012). Shen et al. (2014) obtiveram eficiências de encapsulação entre 63 até 95 %, usando como

material de parede misturas de proteínas de leite e fibra, através da secagem por aspersão de emulsões de astaxantinas. Também pode ser usado caseinato de sódio, proteína isolada de soro (WPI), proteína isolada de soja através do método de homogeneização e evaporação. Os autores sugerem que WPI poderia ser o melhor veículo para a liberação controlada de betacaroteno (YI et al., 2015). Boscheto et al. (2014) investigaram as características de liberação do betacaroteno coprecipitado em poli-hidroxibutirato-co-valerato, utilizando dióxido de carbono supercrítico, reportaram eficiências de encapsulação entre 7,75 até 55,54 %. Outras metodologias como a coacervacão complexa de betacaroteno em misturas de caseína e goma traganta, também têm sido utilizadas com eficiência de encapsulação próxima de 82,51 % (JAIN et al., 2016). Extrato de pimenta vermelha rico em carotenoide foi microencapsulado com goma arábica, com eficiências de encapsulação de 73 a 77 % (ROMO-HUALDE et al., 2012).

1.1.1 Emulsões e nanoemulsões

As emulsões e nanoemulsões podem ser distinguidas pelo tamanho da partícula em suspensão. As emulsões têm um diâmetro de partícula entre 100 nm a 100 μm, enquanto que as nanoemulsões têm diâmetros entre 10 nm a 100 nm. Basicamente são preparadas e estabilizadas pela interação de um lipídeo e um agente emulsificante, cujo balanço hidrofílico-lipofílico determina o balanço de cargas na interface, assim como o comportamento reológico e estabilidade às mudanças de pH. O balanço de cargas na interface entre o emulsificante e o lipídeo pode ser afetado, gerando-se mudanças nas propriedades reológicas da emulsão e na velocidade de liberação do composto bioativo de interesse. No entanto, as caraterísticas desses sistemas de liberação podem ser modificadas pelo incremento ou diminuição do tamanho de partícula suspensos no sistema. Alguns sistemas de liberação desse tipo têm sido produzidos a partir de misturas de triglicerídeos, ceras ou ácidos graxos com lipídeos. Geralmente, a emulsão é preparada pela combinação a quente de uma fase lipofílica e uma fase aquosa na presença de um emulsificante hidrófilo, a qual é posteriormente resfriada de maneira controlada, provocando a cristalização do lipídeo dentro da emulsão, o que permite obter sistemas com caraterísticas específicas. Nessa mesma categoria encontram-se as emulsões em multicamada, as quais consistem na dispersão clássica de um lipídeo em uma fase aquosa, mas cobertos por nano-camadas de um ou mais biopolímeros (AOKI; DECKER; MCCLEMENTS, 2005; SCHUBERT; MÜLLER-GOYMANN, 2005; LI et al., 2010)

1.1.2 Lipossomas, hidrogéis e criogéis

Os lipossomas são uma tecnologia usada como meio de liberação oral de moléculas como o resveratrol, com boa proteção e estabilidade. O sistema consiste na formação de vesículas lipídicas microscópicas, preparadas em alguns casos por fosfolipídios, e cuja estabilidade é determinada pelo tamanho da vesícula, concentração do lipídeo e da molécula hóspede dentro do lipossoma (AMRI, A., CHAUMEIL; SFAR; CHARRUEAU, 2012). Como alternativa para a produção de sistemas de liberação encontram-se os hidrogéis, os quais são produzidos por emulsões duplas, ou mediante metodologias como a coacervação simples ou complexa, ou por métodos de extrusão e molde (MATALANIS; JONES; MCCLEMENTS, 2011b; BRAITHWAITE et al., 2013). Pesquisas sobre o uso dos criogéis na microencapsulação de moléculas bioativas foram avaliadas por Ahuja et al. (2015), que estudou a incorporação de metronidazol em hidrogéis de polissacarídeo carboximetilcelulose de semente de tamarindo e álcool polivinílico. Os criogéis produzidos nessas matrizes apresentaram boas taxas de adsorção e liberação do metronidazol e uma alta estabilidade térmica. Păduraru et al. (2012) avaliaram a incorporação de vanilina em criogéis a partir de álcool polivinílico e celulose microcristalina, e reportaram que houve uma diminuição no tempo de liberação e que a capacidade de inchamento foi melhorada pela presença da celulose.

1.1.3 Nano esponjas e complexos de inclusão

De modo similar aos complexos de inclusão com amido, os complexos com as ciclodextrinas têm sido usados para melhorar a solubilidade de algumas moléculas bioativas de interesse, assim como sua biodisponibilidade (TONNESEN; MÁSSON; LOFTSSON, 2002; YUAN; JIN; XU, 2012). Nesse mesmo sentido se têm desenvolvido formulações de limão em pó por esta metodologia sem prejuízo às características originais do óleo (BHANDARI et al., 1998). Marques et al. (2010) fizeram uma revisão sobre a aplicação desse tipo de complexos de inclusão com óleos essenciais e compostos voláteis, assim como as metodologias propostas para sua preparação e análise. Também tem sido reportado o desenvolvimento de nano esponjas com grande área superficial interna e boa capacidade de carga, o que melhora a eficiência de liberação (ANSARI et al., 2011).

1.2 O papel do amido nos sistemas de liberação controlada

Como se tem indicado antes, o crescente uso dos sistemas de microencapsulação baseados no amido como material de parede na microencapsulação de compostos bioativos é devido à sua alta eficiência de encapsulação e proteção em comparação às proteínas ou algumas gomas. Uma série de sistemas baseados no amido como matriz para a preparação de sistemas de liberação têm sido investigadas. Investigações desses sistemas têm-se focado no uso dos microporos presentes no amido, na preparação de aerogéis, criogéis e xerogéis, ou na formulação de emulsões e nanopartículas, assim como no uso de amido modificado através de reticulação, hidrolisado, ou ainda na preparação de complexos de amilose (ZHU., 2017). Antes de abordar as metodologias usadas na microencapsulação usando amido como principal material de parede, sua estrutura será descrita brevemente.

1.2.1 Estrutura do grânulo de amido

O amido é o principal carboidrato armazenado em tubérculos, raízes e cereais, estando depositado em grânulos insolúveis constituídos por estruturas semicristalinas. O amido é composto por dois polímeros de D-glicose. O primeiro, denominado amilose, é um glucano constituído principalmente de ligações α[1-4]. O segundo é a amilopectina, a qual tem cadeias de glicose ligadas nas posições α[1-4], arranjadas em uma estrutura ramificada com ligações α[1-6]. Esses dois glucanos representam de 98 a 99 % do material seco do grânulo, dependendo da origem botânica do amido. Assim, os amidos denominados "waxy'' contêm menos de 15 % de amilose, enquanto nos denominados de alto conteúdo de amilose são encontradas concentrações maiores de 40 %. Nos amidos normais a concentração de amilose varia entre 20 a 30 %. No entanto, dentro do grânulo também são encontradas pequenas quantidade de lipídeos, em forma de fosfolipídios, assim como minerais e fosfatos esterificados com os grupos hidroxilas da glicose (TESTER; KARKALAS; QI, 2004; COPELAND et al., 2009).

1.2.1.1 Amilopectina

É um polímero ramificado com massa molar de aproximadamente 10^7 a 10^8 g/mol e um grau de polimerização entre 9600 a 15900. Uma caraterística da amilopectina é a grande quantidade de ramificações, as quais podem ser descritas em termos da designação

das suas cadeias como A, B, C. Acredite-se que esta é encontrada em cluster discreto como se mostra na Figura 1.1 (TESTER; KARKALAS; QI, 2004).

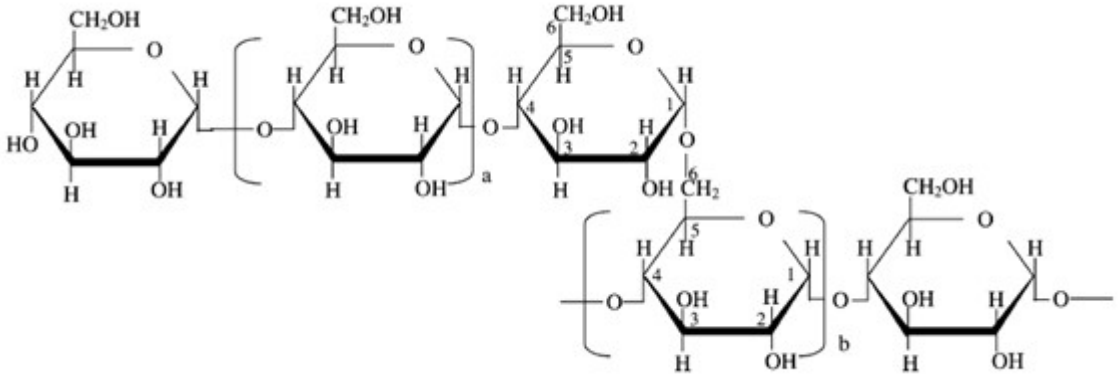

Figura 1.1 Ilustração da estrutura molecular da amilopectina. Adaptado de (TESTER; KARKALAS; QI, 2004).

1.2.1.2 Amilose

A amilose tem uma massa molar de aproximadamente 10^5 - 10^6 g/mol, a qual varia dependendo da sua origem botânica; cada cadeia contém aproximadamente 200 a 700 resíduos de glicose (TESTER;KARKALAS;QI, 2004). Sua estrutura é apresentada na Figura 1.2. A amilose representa uma fração muito pequena da estrutura cristalina do amido, no entanto, esta pode ser recristalizada por resfriamento de uma solução ou pela adição de um precipitante até recristalizar por meio da auto-organização de suas cadeias formando cristalitos A, B, assim como agregados, géis ou esferulitos (BULÉON; VÉRONÈSE; PUTAUX, 2007). Outro aspecto interessante da amilose é sua capacidade para se ligar com pequenas moléculas, formando complexos de inclusão com iodo, lipídeos, álcoois ou flavors, formando estruturas cristalinas de apenas uma hélice denominada de tipo-V (MOTTIAR; ALTOSAAR, 2011).

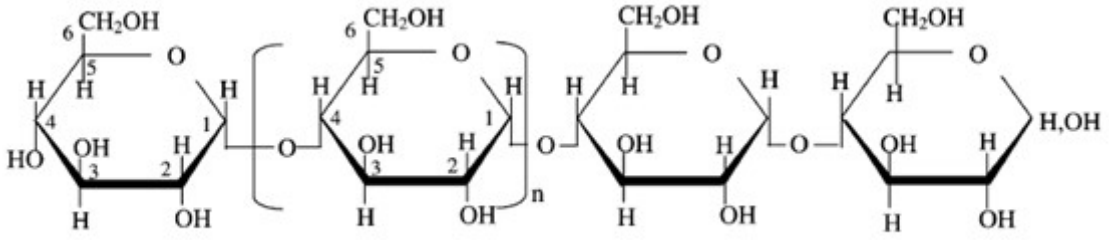

Figura 1.2 Ilustração da estrutura molecular da amilose. Adaptado de (TESTER; KARKALAS; QI, 2004).

No grânulo de amido, a amilose e a amilopectina se encontram ligadas. Uma vez que se realiza o processo de solvatação do grânulo, sua separação é difícil, limitando-se à obtenção de um gel que esteja livre de algum dos dois polímeros. Quando uma suspensão de amido é aquecida acima da sua temperatura de gelatinização, a amilose se difunde mais facilmente para fora do grânulo, o que permite sua separação. Os métodos de separação aproveitam a capacidade da amilose para formar complexos de inclusão com álcoois de baixa massa molar, os quais produzem precipitados insolúveis. É usada também a cromatografia por exclusão de tamanho para sua separação (GARCÍA; MARTINO; ZARITZKY, 1995; MUA; JACKSON, 1995).

1.2.2 Sistemas de encapsulação usando amido

O amido nativo gelatinizado a alta pressão tem sido usado como material de parede na preparação de sistemas de liberação de extratos de ervas (DELADINO et al., 2015). O próprio grânulo de amido possui cavidades que podem ser usadas como carregadores de compostos bioativos. A superfície porosa do grânulo tem sido usada no desenvolvimento de sistemas de liberação de catequina, a qual permanece nas cavidades do grânulo, provavelmente devido às interações entre os grupos benzeno-tetrahidrofurano que se associam com a molécula de amido, formando um sistema de liberação controlada (HAN et al., 2015). O amido microporoso pode ser também preparado por hidrólise enzimática com glicoamilase (WU et al., 2011). Os microporos podem armazenar probióticos, melhorando a sobreviência sob condições do TGI. Estudos mencionam a adição de alginato, o qual ajuda na formação das microcápsulas, porém é o amido o que aumenta a eficiência de encapsulação (XING et al., 2014). O amido pode carregar

polifenóis ou vitaminas em cápsulas em nível nanométrico; o sistema, no caso dos polifenóis, pode ser dissolvido em soluções aquosas e atingir capacidades de carga de até 78%. As nanopartículas de amido carregadas são resistentes à hidrólise ácida e melhoram a biodisponibilidade da molécula hóspede (CHIN; YASID AKMARMOHD; PANG, 2014; HASANVAND et al., 2015). Géis de amido de feijão e arroz também têm sido usados como carregadores para a microencapsulação de betacaroteno emulsificado em óleo de milho e estabilizado com proteína de soro ou Tween 20. Os géis de amido de feijão e arroz apresentam propriedades reológicas diferentes, as quais são causadas pela diferença no conteúdo de amilose. O perfil de liberação sob condições similares às do TGI vê-se afetado pela cristalinidade e baixa solubilidade do gel (MUN et al., 2015).

Amidos substituídos e modificados com trimetafosfato trissódico e oxidados com hipoclorito de sódio e posteriormente reticulados também são usados na preparação de sistemas de liberação. O grupo fosfato que fica livre depois do processo de reticulação aumenta a afinidade do amido pelas moléculas catiônicas (LI et al., 2009). O amido oxidado e reticulado tem sido usado na microencapsulação de carotenoides e antocianinas, sendo que a capacidade de carga pode variar em função de alterações no grau de modificação do amido (WANG et al., 2015). Por outro lado, os amidos substituídos com anidrido octenilsuccínico ou os produzidos por esterificação com o ácido esteárico têm sido usados na encapsulação de ingredientes hidrofóbicos e na preparação de emulsões Pickering. O sistema de liberação é produzido pela mistura entre o ingrediente hidrofóbico e o amido substituído e posteriormente secado por spray drying. Através desta metodologia tem sido encapsulado óleo de peixe, óleo de frutas, carotenoides, coenzima $Q_{10,}$ cúrcuma e probióticos, com eficiências de encapsulação no caso dos carotenoides de até 80%, o tamanho de partícula varia entre 200 a 300 nm no caso do sistema que contém coenzima Q_{10} (YU; HUANG, 2010; DE PAZ; MARTÍN; COCERO, 2013; SWEEDMAN et al., 2013; CORTÉS et al., 2014; CHEUK et al., 2015). Nos amidos esterificados observa-se um aumento da habilidade emulsificante, melhorando a capacidade de retenção, por exemplo, de óleo de soja (HAN et al., 2011). Outro tipo de substituição usada na preparação de amidos modificados são os fosforilados e os acetilados; neste caso, o sistema de liberação é preparado geralmente por spray drying. Têm sido preparadas cápsulas com probióticos e antocianinas, atingindo eficiências de encapsulação maiores que 88 % e tamanhos de partícula entre 2 a 6 μm; a acetilação aumenta a hidrofobicidade e diminui a capacidade de inchamento, no entanto,

parece que esta metodologia (amido fosforilado ou acetilados) não proporciona suficiente proteção contra as condições do TGI (FATHI; MARTÍN; MCCLEMENTS, 2014; GARCÍA-TEJEDA et al., 2016).

Maltodextrinas e amido hidrolisado também têm sido matéria prima na preparação de sistemas de liberação controlada de vitaminas e óleos, podendo ser usados sós ou em combinação com outros agentes tais como gelatina, melhorando a solubilidade da molécula hóspede (SPADA et al., 2012). Dispersões aquosas de betacaroteno também têm sido preparadas com dextrinas de amido com alto teor de amilose; o sistema provê proteção contra a oxidação e a digestão enzimática (KIM; SEO; LIM, 2013). Os amidos hidrolisados possuem a capacidade de reter maior quantidade de carotenoides em comparação com o amido nativo, provavelmente devido ao menor tamanho de partícula que facilita a acomodação do hóspede na matriz (SPADA et al., 2012).

1.2.3 Complexos de amilose

A amilose exibe tendência a formar complexos moleculares denominados V-amilose, os quais podem ser usados para desenvolvimento de sistemas de liberação controlada (GODET; BIZOT; BULÉON, 1995; ZABAR et al., 2010). O padrão de difração apresentado pelos complexos do tipo V mostra que as hélices formadas estão constituídas por seis, sete ou oito unidades de glicose por volta. Esse padrão é similar ao encontrado nos complexos com configurações α-β-γ das ciclodextrinas, os quais serviram como guia para tentar explicar os encontrados na amilose (OBIRO; SINHA RAY; EMMAMBUX, 2012a). Na hélice de amilose os grupos metilenos são orientados para a parte interna, enquanto que as hidroxilas são alinhadas para a parte exterior da hélice. Essa conformação converte a hélice da amilose em uma estrutura com uma cavidade interna hidrofóbica e uma superfície externa hidrofílica. É geralmente aceito que a estrutura helicoidal é estabilizada pelas interações de ligações de hidrogênio e forças de van der Waals entre a glicose presente na amilose, água e a molécula hóspede; dessa forma, a interação hidrofóbica permite ao hóspede localizar-se na cavidade da amilose (LICHTENTHALER; IMMEL, 2000). Uma ilustração da configuração tipo V da amilose é apresentada na Figura 1.3.

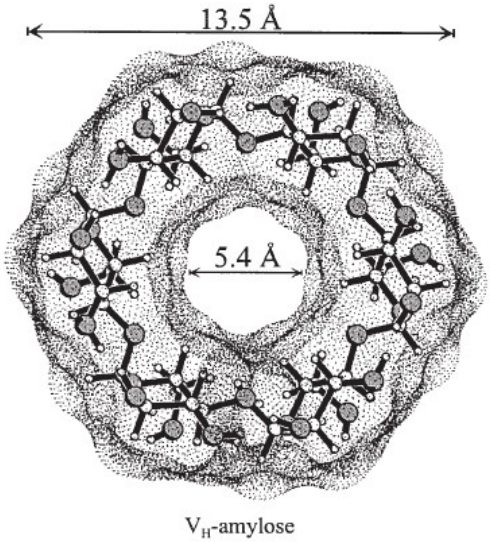

Figura 1.3. Ilustração da geometria molecular e dimensões da configuração da amilose tipo V_h (LICHTENTHALER; IMMEL, 2000).

Os complexos podem ser classificados segundo o número de unidades de glicose em cada volta, ou pela forma de empacotamento das suas hélices, enquanto o diâmetro da cavidade depende da estrutura da molécula hóspede (BILIADERIS; GALLOWAY, 1989). Tem-se estabelecido que os lipídeos ou álcoois lineares podem formar complexos com a amilose usando suas seis unidades de glicose, enquanto que nos compostos com cadeias ramificadas é mais comum o uso de sete unidades, inclusive oito para compostos mais volumosos. Os complexos cuja estrutura é composta por seis unidades de glicose são denominados V_6, os quais são subdivididos em V_h-amilose, também conhecido como V_{6I}, o qual se caracteriza por capturar o composto de interesse dentro da cavidade da hélice (NUESSLI et al., 1997; LICHTENTHALER; IMMEL, 2000; HEINEMANN et al., 2001; LE BAIL; RONDEAU; BULÉON, 2005). A outra forma, denominada V_{6II}, é também conhecida como $V_{butanol}$ e tem a capacidade de complexar tanto dentro da cavidade como na zona compreendida entre suas hélices (HELBERT; CHANZY, 1994; LE BAIL; RONDEAU; BULÉON, 2005). Finalmente, a terceira subdivisão do complexo V_6 é conhecida como V_{6III} ou $V_{isopropanol}$, a qual tem um espaço intersticial maior do que o complexo V_{6II}; isso permite ao hóspede localizar-se dentro e entre a hélice. Flavors e aromas como o timol e o geraniol formam complexos deste tipo (BULÉON et al., 1990; RONDEAU-MOURO; LE BAIL; BULÉON, 2004; LE BAIL; RONDEAU; BULÉON,

2005). Cabe destacar que a secagem pode realizar a conversão dos complexos V_{6II} e V_{6III} a V_{6I} (HELBERT; CHANZY, 1994). Como se tinha indicado antes, os complexos formados com moléculas mais volumosas, como o caso do α-naftol, são formados por hélices com oito unidades de glicose, ou sete, como no caso da mentona. Alguns autores assumem a configuração V_7 como uma V_6 com o hóspede localizado entre as hélices. Os complexos V_7 podem ser convertidos em V_H através de um processo de secagem, porém no caso do complexo V_8 isso não é possível (BULÉON et al., 1990; RONDEAU-MOURO; LE BAIL; BULÉON, 2004). Os complexos da amilose também podem ser classificados em função do solvente usado na sua preparação ou das condições de temperatura e pH. Na primeira classificação encontra-se o denominado tipo I, os quais se caracterizam por ter uma estrutura amorfa e uma temperatura de fusão abaixo de 100 °C. Na segunda categoria está o denominado tipo II, o qual se caracteriza por formar estruturas parcialmente ordenadas, com regiões amorfas e cristalinas distintas. Esses complexos têm uma temperatura de fusão acima dos 100 °C, o que os torna excelentes matrizes resistentes ao calor (KARKALAS et al., 1995; PUTAUX et al., 2008). Os complexos tipo II são subdivididos em tipo IIa e tipo IIb; o último pode atingir temperaturas de fusão até os 120 °C. Tem-se reportado a transição do tipo II ao tipo I quando estes são submetidos ao aquecimento acima de 90 °C (SISWOYO; MORITA, 2002; TUFVESSON; WAHLGREN; ELIASSON, 2003).

1.2.3.1 Métodos de preparação de complexos V-amilose

O processo de complexação ocorre quando a amilose presente no grânulo de amido ganha suficiente mobilidade para se ligar à molécula hóspede. Por essa razão, é necessária a liberação da amilose através do rompimento do grânulo (CONDE-PETIT; ESCHER; NUESSLI, 2006). Para realizar esse processo tem-se usado métodos distintos, os quais podem ser classificados em clássicos, enzimáticos e termomecânicos. Obiro et al. (2012a) fazem uma revisão detalhada dos métodos usados na preparação de complexos de inclusão de amilose.

O método clássico consiste na mistura de amilose, ou amido com alto conteúdo de amilose e a molécula que se deseja complexar em condições de aquecimento e alta umidade. Primeiro é necessária a dissolução da amilose em dimetilsulfóxido ou hidróxido de potássio, depois é adicionada a molécula hóspede e posteriormente eleva-se a

temperatura para permitir a interação das cadeias de amilose e o ligante. No entanto, para aumentar a formação de complexos faz-se necessário o aumento da solubilidade da molécula hóspede na mistura. Na etapa de isolamento do complexo o pH da mistura é diminuído até aproximadamente 4,5 e o complexo é posteriormente isolado por centrifugação (LALUSH et al., 2005a; OBIRO; SINHA RAY; EMMAMBUX, 2012a). Ades et al. (2012) usaram esse método para estudar os complexos de inclusão da amilose com aromas preparados a partir de amido de milho com diferentes concentrações de amilose, usando como modelos mentol e limoneno. Encontraram que o limoneno não gera complexos de V-amilose eficientemente; concluíram também que a eficiência da encapsulação depende da concentração da amilose e que os complexos formados são estáveis às altas temperaturas, às variações de pH e que podem ser usados para liberar aromas na cavidade oral.

Os métodos termomecânicos melhoram a velocidade de inchamento do grânulo, promovendo a formação de complexos. Simultaneamente, é usado o efeito de aquecimento e cisalhamento e, da mesma forma que no método clássico, a etapa final envolve uma diminuição do pH seguida da centrifugação para isolar os complexos (OBIRO; SINHA RAY; EMMAMBUX, 2012a). Esse tipo de método inclui a aplicação da homogeneização e da extrusão.

No caso da preparação de complexos por extrusão, tem-se mostrado que as condições do processo, assim como o aumento da temperatura e da umidade da matéria prima melhora a eficiência de encapsulação (DE PILLI et al., 2011). Meng et al. (2014) estudaram a produção de complexos de amilose e ácido palmítico por homogeneização a alta pressão. Concluíram que existe um efeito positivo no incremento da pressão sobre a formação de complexos. Le Bail et al. (2013) estudaram a formação de complexos de amilose de quatro fontes de amido - de batata, feijão, ervilha e mandioca - e compararam o processo de alta pressão e a gelatinização convencional, concluindo que é possível formar complexos de amilose com ácido decanóico e carvacrol; os complexos formados mostraram ser amorfos e dependentes da temperatura usada durante o processo a alta pressão. Lesmes et al. (2008) propuseram a produção de complexos de inclusão por alta pressão em um processo contínuo, mostrando que as condições de processo geram uma considerável redução do tamanho de partícula, além de apresentar as vantagens do uso de um processo contínuo.

O ultrassom inclui-se dentro da categoria de métodos não convencionais de obtenção de complexos de inclusão. Durante a aplicação do ultrassom acontecem processos de transferência de calor, turbulência e aplicação simultânea de forças devido ao fenômeno de cavitação produzido pela compressão e expansão dos gases dissolvidos no meio e evaporação da água devido à alta temperatura gerada. O colapso das bolhas de gás produz suficiente esforço para romper as ligações do polímero, permitindo uma melhor dissolução no meio reacional. TIAN et al. (2013) avaliaram o efeito do ultrassom na encapsulação através de complexos de inclusão de cinamaldeído com amido de milho usando baixas temperaturas.

O método enzimático baseia-se na síntese da V-amilose a partir de resíduos glicosídicos. Segundo OBIRO et al. (2012a), o método enzimático pode ser subdivido em inteiramente enzimático e parcialmente enzimático. O primeiro destes métodos usa glucofosforilase para catalisar a síntese da V-amilose em presença da molécula hóspede. O método parcialmente enzimático implica na despolimerização do amido ou amilose por catálise enzimática, a qual pode ser realizada pela β-amilase, sendo a enzima colocada antes ou depois da molécula hóspede. ZHANG et al. (2012) estudaram os complexos de V-amilose preparados com amido de milho desramificado usando pululanase e ácido láurico, concluindo que um elevado tempo de despolimerização poderia melhorar a eficiência de formação de complexos e que a inclusão reduz a digestibilidade do amido nativo.

1.2.3.2 Interação da amilose com algumas moléculas hóspede

BILIADERIS et al. (1991) estudaram a interação entre o dodecilsulfato de sódio (SDS), monoesterato de glicerol, brometo de cetil trimetil amônio, l-α-lisofosfatidilcolina e amidos de trigo, arroz, ervilha e grão de bico, através de ensaios reológicos e calorimetria exploratória diferencial (DSC). Esses pesquisadores sugeriram que a presença dos lipídeos induz a formação de complexos com a amilose, reduzindo a entalpia de gelatinização e aumentando o valor do módulo de armazenamento (G') no amido de trigo. Também têm sido reportados estudos que relacionam o decréscimo na produção de amido resistente com a formação de complexos de inclusão. O SDS também tem sido usado no estudo do comportamento térmico dos complexos formados com amido de milho junto com brometo de dodeciltrimetilamonio (DOTAB), hexadecilsulfato de sódio

e 1- monolaurina-rac-glicerol (ML), mostrando que os complexos com DOTAB diminuem a temperatura de fusão à medida que se aumenta a concentração do surfactante, ocasionando finalmente sua desestabilização. O autor sugere que este fenômeno é devido ao caráter iônico dos complexos formados. No caso do amido de milho ceroso com surfactantes iônicos como o DOTAB e o SDS, diminui a temperatura de início da gelatinização, possivelmente pela interação com a amilopectina (VILLWOCK et al., 1999). Chan et al. (2010) estudaram o efeito do dodecilsulfato de sódio e do ultrassom sobre as propriedades físico-químicas de amidos de milho, batata, feijão mungo e sagu, reportando que o ultrassom produz mudanças na superfície do grão, fazendo-a mais rugosa e gerando fissuras. A combinação do ultrassom e do SDS aumenta o conteúdo de amilose, o que se atribui ao efeito do SDS removendo proteínas da superfície e ao enfraquecimento da estrutura do grânulo, o que melhora a lixiviação da amilose. No entanto, não se encontrou evidência de formação de complexos com o SDS. A atuação conjunta desses fatores aumenta a solubilidade do amido de milho, feijão e batata, sem aumento da viscosidade e com diminuição da temperatura de pasta. Radhika et al. (2008) estudaram o efeito do SDS sobre a capacidade de formar complexos de inclusão com amido de mandioca. Eles reportaram um aumento no volume de inchamento do complexo à medida que se aumenta a concentração do SDS. O complexo formado tem maior resistência à hidrólise que o amido nativo. Os autores sugeriram que a amilose presente em regiões amorfas forma complexos mais facilmente que a presente em outras regiões do grânulo de amido.

Sievert et al. (1991) reportaram a formação de amido resistente e de complexos de inclusão do tipo V-amilose entre amido comercial Amylomaize VII starch (70 % de amilose) com lisofosfatidilcolina (LPC), lactilato estearoilo de sódio (SSL), lecitina hidroxilada (OHL), os quais observaram que o aumento de tais complexos gera uma diminuição na produção de amido resistente, uma vez que esses complexos competem com as cadeias de amilose que participam na geração do amido resistente. A amilose parece ter uma grande afinidade pelas cadeias de ácidos graxos presentes em alguns lipídeos ou em alguns emulsificantes. O estearoil-2-lactil lactato de sódio, os monoglicerídeos destilados, monoglicerídeos de ácido tartárico diacetil (DATEM), monoglicerídeos etoxilados têm sido usados para a preparação de complexos de inclusão com amido de cevada (42 % de amilose) através do aquecimento de uma dispersão desse amido a 121 °C por uma hora, obtendo-se complexos do tipo V com temperaturas de

fusão de 100 a 112 °C, assim como a formação de amido resistente (SIEVERT; CZUCHAJOWSKA; POMERANZ, 1991). Por sua vez, Conde-Petit et al. (1992) estudaram a formação de complexos de inclusão em amido de batata nativo e pré-gelatinizado, usando como agentes de inclusão monoestearato de glicerila (GMS) e lecitina; observaram que esse último não forma complexos com o amido, enquanto que, o GMS produz complexos insolúveis e induz a gelificação do amido em dispersões a 2%. Chien et al. (1999) estudaram a formação de complexos de inclusão entre o amido de arroz e várias moléculas hóspedes com diferentes polaridades, tais como o ácido láurico (LA), álcool laurílico (LOH), dodecano (DD) e o laurato de metilo (LM), reportando uma temperatura de fusão para os complexos com LA e LOH entre 93 e 96 °C e uma entalpia de 3,0 J/g, enquanto que os complexos produzidos com LM e DD apresentaram uma entalpia de fusão de 1,87 e 1,8 J/g. Por outro lado, as propriedades reológicas apresentadas pelos complexos de LA e LOH mostraram um incremento no módulo elástico (G') durante o aquecimento e preparação dos complexos. Sugeriram que G' e tan δ aumentam à medida que se aumenta a elasticidade do amido produto da formação dos complexos; no caso de tan δ, o aumento poderia ser causado pela incompatibilidade dos componentes do complexo. Kawai et al. (2012) estudaram o efeito do tipo e concentração de ácido graxo sobre as propriedades térmicas e digestibilidade do amido de batata, encontrando que a concentração de ácido graxo reduz o conteúdo de amido hidrolisado e isto se relaciona com o grau de formação de complexos. Tem-se usado, de igual forma, ácidos graxos insaturados como o mirístico, esteárico e palmítico e seus sais, os quais têm sido submetidos a tratamento térmico (Steam jet cooking) 140 °C junto com amido de milho com um conteúdo de amilose de 70%. Porém, tem-se sugerido que existem diferenças nas estruturas dos complexos formados, possivelmente ocasionadas pela massa molecular e pela baixa solubilidade em água dos ácidos graxos usados, ainda que esta deficiência seja corrigida pela alta temperatura mantida durante o processo térmico (FANTA; SHOGREN; SALCH, 1999).

Por outro lado, Zhou et al. (2007) estudaram o efeito da adição de ácido esteárico e linoleico sobre as propriedades térmicas durante o processo de gelatinização de amido de arroz, concluindo que esses não tem nenhuma influência significativa sobre a gelatinização, no entanto, apresentou-se um decréscimo significativo na endoterma de retrogradação comparada com o amido nativo. Os autores sugerem que a dupla ligação presente no ácido linoleico dificulta a formação dos complexos.

Ácidos graxos insaturados como o oleico e o linoleico podem formar complexos de inclusão com o amido de sorgo e a proteína isolada de soro de leite. A interação da amilose com esse tipo de proteínas tem sido sugerida para a preparação de complexos ternários, os quais seriam formados por dois elementos estruturais: um criado pela relação entre o ácido graxo-amido e o outro formado pela interação ácido graxo-proteína, sendo as ligações dissulfeto da proteína uma peça importante na composição estrutural do complexo ternário formado (ZHANG; MALADEN; HAMAKER, 2003).

Como foi indicado anteriormente, os complexos com ciclodextrinas têm sido propostos como alternativa para melhorar a solubilidade de algumas moléculas insolúveis, porém, nos complexos de inclusão formados a partir de ácido linoleico conjugado (CLA) com amilose e os formados a partir de β-ciclodextrinas, tem sido constatado um maior rendimento de encapsulação das ciclodextrinas em comparação à amilose. No entanto, a amilose mostrou ter uma melhor proteção antioxidante devido à maior interação entre sua estrutura e o CLA (YANG; ZHENGBIAO; ZHANG, 2009).

Heinemann et al. (2005) estudaram os complexos formados entre o amido de batata e a δ-dodecalactona, γ-nonalactona e geraniol, mostrando a resistência dos complexos ao ataque pela α-amilase da boca e a rápida liberação no TGI. Do mesmo modo, Lafargeet al. (2008) estudaram a cinética de liberação de geraniol e do acetato de isoamila em matrizes de amido nativo. Concluíram que a perda de aroma no caso do geraniol é controlada pela interação com o amido. No entanto, o acetato de isoamila não formou complexos de inclusão. Similarmente, na preparação de massas de bolo é possível obter complexos de inclusão como os encontrados no sistema bicomponente aroma-amilose (POZO-BAYON et al., 2008). Cabe ressaltar que a solubilidade em água da molécula que se quer complexar tem um papel importante na preparação de complexos com alguns flavors: aqueles com maior solubilidade terão rendimento maior. No entanto, tem-se encontrado que a presença de lipídeos nativos nos amidos pode melhorar a eficiência de encapsulação de flavors de baixa solubilidade, formando complexos ternários (TAPANAPUNNITIKUL et al., 2008). ZHU e WANG (2013) reportaram a produção de complexos de inclusão entre o amido de trigo modificado química e enzimaticamente com alto teor de amilose e o α-naftol. A caracterização por difração de raios-X indicou que a modificação do amido tem pouca influência sobre o padrão de difração do complexo. A modificação química produz complexos com baixa faixa de termoestabilidade e temperatura de recristalização. As propriedades reológicas do amido

foram afetadas pela formação do complexo, ainda que isto dependa do tipo de modificação.

Outras moléculas de interesse como a genisteína e os polifenóis têm sido encapsuladas por meio de complexos de inclusão. COHEN et al. (2008) reportaram a preparação desses complexos com amilose de batata e amido de milho com alto teor de amilose, ressaltando que os complexos preparados a partir de amilose foram capazes de encapsular uma maior quantidade de genisteína com boa estabilidade sob condições simuladas do estômago, a diferentes valores de pH, e temperatura de 30 e 50 °C, porém, baixa estabilidade a 80 °C. Num trabalho posterior, Cohen et al. (2011) estudaram o efeito da formação de complexos entre a genisteína e amido de batata. Reportaram que tais complexos têm um tempo de trânsito pelo intestino similar àquele encontrado nos alimentos e sua concentração no plasma foi duas vezes mais alta que a do controle. A concentração na urina foi alta, mas baixa nas fezes, o que indica a efetividade dos complexos da amilose no incremento da biodisponibilidade da genisteína. No caso dos polifenóis, Chai et al., (2013a) estudaram a digestão dos complexos formados com amido com alto conteúdo de amilose (>70%), mostrando sua baixa digestão e uma alta e moderada resposta glicêmica. Os autores sugerem que a interação entre os polifenóis e a amilose provocou um aumento do raio hidrodinâmico das moléculas de amilose, assim como uma diminuição na viscosidade e no módulo elástico G' dos géis, interrompendo o processo normal de cristalização da amilose e produzindo um complexo com uma estrutura de baixa cristalinidade.

Algumas outras moléculas cujo uso em alimentos é restringido têm sido encapsuladas em forma de complexos de inclusão, como é o caso de hidrocarbonetos alifáticos e aromáticos e δ- e γ–lactonas. Polazek et al. (2000) compararam a capacidade de formar complexos de inclusão dos amidos de batata, milho, e mandioca com hidrocarbonetos alifáticos e aromáticos, concluindo que a quantidade de complexo formado depende de sua variedade e é o amido de milho o que possui a maior capacidade de inclusão. Destacaram, ainda, que os hidrocarbonetos menos polares e particularmente os aromáticos foram complexados mais facilmente. Cheetham e Tao (1998) reportaram que o teor de água em misturas binárias de dimetilsulfóxido/água afetam as conformações da amilose, já que diminuem as ligações de hidrogênio. Abaixo da concentração de 66,6% em DMSO a conformação helicoidal perde-se progressivamente à medida que se adiciona água. Heinemann et al. (2001) estudaram os complexos de inclusão de amido de batata e

δ e γ–lactonas mediante titulação amperométrica, DSC e difração de raios-X, encontrando que as lactonas de cadeia curta (< 5 carbonos) têm pouca capacidade para formar esses complexos, e que sua estabilidade térmica incrementa-se à medida que a cadeia aumenta.

Também têm sido encapsulados ácidos como o láctico e o clorogênico em amido de batata. HONG et al., (2012) estudaram a encapsulação de ácido láctico por meio de extrusão durante a preparação de embutidos. Apresentou-se uma leve mudança no tamanho de partícula produto da formação dos complexos e da pressão de extrusão. LORENTZ et al. (2012) desenvolveram uma metodologia para encapsular ácido clorogênico submetendo-o a uma reação de lipofilização, que permite sua interação com a amilose. Os complexos formados apresentaram uma baixa temperatura de fusão (80 °C), causada provavelmente por sua baixa cristalinidade.

1.2.3.3 Avaliação da microencapsulação com e sem complexação

A avaliação da microencapsulação pode ser realizada através da verificação da formação de complexos e medindo a capacidade que estes têm para resistir às condições de preparação e consumo. A caracterização dos complexos formados pela amilose e o tipo de estrutura cristalina do complexo de inclusão podem ser estabelecidos por difração de raios-X, o que permite concluir sobre a conformação da hélice de amilose. A calorimetria exploratória diferencial, assim como a reologia, permitem estabelecer as temperaturas de fusão de tais complexos e o efeito do alinhamento das cadeias de amilose durante sua preparação a nível macroscópico (LE BAIL; RONDEAU; BULÉON, 2005; CONDE-PETIT; ESCHER; NUESSLI, 2006). Por outro lado, para avaliar a matriz encapsulante e sua capacidade de liberação são realizados ensaios *in vitro*, que buscam simular as condições ambientais à que se submete a molécula hóspede em seu caminho pelo TGI. O que se pretende com esse tipo de ensaio é estudar as mudanças provocadas sobre a matriz encapsulante ou sobre a molécula de interesse diante das mudanças de pH, ação enzimática, sais biliares e temperatura similares às do sistema digestivo (MCCLEMENTS; LI, 2010).

Finalmente, destaca-se que a bixina pode formar complexos de inclusão com a α-ciclodextrina (α-CD) (LYNG; PASSOS; FONTANA, 2005b) ou com a β-ciclodextrina (MARCOLINO et al., 2011). Devido à similaridade entre a cavidade hidrofóbica da amilose e as ciclodextrinas é razoável considerar a possibilidade de formação de

complexos do tipo V entre a amilose e a bixina, no entanto, é importante considerar o tamanho da molécula de bixina como um fator relevante na formação de complexos de inclusão.

1.3 Aerogéis, criogéis e xerogéis

Esses materiais são caracterizados por sua porosidade, grande área superficial, baixa densidade e condutividade térmica, e são produzidos a partir do intercâmbio do solvente presente no gel por ar (GAUTHIER et al., 2004). Seu processamento começa com a formação de um hidrogel a partir de uma solução aquosa. Isso é realizado através de um processo físico ou químico, pela adição de agente reticulante ou pela modificação do pH ou da temperatura. A seguir, realiza-se a substituição da água presente na estrutura do hidrogel por um solvente, geralmente um álcool, até formar o alcoolgel correspondente. Finalmente o álcool, comumente etanol, é extraído do alcoolgel por alguma metodologia de extração ou secagem (GARCÍA-GONZÁLEZ; ALNAIEF; SMIRNOVA, 2011). A estrutura porosa é produzida durante o processo de secagem, o que é realizado por liofilização para formar os denominados criogéis, sob pressão atmosférica para obter xerogel, ou com dióxido de carbono em estado supercrítico ($scCO_2$) para formar os aerogéis (GLENN; IRVING, 1995; JOB et al., 2006; HOEPFNER; RATKE; MILOW, 2008; COMIN; TEMELLI; SALDAÑA, 2012; DE MARCO et al., 2015). Contudo, o esforço e a tensão superficial a nível capilar produzidos durante o processo de secagem, pode gerar o colapso da estrutura porosa, tornando este fenômeno em um dos principais desafios para sua produção. Nesse sentido, alguns trabalhos têm-se focado em diminuir as forças capilares e melhorar as propriedades mecânicas. Tem-se reportado o aumento do esforço à compressão de aerogéis preparados a partir de alginato com N,N-metilenobisacrilamida e carboximetilcelulose, conseguindo-se gerar fortes interações entre a matriz de alginato e os agentes de reforço; tem-se proposto o uso de surfactantes na busca de diminuir a tensão superficial entre o solvente e o material sólido (CHENG et al., 2012; GARCÍA-GONZÁLEZ et al., 2012).

Esses materiais têm atraído a atenção dos investigadores por sua potencial aplicação em várias áreas da ciência. Regularmente são produzidos a partir de materiais inorgânicos como o dióxido de silício (SiO_2), ou orgânicos como o carbono, resorcinol-formaldeído, alginatos, celulose, quitosana, ágar (TSIOPTSIAS; PANAYIOTOU, 2008; AALTONEN; JAUHIAINEN, 2009; BROWN et al., 2010; LIEBNER et al., 2010;

GRANSTRÖM et al., 2011; AGULHON et al., 2012; KUMAR; VINJAMUR; MUKHOPADHYAY, 2013; LIU et al., 2014). Embora o amido seja abundante, este não tem sido amplamente estudado como matéria prima para a formação desse tipo de materiais em comparação com o alginato e/ou com a celulose, ainda que alguns trabalhos tenham sido publicados, usando como metodologia de secagem o $scCO_2$, a carbonização e a liofilização (SVAGAN; SAMIR; BERGLUND, 2008; MEHLING et al., 2009; CHANG; CHEN; JIAO, 2010; SALAM et al., 2011; GARCÍA-GONZÁLEZ et al., 2012).

Sob o ponto de vista do processo de secagem, a extração do solvente com CO_2 supercrítico ($scCO_2$) tem sido considerada como a técnica que gera o menor impacto sobre o encolhimento e deformação dos poros (LIEBNER et al., 2010; GARCÍA-GONZÁLEZ; ALNAIEF; SMIRNOVA, 2011). No entanto, essa tecnologia tem limitações para atingir as condições supercríticas de forma segura e barata, já que se requer equipamentos com resistência às altas pressões (GAUTHIER et al., 2004). Xerogéis, criogéis e aerogéis têm ganhado interesse na indústria e como uma ferramenta para a microencapsulação de compostos bioativos (GLENN; IRVING, 1995; JOB et al., 2006; HOEPFNER; RATKE; MILOW, 2008; COMIN; TEMELLI; SALDAÑA, 2012; DE MARCO et al., 2015). Tem sido demostrado com sucesso o uso de aerogéis de sílica como sistemas de liberação (SMIRNOVA; MAMIC; ARLT, 2003). No entanto, esses sistemas de liberação têm problemas de biodegradabilidade comparados com matrizes tais como as de polissacarídeos. Por essa razão, os biopolímeros têm se tornado matrizes com potencial de carga de compostos bioativos. Esferas de alginato têm sido usadas como carreadores para a microencapsulação de medicamentos como ibuprofeno, paracetamol, cetoprofeno, e ácido benzoico, a quantidade de material carregado dentro da matriz depende da estrutura e composição do aerogel (HUANG; YUAN; CHEN, 2008; MEHLING et al., 2009; GARCÍA-GONZÁLEZ et al., 2015). Características dos aerogéis com possibilidade de ser usados na indústria alimentar, preparados a partir de polissacarídeos de derivados marinhos e plantas foram reportadas por MIKKONEN et al. (2013), mostrando as grandes vantagens desses materiais.

Os amidos são outra matéria prima biodegradável, os quais são considerados seguros para ser usados no desenvolvimento de matrizes e coberturas de compostos bioativos (LALUSH et al., 2005a). Como já foi mencionado, a amilose presente no grânulo de amido forma complexos de inclusão com compostos hidrofóbicos e, por esta característica, tem sido usada para a preparação de complexos com lipídeos, ácidos graxos

como o palmítico, oleico e linoleico e alguns saborizantes (WULFF; AVGENAKI; GUZMANN, 2005a; ABU-HARDAN; HILL; FARHAT, 2007; ITTHISOPONKUL et al., 2007; RADHIKA; MOORTHY, 2008). Estudos sobre aerogéis, xerogéis e criogéis preparados com amido têm sido reportados (SVAGAN; SAMIR; BERGLUND, 2008; MEHLING et al., 2009; CHANG; CHEN; JIAO, 2010; SALAM et al., 2011). Especificamente, amido com alto conteúdo de amilose foi usado para preparação de microesferas porosas no controle de ácaros parasitas em colônias de abelhas (GLENN et al., 2010a). Recentemente foram desmostradas as vantagens de preparação de aerogéis simultaneamente com a formação de complexos de inclusão; com palmitato de sódio, através de cozimento a vapor (*steam cooking*). A técnica melhora as características de retrogradação, mostrando que este método é uma alternativa para o desenvolvimento de sistemas de liberação controlada, pois elimina as dificuldades do processo de gelatinização (KENAR et al., 2014).

1.4 Referências bibiográficas

AALTONEN, O.; JAUHIAINEN, O. The preparation of lignocellulosic aerogels from ionic liquid solutions. **Carbohydrate Polymers**, v. 75, n. 1, p. 125–129, 2009.

ABU-HARDAN, M. O.; HILL, S. E.; FARHAT, I. a. A Calorimetric Study of the Interaction between Waxy Maize Starch and Lipid. **Starch - Stärke**, v. 59, n. 5, p. 217–223, maio 2007.

ADES, H.; KESSELMAN, E.; UNGAR, Y.; SHIMONI, E. Complexation with starch for encapsulation and controlled release of menthone and menthol. **LWT - Food Science and Technology**, v. 45, n. 2, p. 277–288, 2012.

AGULHON, P.; ROBITZER, M.; DAVID, L.; QUIGNARD, F. Structural regime identification in ionotropic alginate gels: Influence of the cation nature and alginate structure. **Biomacromolecules**, v. 13, n. 1, p. 215–220, 2012.

AHMED, F.; LI, Y.; FANNING, K.; NETZEL, M.; SCHENK, P. M. Effect of drying, storage temperature and air exposure on astaxanthin stability from Haematococcus pluvialis. **Food Research International**, v. 74, p. 231–236, 2015.

AHUJA, M. Metronidazole loaded carboxymethyl tamarind kernel polysaccharide-polyvinyl alcohol cryogels: Preparation and characterization. **International Journal of Biological Macromolecules**, v. 72, p. 931–938, 2015.

AMRI, A., CHAUMEIL, J. C.; SFAR, S.; CHARRUEAU, C. Administration of resveratrol: What formulation solutions to bioavailability limitations? **Journal of Controlled Release**, v. 158, p. 182–193, 2012.

ANSARI, K. a; VAVIA, P. R.; TROTTA, F.; CAVALLI, R. Cyclodextrin-based nanosponges for delivery of resveratrol: in vitro characterisation, stability, cytotoxicity and permeation study. **AAPS PharmSciTech**, v. 12, n. 1, p. 279–86, mar. 2011.

AOKI, T.; DECKER, E. a.; MCCLEMENTS, D. J. Influence of environmental stresses on stability of O/W emulsions containing droplets stabilized by multilayered membranes produced by a layer-by-layer electrostatic deposition technique. **Food Hydrocolloids**, v. 19, n. 2, p. 209–220, mar. 2005.

BELITZ, H.; GROSCH, W.; SCHIEBER LE, P. **Lipids. In Food Chemistry**. 4th ed ed. Berlin: Springer, 2009.

BHANDARI, B. R.; ARCY, B. R. D.; LE, L.; BICH, T. Lemon Oil to B-Cyclodextrin Ratio Effect on the Inclusion Efficiency of B-Cyclodextrin and the Retention of Oil Volatiles in the Complex. **Analysis**, v. 8561, n. 97, p. 1494–1499, 1998.

BILIADERIS, C. G.; GALLOWAY, G. Crystallization behavior of amylose-v complexes: structure-property relationships. **Carbahydrate Research**, v. 189, p. 31–48, 1989.

BILIADERIS, C. G.; TONOGAI, J. R. Influence of lipids on the thermal and mechanical-properties of concentrated starch gels. **Journal of Agricultural and Food Chemistry**, v. 39, p. 833–840, 1991.

BOSCHETTO, D. L.; LOSS, R. A.; PEREIRA, G. N.; AGUIAR, G. S. P.; MACHADO, J. R.; CHAVES, L. M. P. C.; SILVA, M. J. A.; OLIVEIRA, D.; OLIVEIRA, J. V.

Encapsulation of eugenyl acetate in PHBV using SEDS technique and in vitro release evaluation. **Journal of Food Science and Technology**, v. 53, n. 10, p. 3859–3864, 2014.

BRAITHWAITE, M. C.; TYAGI, C.; TOMAR, L. K.; KUMAR, P.; CHOONARA, Y. E.; PILLAY, V. Nutraceutical-based therapeutics and formulation strategies augmenting their efficiency to complement modern medicine: An overview. **Journal of Functional Foods**, p. 1–18, out. 2013.

BROWN, Z. K.; FRYER, P. J.; NORTON, I. T.; BRIDSON, R. H. Drying of agar gels using supercritical carbon dioxide. **Journal of Supercritical Fluids**, v. 54, n. 1, p. 89–95, 2010.

BULÉON, A.; DELAGE, M.; BRISSON, J.; CHANZY, H. Single crystals of V amylose complexed with isopropanol and acetone. **Int. J. Biol. Macromol**, v. 12, p. 25–33, 1990.

BULÉON, A.; VÉRONÈSE, G.; PUTAUX, J. L. Self-association and crystallization of amylose. **Australian Journal of Chemistry**, v. 60, n. 10, p. 706–718, 2007.

CHAI, Y.; WANG, M.; ZHANG, G. Interaction between Amylose and Tea Polyphenols Modulates the Postprandial Glycemic Response to High-Amylose Maize Starch. **Agricultural and Food Chemestry**, 2013.

CHAN, H.-T.; BHAT, R.; KARIM, A. Effects of sodium dodecyl sulphate and sonication treatment on physicochemical properties of starch. **Food Chemistry**, v. 120, n. 3, p. 703–709, 2010.

CHANG, X.; CHEN, D.; JIAO, X. Starch-derived carbon aerogels with high-performance for sorption of cationic dyes. **Polymer**, v. 51, n. 16, p. 3801–3807, 2010.

CHEETHAM, N. W. H.; TAO, L. Amylose conformational transitions in binary DMSO/water mixtures. **Carbohydrate Polymers**, v. 35, p. 287–295, 1998.

CHENG, Y.; LU, L.; ZHANG, W.; SHI, J.; CAO, Y. Reinforced low density alginate-based aerogels: Preparation, hydrophobic modification and characterization. **Carbohydrate Polymers**, v. 88, n. 3, p. 1093–1099, 2012.

CHEUK, S. Y.; SHIH, F. F.; CHAMPAGNE, E. T.; DAIGLE, K. W.; PATINDOL, J. A.; MATTISON, C. P.; BOUE, S. M. Nano-encapsulation of coenzyme Q10 using octenyl succinic anhydride modified starch. **Food Chemistry**, v. 174, p. 585–590, 2015.

CHIEN, J. T.; LIEN, Y. Y.; SHOEMAKER, C. F. Effect of polarity of complexing agents on thermal and rheological properties of rice starch gels. **Cereal Chemistry**, v. 76, n. 6, p. 837–842, 1999.

CHIN, S. F.; YASID AKMARMOHD, S. N.; PANG, S. C. Preparation and characterization of starch nanoparticles for Release of Curcumin. **International Journal of Polymer Science**, v. 2014, p. 292–295, 2014.

COHEN, R.; ORLOVA, Y.; KOVALEV, M.; UNGAR, Y.; SHIMONI, E. Structural and functional properties of amylose complexes with genistein. **Journal of Agricultural and Food Chemistry**, v. 56, p. 4212–4218, 2008.

COHEN, R.; SCHWARTZ, B.; PERI, I.; SHIMONI, E. Improving bioavailability and stability of genistein by complexation with high-amylose corn starch. **Journal of Agricultural and Food Chemistry**, v. 59, p. 7932–7938, 2011.

COMIN, L. M.; TEMELLI, F.; SALDAÑA, M. D. a. Barley beta-glucan aerogels via

supercritical CO2 drying. **Food Research International**, v. 48, n. 2, p. 442–448, 2012.

CONDE-PETIT, B.; ESCHER, F. Gelation of low concentration starch systems induced by starch emulsifier complexation. **Food Hydrocolloids**, v. 6, n. 2, p. 223–229, 1992.

CONDE-PETIT, B.; ESCHER, F.; NUESSLI, J. Structural features of starch-flavor complexation in food model systems. **Trends in Food Science and Technology**, v. 17, n. 5, p. 227–235, 2006.

COPELAND, L.; BLAZEK, J.; SALMAN, H.; TANG, M. C. Form and functionality of starch. **Food Hydrocolloids**, v. 23, n. 6, p. 1527–1534, 2009.

CORTÉS, R. N. F.; MARTÍNEZ, M. G.; GUZMÁN, I. V.; LLANO, S. L. A.; GROSSO, C. R. F.; BUSTOS, F. M. Evaluation of modified amaranth starch as shell material for encapsulation of probiotics. **Cereal Chemistry**, v. 91, n. 3, p. 300–308, 2014.

DE MARCO, I.; BALDINO, L.; CARDEA, S.; REVERCHON, E. Supercritical Gel Drying for the Production of Starch Aerogels for Delivery Systems. **Chemical Engineering Transactions**, v. 43, p. 307–312, 2015.

DE PAZ, E.; MARTÍN, Á.; COCERO, M. J. Production of water-soluble b-carotene formulations by high pressure processes. **III Iberoamerican Conference on Supercritical Fluids**, n. 2008, p. 1–6, 2013.

DE PILLI, T.; DEROSSI, A.; TALJA, R. a.; JOUPPILA, K.; SEVERINI, C. Study of starch-lipid complexes in model system and real food produced using extrusion-cooking technology. **Innovative Food Science & Emerging Technologies**, v. 12, n. 4, p. 610–616, out. 2011.

DELADINO, L.; TEIXEIRA, A. S.; NAVARRO, A. S.; ALVAREZ, I.; MOLINA-GARCÍA, A. D.; MARTINO, M. Corn starch systems as carriers for yerba mate (Ilex paraguariensis) antioxidants. **Food and Bioproducts Processing**, v. 94, n. July, p. 463–472, 2015.

FANTA, G.; SHOGREN, R.; SALCH, J. Steam jet cooking of high-amylose starch–fatty acid mixtures. An investigation of complex formation. **Carbohydrate Polymers**, v. 38, p. 1–6, 1999.

FATHI, M.; MARTÍN, Á.; MCCLEMENTS, D. J. Nanoencapsulation of food ingredients using carbohydrate based delivery systems. **Trends in Food Science and Technology**, v. 39, n. 1, p. 18–39, 2014.

GARCÍA-GONZÁLEZ, C. a.; ALNAIEF, M.; SMIRNOVA, I. Polysaccharide-based aerogels - Promising biodegradable carriers for drug delivery systems. **Carbohydrate Polymers**, v. 86, n. 4, p. 1425–1438, 2011.

GARCÍA-GONZÁLEZ, C. A.; CAMINO-REY, M. C.; ALNAIEF, M.; ZETZL, C.; SMIRNOVA, I. The Journal of Supercritical Fluids Supercritical drying of aerogels using CO2 : Effect of extraction time on the end material textural properties. **The Journal of Supercritical Fluids**, v. 66, p. 297–306, 2012.

GARCÍA-GONZÁLEZ, C. a.; JIN, M.; GERTH, J.; ALVAREZ-LORENZO, C.; SMIRNOVA, I. Polysaccharide-based aerogel microspheres for oral drug delivery. **Carbohydrate Polymers**, v. 117, p. 797–806, 2015.

GARCÍA-TEJEDA, Y. V.; SALINAS-MORENO, Y.; HERNÁNDEZ-MARTÍNEZ, Á.

R.; MARTÍNEZ-BUSTOS, F. Encapsulation of purple maize anthocyanins in phosphorylated starch by spray drying. **Cereal Chemistry**, v. 93, n. 2, p. 130–137, 2016.

GARCÍA, M.; MARTINO, M.; ZARITZKY, N. Comparison of Amylose Enrichment Procedure for Food Applications. **Carbohydrate.**, v. 72, n. 6, p. 552–558, 1995.

GAUTHIER, B. M.; BAKRANIA, S. D.; ANDERSON, A. M.; CARROLL, M. K. A fast supercritical extraction technique for aerogel fabrication. **Journal of Non-Crystalline Solids**, v. 350, p. 238–243, 2004.

GLENN, G. M.; IRVING, D. W. Starch-Based Microcellular Foams. **American Association of Cereal Chemists**, v. 72, n. 2, p. 155–161, 1995.

GLENN, G. M.; KLAMCZYNSKI, A. P.; WOODS, D. F.; CHIOU, B.; ORTS, W. J.; IMAM, S. H. Encapsulation of Plant Oils in Porous Starch Microspheres. **Journal of Agricultural and Food Chemistry**, v. 58, n. 7, p. 4180–4184, 2010.

GODET, M. C.; BIZOT, H.; BULÉON, A. Crystallization of amylose-fatty acid complexes prepared with different amylose chain lengths. **Carbohydrate Polymer**, v. 1, n. 27, p. 47–52, 1995.

GONNET, M.; LETHUAUT, L.; BOURY, F. New trends in encapsulation of liposoluble vitamins. **Journal of controlled release: official journal of the Controlled Release Society**, v. 146, n. 3, p. 276–90, 15 set. 2010.

GRANSTRÖM, M.; NÉE PÄÄKKÖ, M. K.; JIN, H.; KOLEHMAINEN, E.; KILPELÄINEN, I.; IKKALA, O. Highly water repellent aerogels based on cellulose stearoyl esters. **Polymer Chemistry**, v. 2, n. 8, p. 1789, 2011.

HAN, L.; LI, L.; LIU, G.; LI, B. Starch stearate as a novel encapsulation wall material and its effect on oil-water interfacial tension. **Journal of controlled release: official journal of the Controlled Release Society**, v. 152 Suppl, n. 2011, p. e226-7, 2011.

HAN, S.; CHOI, S. H.; KIM, W.; KIM, B. Y.; BAIK, M. Y. Infusion of catechin into native corn starch granules for drug and nutrient delivery systems. **Food Science and Biotechnology**, v. 24, n. 6, p. 2035–2040, 2015.

HASANVAND, E.; FATHI, M.; BASSIRI, A.; JAVANMARD, M.; ABBASZADEH, R. Novel starch based nanocarrier for Vitamin D fortification of milk: Production and characterization. **Food and Bioproducts Processing**, v. 96, p. 264–277, 2015.

HEINEMANN, C.; CONDE-PETIT, B.; NUESSLI, J.; ESCHER, F. Evidence of starch inclusion complexation with lactones. **Journal of Agricultural and Food Chemistry**, v. 49, n. 3, p. 1370–1376, 2001.

HEINEMANN, C.; ZINSLI, M.; RENGGLI, A.; ESCHER, F.; CONDE-PETIT, B. Influence of amylose-flavor complexation on build-up and breakdown of starch structures in aqueous food model systems. **LWT - Food Science and Technology**, v. 38, p. 885–894, 2005.

HELBERT, W.; CHANZY, H. Single crystals of V amylose complexed with n-butanol or n-pentanol: Structural features and properties. **International Journal of Biological Macromolecules**, v. 16, n. 4, p. 207–213, 1994.

HOEPFNER, S.; RATKE, L.; MILOW, B. Synthesis and characterisation of nanofibrillar cellulose aerogels. **Cellulose**, v. 15, n. 1, p. 121–129, 2008.

HONG, G. P.; LEE, Y. S.; BAEK, J. Y.; CHOI, M. J. Encapsulation of lactic acid in starch by extrusion forusing as pH regulated binder of meat products. **Korean Journal for Food Science of Animal Resources**, v. 32, n. 2, p. 155–161, 2012.

HUANG, H.-J.; YUAN, W.-K.; CHEN, X. D. Microencapsulation Based on Emulsification for Producing Pharmaceutical Products: A Literature Review. **Developments in Chemical Engineering and Mineral Processing**, v. 14, n. 3–4, p. 515–544, 2008.

ITTHISOPONKUL, T.; MITCHELL, J. R.; TAYLOR, A. J.; FARHAT, I. a. Inclusion complexes of tapioca starch with flavour compounds. **Carbohydrate Polymers**, v. 69, n. 1, p. 106–115, 1 maio 2007.

JAIN, A.; THAKUR, D.; GHOSHAL, G.; KATARE, O. P.; SHIVHARE, U. S. Characterization of microcapsulated β-carotene formed by complex coacervation using casein and gum tragacanth. **International Journal of Biological Macromolecules**, v. 87, p. 101–113, 2016.

JANISZEWSKA-TURAK, E. Carotenoids microencapsulation by spray drying method and supercritical micronization. **Food Research International**, v. 99, p. 891–901, 2017.

JOB, N.; PANARIELLO, F.; MARIEN, J.; CRINE, M.; PIRARD, J. P.; LÉONARD, A. Synthesis optimization of organic xerogels produced from convective air-drying of resorcinol-formaldehyde gels. **Journal of Non-Crystalline Solids**, v. 352, n. 1, p. 24–34, 2006.

KARKALAS, J.; MA, S.; MORRISON, W. R.; PETHRICK, R. a. Some factors determining the thermal properties of amylose inclusion complexes with fatty acids. **Carbohydrate Research**, v. 268, n. 2, p. 233–247, 1995.

KAWAI, K.; TAKATO, S.; SASAKI, T.; KAJIWARA, K. Complex formation, thermal properties, and in-vitro digestibility of gelatinized potato starch e fatty acid mixtures. **Food hydrocolloids**, v. 27, n. 1, p. 228–234, 2012.

KENAR, J. A.; ELLER, F. J.; FELKER, F. C.; JACKSON, A.; FANTA, G. F. complexes prepared from high amylose starch and sodium palmitate. **Green Chem**, v. 16, p. 1921–1930, 2014.

KIM, J.; SEO, T.; LIM, S. Preparation of aqueous dispersion of b-carotene nano-composites through complex formation with starch dextrin. **Food hydrocolloids**, v. 33, n. 2, p. 256–263, 2013.

KUMAR, R. S.; VINJAMUR, M.; MUKHOPADHYAY, M. A Simple Process to Prepare Silica Aerogel Microparticles from Rice Husk Ash. **International Journal of Chemical Engineering and Applications**, v. 4, n. 5, p. 321–325, 2013.

LAFARGE, C.; BARD, M. H.; BREUVART, a.; DOUBLIER, J. L.; CAYOT, N. Influence of the structure of cornstarch dispersions on kinetics of aroma release. **Journal of Food Science**, v. 73, n. 2, 2008.

LALUSH, I.; BAR, H.; ZAKARIA, I.; EICHLER, S.; SHIMONI, E. Utilization of amylose-lipid complexes as molecular nanocapsules for conjugated linoleic acid. **Biomacromolecules**, v. 6, n. 1, p. 121–130, 2005.

LE BAIL, P.; CHAUVET, B.; SIMONIN, H.; RONDEAU-MOURO, C.; PONTOIRE, B.; CARVALHO, M. De; LE-BAIL, A. Formation and stability of amylose ligand

complexes formed by high pressure treatment. **Innovative Food Science and Emerging Technologies**, v. 18, p. 1–6, 2013.

LE BAIL, P.; RONDEAU, C.; BULÉON, A. Structural investigation of amylose complexes with small ligands: Helical conformation, crystalline structure and thermostability. **International Journal of Biological Macromolecules**, v. 35, n. 1–2, p. 1–7, 2005.

LESMES, U.; BARCHECHATH, J.; SHIMONI, E. Continuous dual feed homogenization for the production of starch inclusion complexes for controlled release of nutrients. **Innovative Food Science & Emerging Technologies**, v. 9, n. 4, p. 507–515, out. 2008.

LI, B. zheng; WANG, L. jun; LI, D.; CHIU, Y. L.; ZHANG, Z. jie; SHI, J.; CHEN, X. D.; MAO, Z. huai. Physical properties and loading capacity of starch-based microparticles crosslinked with trisodium trimetaphosphate. **Journal of Food Engineering**, v. 92, n. 3, p. 255–260, 2009.

LI, Y.; HU, M.; XIAO, H.; DU, Y.; DECKER, E. A.; MCCLEMENTS, D. J. Controlling the functional performance of emulsion-based delivery systems using multi-component biopolymer coatings. **European journal of pharmaceutics and biopharmaceutics: official journal of Arbeitsgemeinschaft für Pharmazeutische Verfahrenstechnik e.V**, v. 76, n. 1, p. 38–47, set. 2010.

LICHTENTHALER, F.; IMMEL, S. The Hydrophobic Topographies of Amylose and its Blue Iodine. **Starch/Stärke**, v. 52, n. 1, p. 1–8, 2000.

LIEBNER, F.; HAIMER, E.; WENDLAND, M.; NEOUZE, M. A.; SCHLUFTER, K.; MIETHE, P.; HEINZE, T.; POTTHAST, A.; ROSENAU, T. Aerogels from unaltered bacterial cellulose: Application of scCO 2 drying for the preparation of shaped, ultra-lightweight cellulosic aerogels. **Macromolecular Bioscience**, v. 10, n. 4, p. 349–352, 2010.

LIU, J.; WANG, H.; WU, C.; ZHAO, Q.; WANG, X.; YI, L. Preparation and characterization of nanoporous carbon-supported platinum as anode electrocatalyst for direct borohydride fuel cell. **International Journal of Hydrogen Energy**, v. 39, n. 12, p. 6729–6736, 2014.

LOKSUWAN, J. Characteristics of microencapsulated β-carotene formed by spray drying with modified tapioca starch, native tapioca starch and maltodextrin. **Food Hydrocolloids**, v. 21, n. 5–6, p. 928–935, 2007.

LORENTZ, C.; PENCREAC'H, G.; SOULTANI-VIGNERON, S.; RONDEAU-MOURO, C.; DE CARVALHO, M.; PONTOIRE, B.; ERGAN, F.; LE BAIL, P. Coupling lipophilization and amylose complexation to encapsulate chlorogenic acid. **Carbohydrate Polymers**, v. 90, n. 1, p. 152–158, 2012.

LYNG, S. M.; PASSOS, M.; FONTANA, J. D. Bixin and α-cyclodextrin inclusion complex and stability tests. **Process Biochemestry**, v. 40, n. 2, p. 865–872, 2005.

MARCOLINO, V. A.; ZANIN, G. M.; DURRANT, L. R.; BENASSI, M. D. T.; MATIOLI, G. Interaction of curcumin and bixin with β-cyclodextrin: Complexation methods, stability, and applications in food. **Journal of Agricultural and Food Chemistry**, v. 59, n. 7, p. 3348–3357, 2011.

MARQUES, H. M. C. A review on cyclodextrin encapsulation of essential oils and volatiles. **Flavour and Fragrance Journal**, v. 25, n. July, p. 313–326, 2010.

MATALANIS, A.; JONES, O. G.; MCCLEMENTS, D. J. Structured biopolymer-based delivery systems for encapsulation, protection, and release of lipophilic compounds. **Food Hydrocolloids**, v. 25, n. 8, p. 1865–1880, dez. 2011.

MCCLEMENTS, D. J.; LI, Y. Structured emulsion-based delivery systems: controlling the digestion and release of lipophilic food components. **Advances in colloid and interface science**, v. 159, n. 2, p. 213–28, 15 set. 2010.

MEHLING, T.; SMIRNOVA, I.; GUENTHER, U.; NEUBERT, R. H. H. Polysaccharide-based aerogels as drug carriers. **Journal of Non-Crystalline Solids**, v. 355, n. 50–51, p. 2472–2479, 2009.

MENG, S.; MA, Y.; SUN, D.; WANG, L.; LIU, T. Properties of starch-palmitic acid complexes prepared by high pressure homogenization. **Journal of Cereal Science**, v. 59, n. 1, p. 25–32, jan. 2014.

MIKKONEN, K. S.; PARIKKA, K.; GHAFAR, A.; TENKANEN, M. Prospects of polysaccharide aerogels as modern advanced food materials. **Trends in Food Science and Technology**, v. 34, n. 2, p. 124–136, 2013.

MOTTIAR, Y.; ALTOSAAR, I. Iodine sequestration by amylose to combat iodine deficiency disorders. **Trends in Food Science and Technology**, v. 22, n. 6, p. 335–340, 2011.

MUA, J. P.; JACKSON, D. S. Fractionation of Regular Corn Starch: A Comparison of Aqueous Leaching and Aqueous Dispersion Methods. **Carbohydrate.**, v. 72, n. 5, p. 508–511, 1995.

MUN, S.; KIM, Y. R.; SHIN, M.; MCCLEMENTS, D. J. Control of lipid digestion and nutraceutical bioaccessibility using starch-based filled hydrogels: Influence of starch and surfactant type. **Food Hydrocolloids**, v. 44, p. 380–389, 2015.

NACKA, F.; CANSELL, M.; MÉLÉARD, P.; COMBE, N. Incorporation of alpha-tocopherol in marine lipid-based liposomes: in vitro and in vivo studies. **Lipids**, v. 36, n. 12, p. 1313–20, dez. 2001.

NUESSLI, J.; SIGG, B.; CONDE-PETIT, B.; ESCHER, F. Characterization of amylose—flavour complexes by DSC and X-ray diffraction. **Food Hydrocolloids**, v. 11, n. 1, p. 27–34, jan. 1997.

OBIRO, W. C.; SINHA RAY, S.; EMMAMBUX, M. N. V-amylose Structural Characteristics, Methods of Preparation, Significance, and Potential Applications. **Food Reviews International**, v. 28, n. 4, p. 412–438, 2012.

PĂDURARU, O. M.; CIOLACU, D.; DARIE, R. N.; VASILE, C. Synthesis and characterization of polyvinyl alcohol/cellulose cryogels and their testing as carriers for a bioactive component. **Materials Science and Engineering C**, v. 32, n. 8, p. 2508–2515, 2012.

POLACZEK, E.; STARZYK, F.; MALEŃKI, K.; TOMASIK, P. Inclusion complexes of starches with hydrocarbons. **Carbohydrate Polymers**, v. 43, p. 291–297, 2000.

POZO-BAYON, M.; BIAIS, B.; RAMPON, V.; CAYOT, N.; LE BAIL, P. Influence of

complexation between amylose and a flavored model sponge cake on the degree of aroma compound release. **Journal of Agricultural and Food Chemistry**, v. 56, p. 6640–6647, 2008.

PUTAUX, J.-L.; CARDOSO, M. B.; DUPEYRE, D.; MORIN, M.; NULAC, A.; HU, Y. Single Crystals of V-Amylose Inclusion Complexes. **Macromolecular Symposia**, v. 273, n. 1, p. 1–8, nov. 2008.

RADHIKA, G. S.; MOORTHY, S. N. Effect of sodium dodecyl sulphate on the physicochemical, thermal and pasting properties of cassava starch. **Starch/Staerke**, v. 60, p. 87–96, 2008.

RADHIKA, G. S.; SHANAVAS, S.; MOORTHY, S. N. Influence of lipids isolated from soybean seed on different properties of cassava starch. **Starch/Starke**, v. 60, n. 9, p. 485–492, 2008.

ROCHA, G. A.; FÁVARO-TRINDADE, C. S.; GROSSO, C. R. F. Microencapsulation of lycopene by spray drying: Characterization, stability and application of microcapsules. **Food and Bioproducts Processing**, v. 90, n. 1, p. 37–42, 2012.

ROMO-HUALDE, A.; YETANO-CUNCHILLOS, A. I.; GONZÁLEZ-FERRERO, C.; SÁIZ-ABAJO, M. J.; GONZÁLEZ-NAVARRO, C. J. Supercritical fluid extraction and microencapsulation of bioactive compounds from red pepper (Capsicum annum L.) by-products. **Food Chemistry**, v. 133, n. 3, p. 1045–1049, 2012.

RONDEAU-MOURO, C.; LE BAIL, P.; BULÉON, A. Structural investigation of amylose complexes with small ligands: Inter- or intra-helical associations? **International Journal of Biological Macromolecules**, v. 34, n. 5, p. 251–257, 2004.

SALAM, A.; VENDITTI, R. a.; PAWLAK, J. J.; EL-TAHLAWY, K. Crosslinked hemicellulose citrate-chitosan aerogel foams. **Carbohydrate Polymers**, v. 84, n. 4, p. 1221–1229, 2011.

SCHUBERT, M; MÜLLER-GOYMANN, C. . . Characterisation of surface-modified solid lipid nanoparticles (SLN): influence of lecithin and nonionic emulsifier. **European journal of pharmaceutics and biopharmaceutics**, v. 61, n. 1–2, p. 77–86, set. 2005.

SHARIF, H. R.; GOFF, H. D.; MAJEED, H.; SHAMOON, M.; LIU, F.; NSOR-ATINDANA, J.; HAIDER, J.; LIANG, R.; ZHONG, F. Physicochemical properties of β-carotene and eugenol co-encapsulated flax seed oil powders using OSA starches as wall material. **Food Hydrocolloids**, v. 73, p. 274–283, 2017.

SHEN, Q.; QUEK, S. Y. Microencapsulation of astaxanthin with blends of milk protein and fiber by spray drying. **Journal of Food Engineering**, v. 123, p. 165–171, 2014.

SIEVERT, D.; CZUCHAJOWSKA, Z.; POMERANZ, Y. Enzyme-resistant starch. III. X-ray diffraction of autoclaved amylomaize VII starch and enzyme-resistant starch residues. **Cereal Chem**, v. 68, n. 1, p. 86–91, 1991.

SISWOYO, T. A.; MORITA, N. Thermal properties and kinetic parameters of amylose-glycerophosphatidylcholine complexes with various acyl chain lengths. **Food Research International**, v. 35, p. 737–744, 2002.

SMIRNOVA, I.; MAMIC, J.; ARLT, W. Adsorption of drugs on silica aerogels. **Langmuir**, v. 19, n. 20, p. 8521–8525, 2003.

SPADA, J. C.; MARCZAK, L. D. F.; TESSARO, I. C.; NOREÑA, C. P. Z. Microencapsulation of β-carotene using native pinhão starch, modified pinhão starch and gelatin by freeze-drying. **International Journal of Food Science and Technology**, v. 47, n. 1, p. 186–194, 2012.

SVAGAN, A. J.; SAMIR, M. a S. a; BERGLUND, L. a. Biomimetic foams of high mechanical performance based on nanostructured cell walls reinforced by native cellulose nanofibrils. **Advanced Materials**, v. 20, n. 7, p. 1263–1269, 2008.

SWEEDMAN, M. C.; TIZZOTTI, M. J.; SCHÄFER, C.; GILBERT, R. G. Structure and physicochemical properties of octenyl succinic anhydride modified starches: A review. **Carbohydrate Polymers**, v. 92, n. 1, p. 905–920, 2013.

TAPANAPUNNITIKUL, O.; CHAISERI, S.; PETERSON, D. G.; THOMPSON, D. B. Water solubility of flavor compounds influences formation of flavor inclusion complexes from dispersed high-amylose maize starch. **Journal of Agricultural and Food Chemistry**, v. 56, n. 1, p. 220–226, 2008.

TESTER, R. F.; KARKALAS, J.; QI, X. Starch composition, fine structure and architecture. **Journal of Cereal Science**, v. 39, n. 2, p. 151–165, mar. 2004.

TIAN, Y.; ZHU, Y.; BASHARI, M.; HU, X.; XU, X.; JIN, Z. Identification and releasing characteristics of high-amylose corn starch-cinnamaldehyde inclusion complex prepared using ultrasound treatment. **Carbohydrate polymers**, v. 91, n. 2, p. 586–9, 16 jan. 2013.

TONNESEN, H. H.; MÁSSON, M.; LOFTSSON, T. Studies of curcumin and curcuminoids. XXVII. Cyclodextrin complexation: solubility, chemical and photochemical stability. **International journal of pharmaceutics**, v. 244, n. 1–2, p. 127–35, 5 set. 2002.

TSIOPTSIAS, C.; PANAYIOTOU, C. Foaming of chitin hydrogels processed by supercritical carbon dioxide. **Journal of Supercritical Fluids**, v. 47, n. 2, p. 302–308, 2008.

TUFVESSON, F.; WAHLGREN, M.; ELIASSON, A.-C. Formation of amylose-lipid complexes and effects of temperature treatment. Part 2. Fatty acids. **Starch/Stärke**, v. 55, p. 138–149, 2003.

VILLWOCK, V. K.; ELIASSON, A.-C.; SILVERIO, J.; BEMILLER, J. N. Starch-lipid interactions in common, Waxy, ae du, and ae su2 maize starches examined by differential scanning calorimetry. **Cereal Chemistry**, v. 76, n. 2, p. 292–298, 1999.

WANG, S.; CHEN, Y.; LIANG, H.; CHEN, Y.; SHI, M.; WU, J.; LIU, X.; LI, Z.; LIU, B.; YUAN, Q.; LI, Y. Intestine-Specific Delivery of Hydrophobic Bioactives from Oxidized Starch Microspheres with an Enhanced Stability. **Journal of Agricultural and Food Chemistry**, v. 63, n. 39, p. 8669–8675, 2015.

WU, Y.; DU, X.; GE, H.; LV, Z. Preparation of microporous starch by glucoamylase and ultrasound. **Starch/Staerke**, v. 63, n. 4, p. 217–225, 2011.

WULFF, G.; AVGENAKI, G.; GUZMANN, M. S. P. Molecular encapsulation of flavours as helical inclusion complexes of amylose. **Journal of Cereal Science**, v. 41, n. 3, p. 239–249, 2005.

XING, Y.; XU, Q.; MA, Y.; CHE, Z.; CAI, Y.; JIANG, L. Effect of porous starch concentrations on the microbiological characteristics of microencapsulated Lactobacillus

acidophilus. **Food & Function**, v. 5, n. 5, p. 972, 2014.

YANG, Y.; ZHENGBIAO, G. U.; ZHANG, G. Delivery of Bioactive Conjugated Linoleic Acid with Self-Assembled Amylose-CLA Complex. **Journal of Agricultural and Food Chemistry**, v. 57, p. 7125–7130, 2009.

YI, J.; LAM, T. I.; YOKOYAMA, W.; CHENG, L. W.; ZHONG, F. Beta-carotene encapsulated in food protein nanoparticles reduces peroxyl radical oxidation in Caco-2 cells. **Food Hydrocolloids**, v. 43, p. 31–40, 2015.

YU, H.; HUANG, Q. Enhanced in vitro anti-cancer activity of curcumin encapsulated in hydrophobically modified starch. **Food Chemistry**, v. 119, n. 2, p. 669–674, 2010.

YUAN, C.; JIN, Z.; XU, X. Inclusion complex of astaxanthin with hydroxypropyl-β-cyclodextrin: UV, FTIR, (1)H NMR and molecular modeling studies. **Carbohydrate polymers**, v. 89, n. 2, p. 492–6, 20 jun. 2012.

ZABAR, S.; LESMES, U.; KATZ, I.; SHIMONI, E.; BIANCO-PELED, H. Structural characterization of amylose-long chain fatty acid complexes produced via the acidification method. **Food Hydrocolloids**, v. 24, n. 4, p. 347–357, jun. 2010.

ZHANG, B.; HUANG, Q.; LUO, F.; FU, X. Structural characterizations and digestibility of debranched high-amylose maize starch complexed with lauric acid. **Food hydrocolloids**, v. 28, n. 1, p. 174–181, 2012.

ZHANG, G.; MALADEN, M. D.; HAMAKER, B. R. Detection of a novel three component complex consisting of starch, protein, and free fatty acids. **Journal of Agricultural and Food Chemistry**, v. 51, n. 9, p. 2801–2805, 2003.

ZHOU, Z.; ROBARDS, K.; HELLIWELL, S.; BLANCHARD, C. Effect of the addition of fatty acids on rice starch properties. **Food Research International**, v. 40, p. 209–214, 2007.

ZHU., F. Encapsulation and delivery of food ingredients using starch based systems. **Food Chemistry**, v. 229, p. 542–552, 2017.

ZHU, F.; WANG, Y. J. Characterization of modified high-amylose maize starch-alpha-naphthol complexes and their influence on rheological properties of wheat starch. **Food Chemistry**, v. 138, n. 1, p. 256–262, 2013.

CAPÍTULO 2. MICROENCAPSULAÇÃO DE BIXINA EM MATRIZ DE AMIDO ASSISTIDA PELO ULTRASSOM

ULTRASOUND ASSISTED MICROENCAPSULATION OF BIXIN IN STARCH MATRIX

Ezequiel José Pérez-Monterroza[1*], Ana María Chaux-Gutiérrez[1], Célia Maria Landi Franco[1], Vânia Regina Nicoletti[1]

[1] Department of Food Engineering and Technology; São Paulo State University (Unesp), Institute of Biosciences, Humanities and Exact Sciences (Ibilce), Campus São José do Rio Preto; Rua Cristovão Colombo 2265, Zip Code 15054-000 São José do Rio Preto, SP, Brazil.

*Correspondence:

Ezequiel José Pérez-Monterroza

Email: eperez494@gmail.com, ejperezm@unalmed.edu.co

Abstract

The impact of ultrasound treatment on the microencapsulation of bixin using high amylose corn starch was evaluated. The physicochemical interactions were analyzed by X-ray diffractometry, FT-IR spectrometry, oscillatory rheological tests, color, scanning electron microscopy, encapsulated bixin content, and release profile. The effect of ultrasound was investigated at three different power levels (150, 210 and 300 W) and the results obtained from X-ray diffraction and FT-IR spectroscopy indicated the interaction between bixin and amylose. Frequency sweep tests showed a slight frequency dependence of the storage (G') and loss (G") moduli, with G' > G". The sonicated samples showed G' lower than the control, but this increased with storage. Bixin content on the surface varied between 162.2 and 1979.8 μg bixin·g^{-1}, whilst encapsulated bixin contents were of 381.2, 1206.0, 1477.8 and 2042.5 μg bixin·g^{-1}, to control, BC3 (300 W), BC2 (210 W), and BC1 (150 W), respectively. The morphology of sonicated samples showed eroded and irregular surfaces with protrusions probably occasioned by aggregation of amylose molecules. After 150 min the bixin release from samples BC1 and BC2 were 3.0 and 3.8 %, respectively, being lower than that observed in samples BC3 and control, with values of 6.9 and 21.8 %, respectively.

Keywords: annatto, microencapsulation, amylose, physicochemical interactions, release profile

2.1 Introduction

Starch-based systems have gained interest as an alternative for the microencapsulation of ingredients with high nutritional value. Starch is considered as a GRAS and ideal matrix for use in encapsulation of bioactive compounds (LALUSH et al., 2005a). The granule of starch consists of two major types of α-glucans, amylose and amylopectin, which represent approximately 98 % of starch granule dry matter. The amylose content depend on botanical origin; in starches called as waxy, the amylose content is less than 15 %, whereas in the so-called high-amylose starches it is higher than 40 % (TESTER; KARKALAS; QI, 2004). Amylose can complexate with hydrophobic ligands, which are called guest molecules, generating a left-handed single helical conformation. The single helical conformation presents a V-type lattice that can host flavors, lipids, fatty acids as palmitic, oleic, and conjugated linoleic inside the helical cavity (WULFF; AVGENAKI; GUZMANN, 2005a; ABU-HARDAN; HILL; FARHAT, 2007; ITTHISOPONKUL et al., 2007; RADHIKA; SHANAVAS; MOORTHY, 2008; ZABAR et al., 2010). Bixin can form inclusion complexes with α-cyclodextrin (α-CD) (LYNG; PASSOS; FONTANA, 2005b) and, due to the similarity between the hydrophobic helical cavity of amylose with that of α-CD, it is reasonable to consider the possibility of producing amylose-bixin complexes. Nevertheless, the guest molecule size is a relevant factor, as it may hinder the guest inclusion into the amylose helical cavity. Despite Zhu (2015) reported that polyphenols do not form inclusion complex with amylose, non-hydrophobic interactions have been observed between starch and some phenolic compounds, such as ferulic acid and tea polyphenols, which lead to formation of complex structures with different physicochemical properties (CHAI; WANG; ZHANG, 2013b; KARUNARATNE; ZHU, 2016; ZHU., 2017). Sonication is a non-conventional process of microencapsulating bioactive compounds being a thermomechanical method that involves turbulence, high shear, simultaneous heating, and acoustic cavitation. A viscosity decrease accompanied by an increase in swelling capacity, solubility, and pasting temperature has been observed in starchy systems subjected to ultrasound (LIMA; ANDRADE, 2010). Ultrasound treatment induced groove and pores formation on granule surface and slight changes in the crystallinity (HUANG; LI; FU, 2007; ZHU et al., 2012), as well as a decrease in the molecular weight of starch molecules, resulting in the formation of starch nanoparticles. After ultrasound treatment, the diffraction peaks can decrease their intensity or even vanish, depending on the treatment time. However, V-diffraction peak seems not to be

affected (HAAJ et al., 2013). Few studies show the effect of ultrasound on the microencapsulation process. Tian et al. (2013) reported that it is possible to encapsulate cinnamaldehyde using ultrasound at low temperature, delaying the release kinetics of the essential oil.

Carotenoids such as bixin are of great importance in the human diet. Bixin is the main component extracted from annatto seeds and widely used as a natural colorant in the food industry. Bixin is not stable in the presence of oxygen or light and, for this reason, the microencapsulation has become an alternative for improving its stability and decreasing its degradation rate (BARBOSA; BORSARELLI; MERCADANTE, 2005; LYNG; PASSOS; FONTANA, 2005b; PARIZE et al., 2008; DE SOUSA LOBATO et al., 2013). The microencapsulation of bixin was reported by Parize et al. (2008) using chitosan and different solutions of acetic acid. It was also reported by Barbosa et al. (2005) using gum Arabic or maltodextrin as wall materials; in both studies, bixin encapsulation was achieved by spray drying. De Sousa Lobato et al. (2013) studied the formation of bixin nanocapsules by interfacial deposition on preformed poly(ε-caprolactone).

Taking into account the possible protection offered by starch combined with the functional properties of bixin, microencapsulation using starchy matrices could be a tool to expanding the range of new formulations available to the food industry. Thus, following the strategy of formulating controlled-release systems, the current study explores the possibility of bixin microencapsulation and amylose-based microparticles using an ultrasound-assisted route.

2.2 Material and Methods

High-amylose (72 % of amylose, according to manufacturer) corn starch (Hylon VII) was obtained from Ingredion Brasil Ing. Ind. Ltda (Mogi Guaçu, SP, Brazil). Bixin was obtained from BKG (Adicon, Brazil). Sodium hydroxide (NaOH) was supplied by Synth (Diadema, Brazil), hydrochloric acid was provided by Quimis (Diadema, Brazil), and pancreatin was provided by Sigma-Aldrich (St. Louis, MO). Starch suspensions were prepared using deionized water. All chemicals were of analytical grade.

2.2.1 Microencapsulation

Ninety grams of high-amylose corn starch in 2350 g of water were gelatinized at 130 °C for 45 min. Then, 90 g of the gelatinized starch suspension (GS) was mixed with bixin (0.18 g) in 0.01 M KOH solution (50 g) at 60 °C for 1 min. This mixture was subjected to ultrasound treatment at three different power levels (150, 210 and 300 W, 20 kHz) at 78 °C for 45 min in an ultrasonic homogenizer (Omni Ruptor 4000, Omni International, Marietta, USA) equipped with a standard probe 1.9 mm in diameter. The pH was adjusted to 4.7 using 0.01 M HCl solution and the samples BC1 (150 W), BC2 (210 W) and BC3 (300 W) were stored at 47 °C for 12 h. After that, the gels formed were frozen at -18 °C and lyophilized. A control sample, consisting of GS and bixin at the same concentration, was mixed at 60 °C for 45 min without sonication.

2.2.1 X-ray diffraction

X-ray diffraction was carried out with a diffractometer RINT 2000 wide angle Goniometer unit (Rigaku, Tokio, Japan). The diffractometer was operated at a voltage of 45 kV and current of 40 mA. The samples were scanned from 5 to 40° in 2θ, at a rate of $1°{\cdot}min^{-1}$ and step size of 0.1°. The relative crystallinity was calculated based on the relationship between the peak area and total area of the X-ray diffractograms, according to Itthisoponkul et al. (2007), by using the Origin 8 software (Microcal Inc, Northampton, USA). Diffractograms were smoothed and the baseline was corrected. The analyses were carried out in duplicate.

2.2.3 Rheological characterization

Small-amplitude oscillatory rheological tests were carried out in the linear viscoelastic region (5 % strain) using an AR-2000EX rheometer (TA Instruments, Delaware, USA), with geometry of serrated parallel plates (40 mm of diameter), and a gap of 700 μm. Frequency sweep tests were carried out at 25 °C in the range of 0.1 to 10 Hz. Gels were carefully sampled with a metal scoop without disturbing its structure. The effects of complexation process on dynamic rheological properties were studied by measurements of the storage (G') and loss (G") moduli in sonicated samples after adjustment of pH at 4.7 and storage at 47 °C for 12h. The analyses were carried out in duplicate.

2.2.4 FT-IR spectroscopy

Infrared spectra were recorded on spectrophotometer Spectrum One (Perkin-Elmer Corp, Shelton, CT, USA) with attenuated total reflectance accessory with a ZnSe crystal.

Samples were analyzed directly after pressing them on the crystal (80 psi) and FT-IR scanning was conducted at ambient conditions. The resolution was set to 4 cm^{-1} and the operating range was 400 to 4000 cm^{-1}. In all cases, 20 scans per sample were recorded. The data were processed using Origin Pro 8 Software (Microcal Inc, Northampton, USA). The analyses were carried out in duplicate.

2.2.5 Content of bixin on surface and inside of matrix

The surface and encapsulated bixin content were determined according to Lalush et al. (2005a) and Sutter et al. (2007) with modifications. Surface bixin was determined by washing 0.010 g of the complex with 4 mL of acetone in a test tube and shaking in a vortex for 2 min. After sedimentation, the powder was separated and the concentration of bixin in the acetone was measured spectrophotometrically at 457 nm. Encapsulated bixin in the remaining powder was determined by degradation of the complex with pancreatin. The powder was incubated in 4 mL of pancreatin solution at 37 °C for 36 h. Then, bixin was extracted with 7 mL of acetona, centrifuged, filtered and quantified spectrophotometrically at 457 nm. This wavelength was found to correspond to the maximum absorbance of the used bixin, in the spectrum range of 200 to 800 nm. For preparing the pancreatin solution, 0.18 g of pancreatin was dissolved in 20 mL of phosphate buffer 20 mM (pH 7.0) containing NaCl (0.04 % w/w). This solution was centrifuged (9000×g, 10 min), the supernatant was filtered and used for the test. Bixin content in the complex (BC) was calculated for each formulation as μg of bixin per g (RODRIGUEZ-AMAYA, 2001; RAHMALIA et al., 2014). The analyses were carried out in duplicate.

2.2.6 Release profile of bixin in simulated intestinal fluid (SIF)

Determination of the release profile was carried out according to Lesmes et al. (2008) with modification. Samples (0.010 g) were dispersed in 15 mL of simulated intestine fluid (SIF), which was prepared by dissolving 0.18 g of pancreatin in a phosphate buffer solution (20 mM, pH 7.0) containing NaCl (0.04% w/w). This dispersion was centrifuged (9000×g, 10 min) and the supernatant was filtered and used to incubate complexes at 37 °C. At intervals of time (30, 60, 90, 150, 210 and 270 min), aliquots of 1 mL of this dispersion were separated and immediately subjected to bixin extraction with 4 mL of acetone, which was centrifuged and measured spectrophotometrically at 457 nm. The volume taken was replaced with fresh SIF. The analyses were carried out in duplicate.

2.2.7 Color analysis

The color of the freeze-dried samples was determined using a ColorFlex model 45/0 spectrophotometer (Hunterlab, USA) with the D65 illuminant and observer at 10º. The 4.10 version of Universal software was used to determine the absolute values of L^*, a^*, and b^*. The system used for specification of color was CIELAB. Values of L^* (lightness) range between zero (black) and one hundred (white), a^* between -a^* (green) and +a^* (red), and b^* between -b^* (blue) and +b^* (yellow). The chroma (C*), which expresses the degree of intensity or saturation of the color (Eq. 1), and the hue angle (°*hue*), which represents the tonality of the color (Eq. 2), were calculated. The analyses were carried out in triplicate.

$$C^* = \sqrt{(a^*)^2 + (b^*)^2} \quad (1)$$

$$^\circ hue = arctg\left(\frac{b^*}{a^*}\right) \quad (2)$$

2.2.8 Scanning electron microscopy (SEM)

SEM was used to visualize the morphology of samples, which were coated with gold in a sputter under vacuum for 3 min, 2.0 kV. The images were made using a scanning electron microscope (JSM7500F, FEG-MEV JEOL, Germany).

2.3 Results and Discussion

2.3.1 X-ray diffraction

Figure 2.1 shows the diffractograms of sonicated, control, and GS (without ultrasound or bixin) samples, all of them freeze-dried at the same conditions. GS showed two reflections in the Bragg angle at 17° and 22° (2θ), which are characteristic of B-type crystallites; this reflection pattern was due to retrograded amylose (Figure 2.1a) (SIEVERT; CZUCHAJOWSKA; POMERANZ, 1991). The B-type diffraction pattern exhibits a hexagonal arrangement, which is more open than A-type and contains 36 water molecules attached to the double helices (IMBERTY; PEREZ, 1988). A partial disruption of B-type crystallinity was observed in the samples subjected to ultrasound, with a residual reflection at 17° that was present in all the samples. The reflection at 20° (2θ), which was not observed in the control or in the GS is similar with the single helical or V6-type conformation of the amylose. This diffraction pattern was found in complexes formed

between menthone, fatty acids, and flavor and high-amylose corn starch, as well as of amylose complexes formed by decanal and potato amylose, native potato starch and lactones (HEINEMANN et al., 2001; LE BAIL; RONDEAU; BULÉON, 2005; TAPANAPUNNITIKUL et al., 2008; ADES et al., 2012; FELKER et al., 2013).

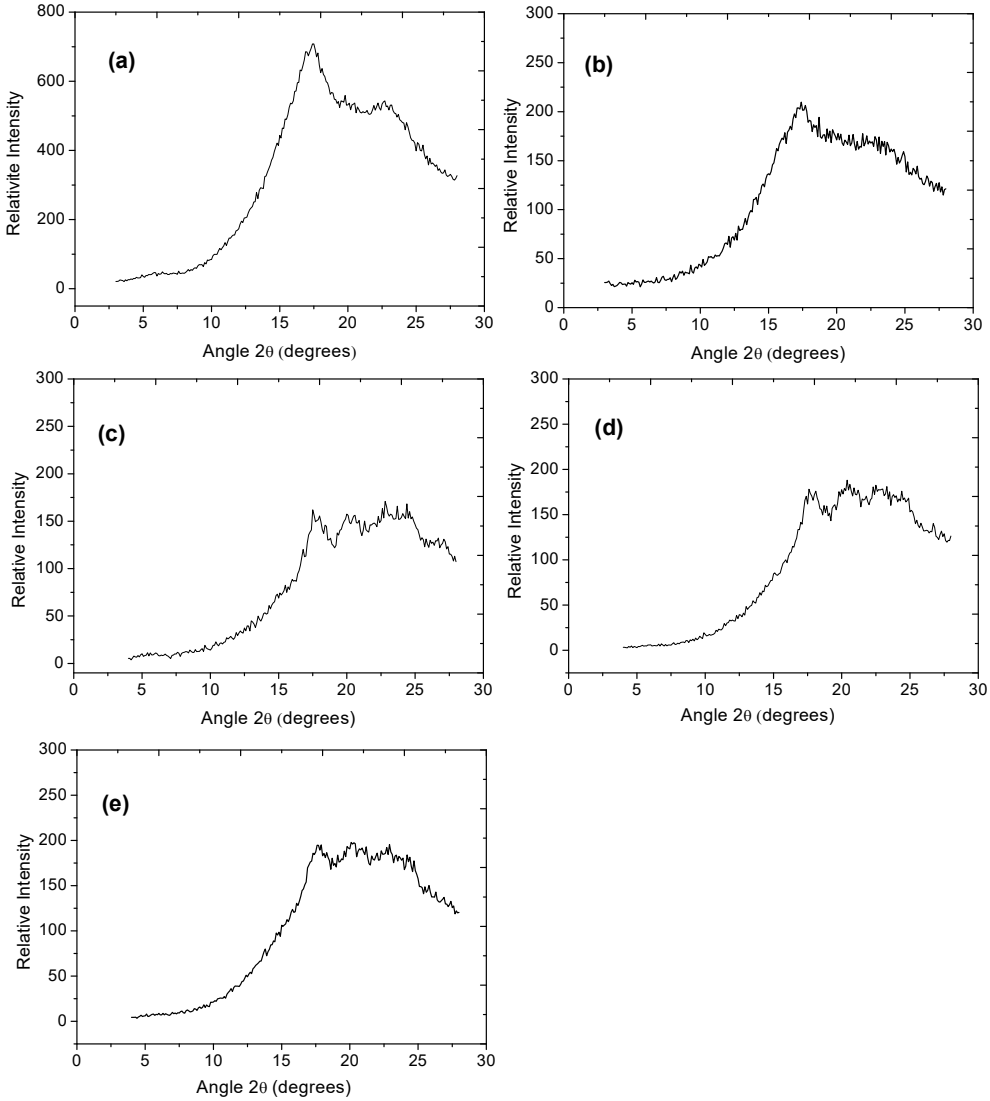

Figure 2.1. X-ray diffraction patterns of high-amylose corn starch gelatinized (GS) (a), GS-B mixture (Control) (b) and sonicated samples BC1 150 W (c), BC2 210 W (d), BC3 300 W (e).

The V6-type complexes are characterized by entrapment of the guest molecule inside of the helical cavity (HEINEMANN; ESCHER; CONDE-PETIT, 2003; RONDEAU-MOURO; LE BAIL; BULÉON, 2004; LALUSH et al., 2005a; BIAIS et al., 2006; ITTHISOPONKUL et al., 2007). Reflections in the Bragg angle close to 22° and

24° (2θ) belong to the double helical conformation of the retrograded amylose (SIEVERT; CZUCHAJOWSKA; POMERANZ, 1991). This retrogradation pattern is caused by the trend of amylose chains to reorganization, due to higher amylose content present in the samples (SINGH et al., 2012).

Table 2.1. Values of relative crystallinity, surface and encapsulated bixin.

Sample	Relative Crystallinity (%)	Bixin on surface (μg bixin·g^{-1})	Encapsulated bixin (μg bixin·g^{-1})
BC1	24.9 ± 1.4 ^{a}	162.2 ± 4.5 ^{d}	2042.5 ± 12.0 ^{a}
BC2	22.0 ± 1.2 ^{a}	2077.4 ± 46.1 ^{a}	1477.8 ± 5.4 ^{b}
BC3	22.9 ± 0.5 ^{a}	1861.6 ± 4.7 ^{c}	1206.0 ± 16.9 ^{c}
Control	14.8 ± 0.6 ^{b}	1979.8 ± 5.9 ^{b}	381.2 ± 5.4 ^{d}
GS	13.5 ± 0.1 ^{b}	-	-

Mean value ± Standard deviation. Means with the same letter in the same column indicate no significant difference by Tukey's test (P< 0.05).

Amini and Razavi (2015) and Zhu et al. (2012) reported that ultrasound treatment does not induce change in the percentage of crystallinity of corn and potato starch granules. Other authors reported changes in the crystalline region, which depends on the ultrasound frequency and its preferential degradation of the amorphous region (HUANG; LI; FU, 2007; ZHENG et al., 2013). In this study, a decrease in peak intensity of sonicated samples was observed compared with gelatinized starch (GS). In addition, a decreasing in peak intensity at 17 ° (2θ) associated with B-type was observed, at the same time that the peak intensity at 20° (2θ) increased. The appearance of reflection at 20° (2θ) suggested reordering of the amylose chains and the formation of a new structure. The application of higher sonication power increased the relative crystallinity in sonicated samples compared with the control (Table 2.1). The retrogradation caused by the reorganization of amylose chains in double helices configuration was affected by the presence of bixin. Indeed, tea polyphenols and black tea extract were able to reduce retrogradation extent of starch from rice and maize (WU et al., 2009; XIAO et al., 2013). The hydroxyl group of polyphenols may be linked with the hydroxyl group of starch through hydrogen bonding, preventing the retrogradation (CHAI; WANG; ZHANG, 2013b). Although bixin does not have a similar structure to polyphenols, the carboxyl group is available to interact with hydroxyl groups of starch chain, avoiding the double helix formation. The interaction between the hydroxyl and carboxyl groups is supported by the FT-IR analysis results

Figure (2.3). The presence of B-type pattern that is still observed in the sonicated samples is probably due to the fact that the bixin content used during encapsulation process was lower than available amylose, allowing the appearance (retrograded amylose) of this diffraction pattern. The diffraction patterns observed in sonicated samples are a mixture of B-type and V-type patterns. Nevertheless, the V-type pattern did not show the typical peaks at of 7.5°, 13°, and 19.9° (2θ). This result suggests that the bixin has not been encapsulated efficiently within the helical cavity, probably due to the molecule size. Thus, bixin and amylose are not linked by hydrophobic interactions. Also, the slight V-type diffraction pattern observed in the sonicated samples suggests that the short chains produced by higher ultrasound power levels can form structures with lower stability.

2.3.2 Rheological characterization

The dynamic rheological test is appropriate for evaluating the viscoelastic behavior of materials. This assay allows studying the characteristics of gels in the linear viscoelasticity region, as well as obtaining rheological parameters such as storage modulus (G') and loss modulus (G"), which are important to evaluate the mechanical properties of these materials (LOPES DA SILVA; RAO, 1999). Results of frequency sweep tests at 25 °C showed that both G' and G" had a slight frequency dependence in the range between 0.6283 rad·s-1 to 62.83 rad·s-1 (0.1 to 10 Hz). The samples coded as BC1 and BC2 presented both G' and G" values lower than the control (Figure 2.2).

Storage module (G') was always greater than G", indicating an elastic behavior and suggesting the presence of a three-dimensional network, exhibiting a gel-like behavior (LOPES DA SILVA; RAO, 1999). Regarding sample BC3, both G' and G" were only slightly lower than those presented by the control, and the same gel-like behavior with G' > G" was observed. The frequency dependence of G' and G" indicates in turn that there was no relaxation process. Chien et al. (1999) reported a slight frequency dependence of G' and G" in a lower range of frequency from 0.1 to 2.5 Hz at 30 °C, during analysis of inclusion complexes using rice starch. Chai et al. (2013b) reported a similar behavior (G' > G") in amylose gels with polyphenols; although they did not report complex formation, they observed a decrease of G' and G" after addition of polyphenol to the amylose gels.

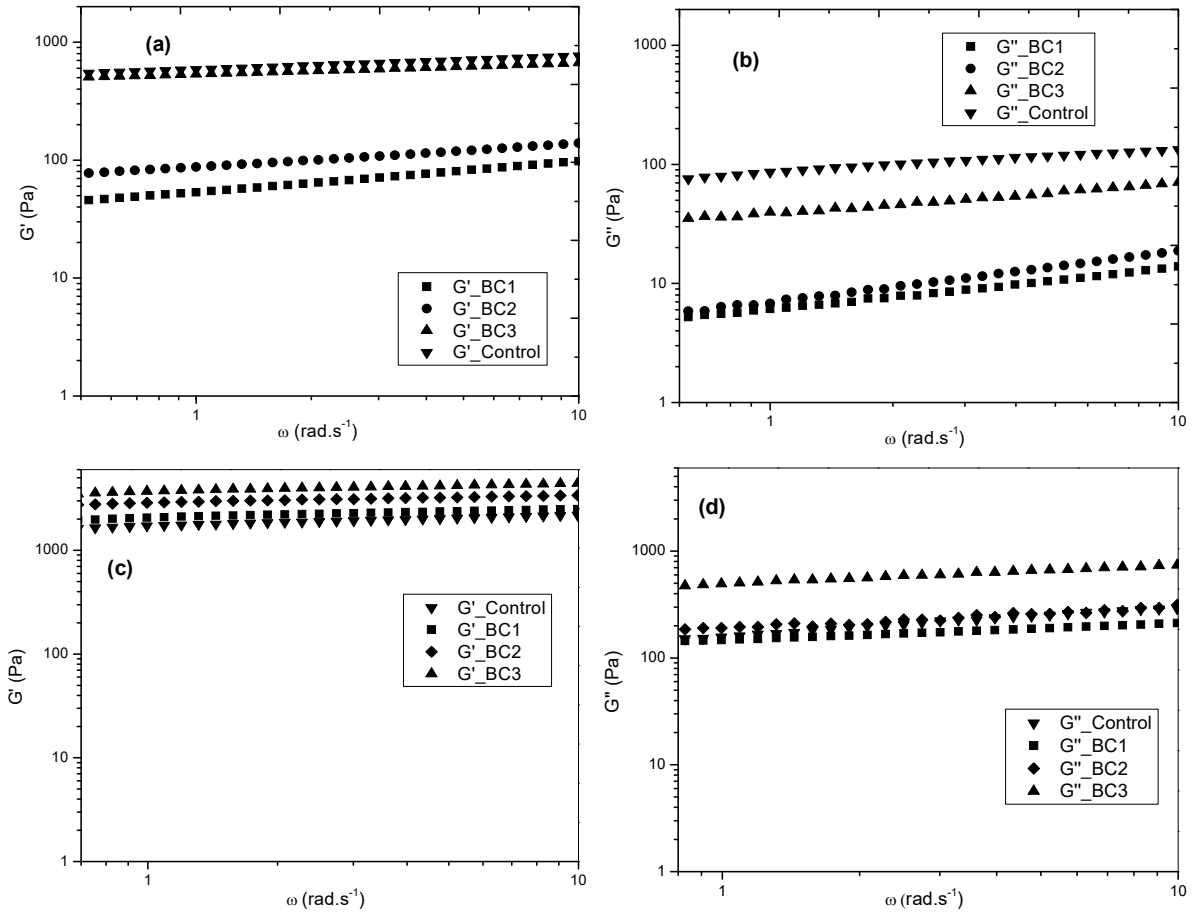

Figure 2.2 Results of frequency sweep assays at 25 °C in terms of G' (a) and G" (b) for sonicated and control samples. G' (c) and G'' (d) for the sonicated and control samples after storage at 47 °C for 12 h.

Ahmadi-abhari et al. (2015) reported also a decrease of G' and G" in inclusion complexes from native wheat starch with 23.5 % of amylose, due to the addition of lysophosphatidylcholine (LPC). In the present study, the decreasing in G' may have been caused by the applied ultrasound treatment. High ultrasound power level applied affected amylose chains and led to formation of a gel with a randomly arranged network and with a twisted structure. On the other hand, at low ultrasound power level, amylose helix chains might be able to arrange themselves in more organized segments, which results in a less elastic network.

Control and sonicated samples showed an increase in G' and G'' after 12-hours storage, with G' of sonicated samples becoming higher than the control (Figure 2c). Chien et al. (1999) studied rice starch gels complexed with different guest molecules, after 12 h storage at room temperature. They carried out an oscillatory temperature sweep and reported an increase in both G' and G'' with heating and proposed that this behavior was due to the addition of ligand and storage, i.e. the strength of the junction zones in the gel structure increased with formation of inclusion complexes and they were reinforced with storage time. Whilst, Ahmadi-Abhari et al. (2015) carried out an oscillatory time sweep and reported increased elasticity (higher G') in the complexes with LPC and native starch after storage at 20 °C for 16 h. Results of frequency sweep assays suggest that amylose chains and bixin have different degrees of interaction due to differences between linear and helical segments of amylose, affecting the normal process formation of double helical conformation of amylose.

According to Chamberlain and Rao (2000), gels can be classified as true-gels or weak-gels (easily broken). The true-gels have G' independent of frequency and G' > G'', unlike to weak-gels that have G' dependent of frequency and G' > G''. Based on this classification, the amylose gels produced by ultrasound can be considered as weak-gels, since despite presenting G' > G'', there was a slight frequency dependence of G' in the range of frequency studied. Power law was applied to describe the frequency-dependence of G' and G'', according to equations 3 and 4.

$$G' = A'\omega^{n'} \quad (3)$$

$$G'' = A''\omega^{n''} \quad (4)$$

in which A is a constant related to gel strength and n is the relaxation exponent.

Parameters A, n and the determination coefficient (R^2) obtained from the adjustment of Power Law are shown in Table 2.2. The Power Law could be fitted to the experimental data with a high coefficient of determination (R2 >0.99). Considering the samples assayed before storage, the A' and A'' parameters that describe the strength of interaction within gel network were higher in the control than in sonicated samples, with A' and A'' being higher in treatment BC3, followed by BC2 and finally BC1. Regarding the parameter n', it followed an opposite trend and decreased with increasing ultrasound power levels

applied. Nevertheless, this power-dependency in n'' was not observed. Considering the behavior of samples after storage at 47 °C for 12 h, the higher elastic character of stored samples is indicated by an increase in the A' values, although n' and n'' were independent on ultrasound power levels applied but were generally lower than the corresponding values before storage. Values of n' and n" approaching zero suggests a purely elastic gel (WINTER; CHAMBON, 1986), indicating the development of elastic properties with storage. At low ligand concentrations, amylose can compete to form double helical or single helical conformation (PUTSEYS; LAMBERTS; DELCOUR, 2010). Thus, a high concentration of free amylose in the control sample contributed to development of double helical conformation during storage, resulting in local organized arrangements which are less elastic (lower A' value) when compared to sonicated samples, in which a possible twisted structure could have been reinforced after storage. This double helical conformation was verified with the X-ray diffraction patterns of the samples after storage.

Table 2.2. Effect of ultrasound treatment on the Power law fitting parameters of sonicated sample and the control.

Sample treatment		A'	n'	R^2	A''	n''	R^2
Before storage	GS-B	588.2	0.11	0.99	81.9	0.23	0.99
	BC1	53.5	0.26	0.99	6.0	0.35	0.99
	BC2	87.3	0.20	0.99	7.2	0.41	0.99
	BC3	534.1	0.10	0.99	39.7	0.24	0.99
After storage	GS-B	2082.4	0.11	0.99	252.6	0.21	0.99
	BC1	2399.6	0.08	0.99	196.9	0.17	0.99
	BC2	3293.6	0.07	0.99	277.0	0.22	0.99
	BC3	4318.8	0.08	0.99	681.9	0.17	0.99

2.3.4 FT-IR spectra analysis

Figure 2.3 shows FT-IR spectra of bixin, the control, GS and sonicated samples. Spectra of the bixin showed two characteristic bands in 2902 and 2853 cm-1 for asymmetric and symmetric stretching vibration from -CH2 group from the hydrocarbon skeleton, respectively. Band in 1744 cm-1 was associated with stretching vibration of –C=O group from aliphatic carboxylic acid, and 1613 cm-1 with stretching vibration of conjugated C=C group. Gelatinized corn starch (GS) showed bands between 2837 to 3010 cm-1 associated with stretching vibration from –C-H, and bands between 920 to 1180 cm-1

associated with stretching from C-O, C-C and -C-O-H respectively (SOEST; VLIEGENTHART, 1997).

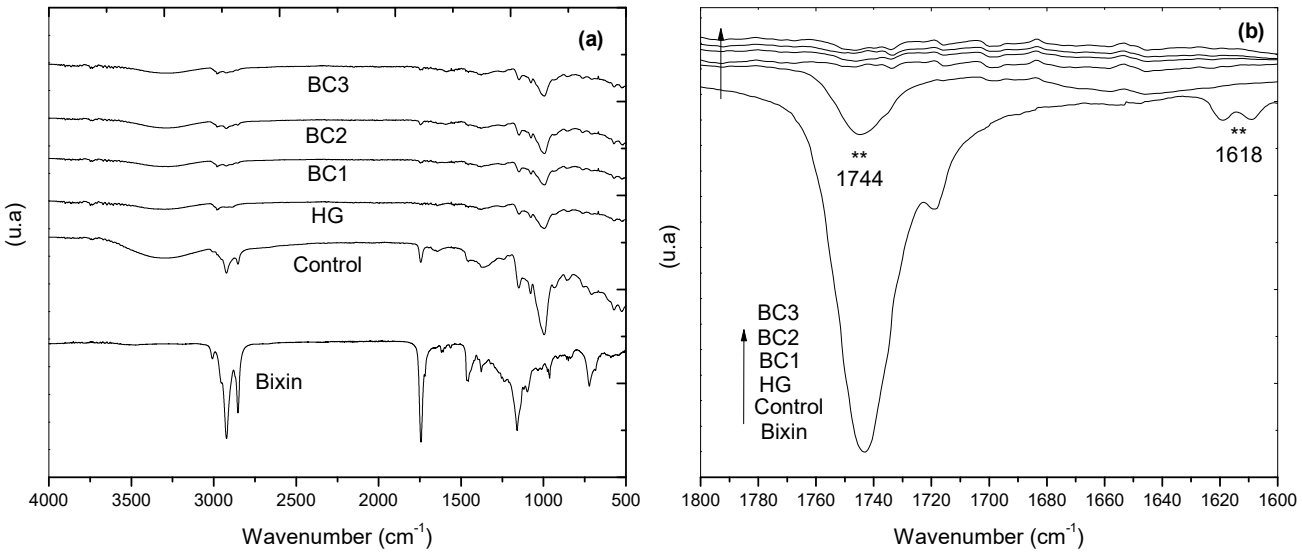

Figure 2.3 FT-IR analysis of Bixin, HG, GS-B mixture (Control) and sonicated samples BC1 150 W, BC2 210 W, BC3 300 W (a), and detail in (b).

When comparing FT-IR spectra, it is possible to see that the spectrum of the control treatment was similar to bixin, although with a lower absorbance in their characteristic bands, due to the low bixin content in the control. Nevertheless, some bands of the FT-IR spectra changed in sonicated samples. The band at 1744 cm-1, which is typical of the –C=O group of bixin and the band at 1618 cm-1 disappeared (detail in Figure 3b), indicating that stretching vibration from -C=O, C=C groups in the bixin were restricted after sonication. These changes probably occurred because these groups were entrapped by the starch matrix, restricting their vibrations. The vibration constraint could be caused by interactions of hydrogen bonds and Van der Waals forces between glucose, water and bixin, stabilizing the amylose-ligand interaction. These results are in agreement with X-ray diffraction patterns, which indicated the reordering of the amylose chains and formation of a new structure. In fatty acids, the carboxylic group may be located outside the helical cavity of amylose and thus remaining only partially entrapped. For fatty acids as palmitic or lauric, the amylose chain may require 30 to 40 glucose units that could

allow the complexation of two molecules of fatty acid. In this way, the steric hindrance and the repulsion forces may affect the location of the guest (GODET; TRAN; DELAGE, 1993; GODET; BIZOT; BULÉON, 1995). The double bond in the structure of bixin could increase steric hindrance by a 'kink' in its chain, which would make it difficult to be entrapped inside of the helical cavity of the amylose. Results suggest that there are interactions between bixin and amylose chain, but these interactions probably are not of the V-type conformation.

2.3.5 Surface and encapsulated bixin

Encapsulated bixin may be divided into a fraction that remains on the surface of starch matrix and another one that is protected by starch. Table 2.1 shows the values of bixin content on the surface and inside the starch matrix. The treatment BC1 (150 W) resulted in higher encapsulated bixin content than BC2 (210 W) and BC3 (300 W), suggesting a decrease in the interaction between bixin and amylose, due to the application of higher ultrasound power levels. The results suggest that the lower power level studied might be more appropriate to increase the content of microencapsulated bixin, leading to the amount of 2042.5 ± 12.0 μg bixin·g^{-1}. Ultrasound treatment can break the starch chains and degrade the amorphous regions, which are most constituted by linear amylose chains instead of branched amylopectin chains (LUO et al., 2008), resulting in the formation of short chains of amylose, which are more available to interact with the bixin.

2.3.6 Release profile of bixin complexes

The release profile of microencapsulated bixin in the simulated intestinal fluid is shown in Figure 2.4. Sonicated samples presented greater stability against the action of the SIF compared to the control treatment. In the control about 25 % of release was observed. The starch seems to be a good wall material, providing protection to bixin in the SIF conditions. Sonicated samples presented a fast release in the first hour, followed by stabilization at a nearly constant value. Sonicated samples also presented a lower release percent compared to the control sample. The release of bixin from control was different of observed in the control, which indicate that bixin was encapsulate in different form in the amorphous region. The sonicated samples were less susceptible to SIF action than control, due to the major intramolecular binding with the guest. These interactions cause a lower bixin release percent.

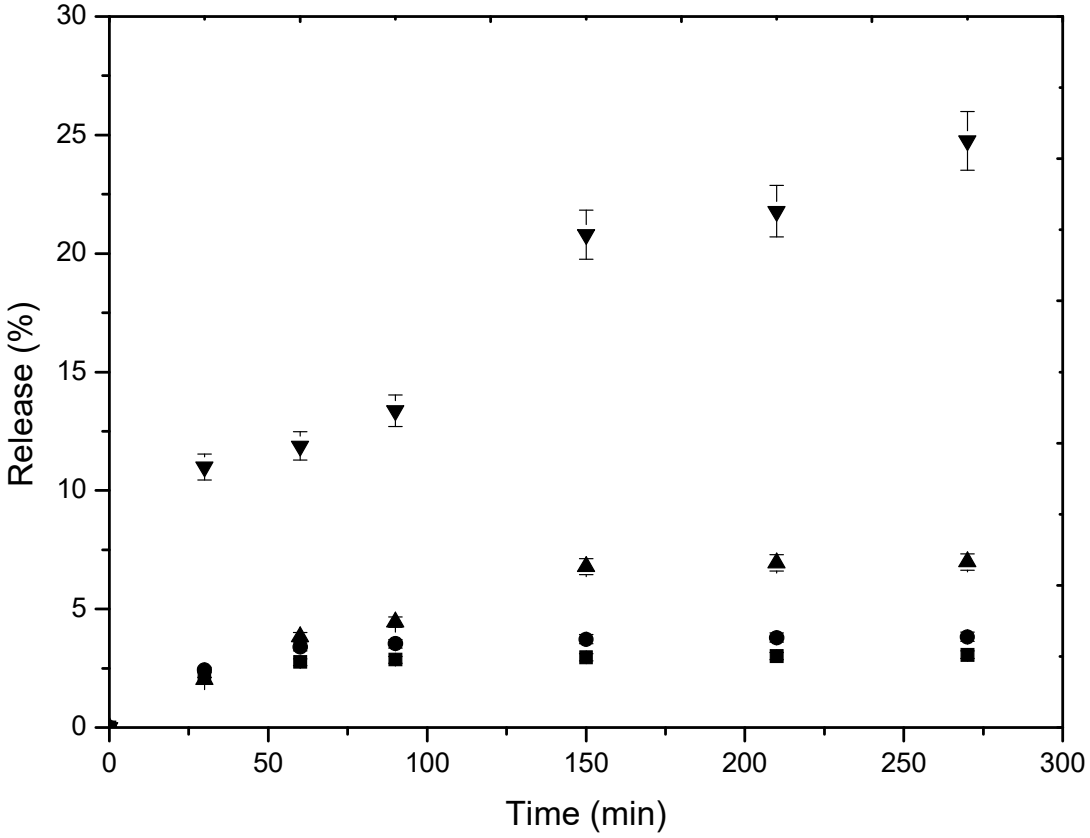

Figure 2.4. Bixin-release profiles of the sonicated samples in simulated intestinal fluid. BC1 150 W (■), BC2 210 W (●), BC3 300 W (▲) and control (▼).

2.3.7 Color analysis

Table 2.3 shows the color parameters *L**, *a**, *b**, *C**, and °*hue* of sonicated and control samples in addition to pure bixin. The parameter *a** varied between 32.0 and 36.7, with higher values indicating increased redness of the sonicated samples. BC2 showed *a** value greater than BC1 and BC3, followed by the control. Nevertheless, sonicated samples had *a** values lower than pure bixin (*a** = 40.1). The parameter *b** of BC1 and BC3 was close to the value of pure bixin, indicating that the ultrasound did not affect this parameter. Sonicated samples had *L** values lower than the control, which may be due to the temperature increase caused by sonication. Nevertheless, *L** values of sonicated and control samples were higher than pure bixin, because of the presence of starch that increases lightness. The °*hue,* which represents the color tonality, varied between 51 and,

54 standing in the second quadrant of the chromaticity diagram, between red (°*hue* = 0) and yellow (°*hue* = 90). Ultrasound caused a decrease in the °*hue* of sonicated samples in comparison to the control, indicating that samples treated with ultrasound were more reddish than the control Figure 2S (Supplementary Figure-Apêndice A) shows UV-vis absorption spectra of the bixin and sonicated samples, indicating that there was no hydrolysis or degradation product formation during complexation process. Concerning chroma, *C**, the complexes presented values in the range between 54.5 and 64.8. Lower values of chroma indicate less saturation and consequently a less intense color. Both *a** and °*hue* are of great importance, since they indicate the redness and tonality of samples treated with ultrasound compared to the original bixin color. The results present in Table 3 show a tendency of samples prepared by ultrasound to be slightly less reddish than the original color of pure bixin. The color parameters *a** and *b** of the sonicated samples were higher than reported by De Sousa Lobato et al. (2013) for nanocapsules of bixin in a suspension prepared by interfacial deposition, with *a* and b** values of 13.54 and 25.50 respectively. Whilst, *L** had a value close to the observed in the sonicated samples.

Table 2.3 Color parameters for amylose-bixin complexes and the control.

Sample	*L**	*a**	*b**	*C**	°*hue*
Control	53.3 ± 0.9 [a]	33.9 ± 0.1 [a]	55.4 ± 0.9 [a]	64.8 ± 0.9 [a]	58.9 ± 0.6 [a]
BC1	44.8 ± 0.9 [b]	34.8 ± 0.2 [b]	43.1 ± 1.0 [b]	55.4 ± 0.8 [b]	51.0 ± 0.7 [b]
BC2	44.3 ± 0.4 [b]	36.7 ± 0.1 [c]	48.3 ± 0.1 [c]	60.7 ± 0.1 [c]	52.7 ± 0.2 [c]
BC3	43.6 ± 0.3 [b]	32.0 ± 0.2 [d]	44.1 ± 0.3 [b]	54.5 ± 0.3 [b]	53.9 ± 0.1 [c]
Bixin	30.6 ± 0.8 [c]	40.1 ± 0.2 [e]	44.9 ± 0.9 [b]	59.9 ± 0.6 [c]	48.4 ± 0.8 [d]

Mean value ± Standard deviation. Means with the same letter in the same column indicate no significant difference by Tukey´s test (P< 0.05).

2.3.8 Scanning electron microscopy (SEM)

Figure 2.5 shows the SEM photographs of the sonicated samples and control at different magnification. The control sample presented particles with a form of compact and homogeneous plate-like structure, while that the sonicated samples presented a surface eroded and irregular with protrusions about 1 μm in size. Exarhopoulos and Raphaelides (2012) suggested that this type of protrusions could be caused by aggregates of amylose molecules. The sonicated samples presented a hollow surface. The ultrasound treatment

produced a porous material due probably to the combined effect of cavitation process during application of ultrasound.

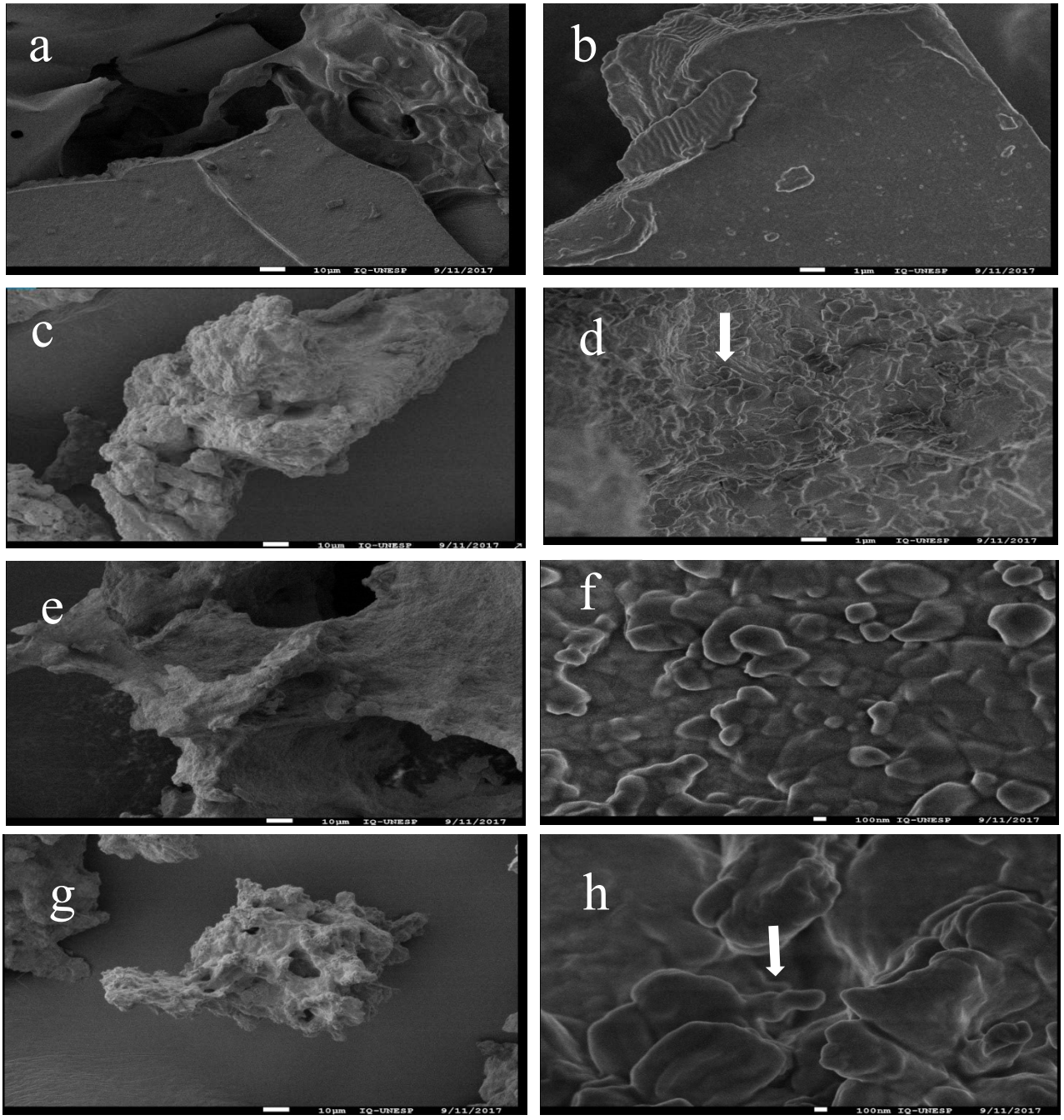

Figure 2.5 SEM micrographs of control (a, b); sonicated samples BC1 (c, d), BC2 (e, f), BC3 (g, h). Magnification 600× (a, c, e, g); 6000× (b, d); 30,000× (f, h).

2.4 Conclusion

Bixin was encapsulated in a starch matrix using ultrasound. The three power levels applied in the ultrasound treatment affected the encapsulated bixin content, as well as the profile and total amount of bixin released when exposed to a simulated gastrointestinal fluid, in comparison with encapsulated bixin without ultrasound treatment. Future studies are desirable to optimize the ultrasound treatment and selecting the best conditions of power level and treatment time to maximize the encapsulated bixin content. The encapsulation of bixin using ultrasound can be an alternative to formulate functional foods enriched with carotenoids and enabling controlled release.

2.4 Acknowledgements

The authors thank Coordenação de Aperfeiçoamento de Pessoal de Nível Superior (CAPES) for financial support.

2.5 References

ABU-HARDAN, M. O.; HILL, S. E.; FARHAT, I. a. A Calorimetric Study of the Interaction between Waxy Maize Starch and Lipid. **Starch - Stärke**, v. 59, n. 5, p. 217–223, maio 2007.

ADES, H.; KESSELMAN, E.; UNGAR, Y.; SHIMONI, E. Complexation with starch for encapsulation and controlled release of menthone and menthol. **LWT - Food Science and Technology**, v. 45, n. 2, p. 277–288, 2012.

AHMADI-ABHARI, S.; WOORTMAN, A. J. .; HAMER, R. .; LOOS, K. Rheological Properties of wheat starch influenced by amylose-lysophosphatidylcholine complexation at different gelation phases. **Carbohydrate Polymers**, v. 122, p. 197–201, 2015.

BARBOSA, M. I. M. .; BORSARELLI, C. .; MERCADANTE, A. . Light stability of spray-dried bixin encapsulated with different edible polysaccharide preparations. **Food Research International**, v. 38, n. 8–9, p. 989–994, 2005.

BIAIS, B.; LE BAIL, P.; ROBERT, P.; PONTOIRE, B.; BULÉON, A. Structural and stoichiometric studies of complexes between aroma compounds and amylose. Polymorphic transitions and quantification in amorphous and crystalline areas. **Carbohydrate Polymers**, v. 66, n. 3, p. 306–315, 2006.

CHAI, Y.; WANG, M.; ZHANG, G. Interaction between amylose and tea polyphenols modulates the postprandial glycemic response to high-amylose maize starch. **Journal of Agricultural and Food Chemistry**, v. 61, n. 36, p. 8608–8615, 2013.

CHAMBERLAIN, E. K.; RAO, M. A. Effect of concentration on rheological properties of acid-hydrolyzed amylopectin solutions. **Food Hydrocolloids**, v. 14, n. 2, p. 163–171, 2000.

CHIEN, J. T.; LIEN, Y. Y.; SHOEMAKER, C. F. Effect of polarity of complexing agents on thermal and rheological properties of rice starch gels. **Cereal Chemistry**, v. 76, n. 6, p. 837–842, 1999.

DE SOUSA LOBATO, K. B.; PAESE, K.; CASANOVA, J.; STANISÇUASKI, S.; JABLONSKI, A.; DE OLIVEIRA, A. Characterisation and stability evaluation of bixin nanocapsules. **Food Chemistry**, v. 141, n. 4, p. 3906–3912, 2013.

EXARHOPOULOS, S.; RAPHAELIDES, S. N. Morphological and structural studies of thermally treated starch-fatty acid systems. **Journal of Cereal Science**, v. 55, n. 2, p. 139–152, 2012.

FELKER, F. C.; KENAR, J. A.; FANTA, G. F.; BISWAS, A. Comparison of microwave processing and excess steam jet cooking for spherulite production from amylose-fatty acid inclusion complexes. **Starch/Starke**, v. 65, n. 9–10, p. 864–874, 2013.

GODET, M. C.; BIZOT, H.; BULÉON, A. Crystallization of amylose-fatty acid complexes prepared with different amylose chain lengths. **Carbohydrate Polymer**, v. 1, n. 27, p. 47–52, 1995.

GODET, M. C.; TRAN, V.; DELAGE, M. M. Molecular modelling of the specific interactions involved in the amylose complexation by fatty acids. **International Journal of Biological Macromolecules**, v. 15, n. 1, p. 11–16, 1993.

HAAJ, S.; MAGNIN, A.; PÉTRIER, C.; BOUFI, S. Starch nanoparticles formation via high power ultrasonication. **Carbohydrate Polymers**, v. 92, n. 2, p. 1625–1632, 2013.

HEINEMANN, C.; CONDE-PETIT, B.; NUESSLI, J.; ESCHER, F. Evidence of starch inclusion complexation with lactones. **Journal of Agricultural and Food Chemistry**, v. 49, n. 3, p. 1370–1376, 2001.

HEINEMANN, C.; ESCHER, F.; CONDE-PETIT, B. Structural features of starch – lactone inclusion complexes in aqueous potato starch dispersions: the role of amylose and amylopectin. **Carbohydrate Polymers**, v. 51, n. 2, p. 159–168, 2003.

HUANG, Q.; LI, L.; FU, X. Ultrasound effects on the structure and chemical reactivity of cornstarch granules. **Starch/Staerke**, v. 59, n. 8, p. 371–378, 2007.

IMBERTY, A.; PEREZ, S. A revisit to the three-dimensional structure of B-type starch. **Biopolymers**, v. 27, n. 8, p. 1205–1221, 1988.

ITTHISOPONKUL, T.; MITCHELL, J. R.; TAYLOR, A. J.; FARHAT, I. a. Inclusion complexes of tapioca starch with flavour compounds. **Carbohydrate Polymers**, v. 69, n. 1, p. 106–115, 1 maio 2007.

KARUNARATNE, R.; ZHU, F. Physicochemical interactions of maize starch with ferulic acid. **Food Chemistry**, v. 199, p. 372–379, 2016.

LALUSH, I.; BAR, H.; ZAKARIA, I.; EICHLER, S.; SHIMONI, E. Utilization of amylose-lipid complexes as molecular nanocapsules for conjugated linoleic acid. **Biomacromolecules**, v. 6, n. 1, p. 121–130, 2005.

LE BAIL, P.; RONDEAU, C.; BULÉON, A. Structural investigation of amylose complexes with small ligands: Helical conformation, crystalline structure and thermostability. **International Journal of Biological Macromolecules**, v. 35, n. 1–2, p. 1–7, 2005.

LESMES, U.; BARCHECHATH, J.; SHIMONI, E. Continuous dual feed homogenization for the production of starch inclusion complexes for controlled release of nutrients. **Innovative Food Science & Emerging Technologies**, v. 9, n. 4, p. 507–515, out. 2008.

LIMA, F.; ANDRADE, C. Ultrasonics Sonochemistry Effect of melt-processing and ultrasonic treatment on physical properties of high-amylose maize starch. **Ultrasonics - Sonochemistry**, v. 17, n. 4, p. 637–641, 2010.

LOPES DA SILVA, J. A.; RAO, A. Rheological Behavior of Food Gel Systems. In: RAO, A. M. (Ed.). **Rheology of Fluid and Semisolid Foods: Principles and Application**. First edit ed. Gaithersburg, Maryland: Aspen Publishers, Inc., 1999. p. 320.

LUO, Z.; FU, X.; HE, X.; LUO, F.; GAO, Q.; YU, S. Effect of ultrasonic treatment on the physicochemical properties of maize starches differing in amylose content. **Starch/Staerke**, v. 60, n. 11, p. 646–653, 2008.

LYNG, S. M.; PASSOS, M.; FONTANA, J. D. Bixin and α-cyclodextrin inclusion complex and stability tests. **Process Biochemestry**, v. 40, n. 2, p. 865–872, 2005.

MOHAMMAD AMINI, A.; RAZAVI, S. M. A. Ultrasound-assisted acid-thinning of corn starch: Morphological, physicochemical, and rheological properties. **Starch/Staerke**, v. 67, n. 7–8, p. 640–653, 2015.

PARIZE, A. L.; CRISTINA, T.; SOUZA, R. De; MARIA, I.; BRIGHENTE, C.; FÁVERE, V. T. De; LARANJEIRA, M. C. M.; SPINELLI, A.; LONGO, E. Microencapsulation of the natural urucum pigment with chitosan by spray drying in different solvents. **African Journal of Biotechnology**, v. 7, n. 17, p. 3107–3114, 2008.

PUTSEYS, J. a; LAMBERTS, L.; DELCOUR, J. a. Amylose-inclusion complexes: Formation, identity and physico-chemical properties. **Journal of Cereal Science**, v. 51, n. 3, p. 238–247, 2010.

RADHIKA, G. S.; SHANAVAS, S.; MOORTHY, S. N. Influence of lipids isolated from soybean seed on different properties of cassava starch. **Starch/Starke**, v. 60, n. 9, p. 485–492, 2008.

RAHMALIA, W.; FABRE, J.-F.; USMAN, T.; MOULOUNGUI, Z. Aprotic solvents effect on the UV-visible absortion spectra of bixin. **Spectrochimica Acta Part A: Molecular and Biomolecular Spectroscopy**, v. 131, p. 455–460, 2014.

RODRIGUEZ-AMAYA, D. B. **A Guide to carotenoide analysis in foods**. Washington, D.C: ILSI PRESS, 2001.

RONDEAU-MOURO, C.; LE BAIL, P.; BULÉON, A. Structural investigation of

amylose complexes with small ligands: Inter- or intra-helical associations? **International Journal of Biological Macromolecules**, v. 34, n. 5, p. 251–257, 2004.

SIEVERT, D.; CZUCHAJOWSKA, Z.; POMERANZ, Y. Enzyme-resistant starch. III. X-ray diffraction of autoclaved amylomaize VII starch and enzyme-resistant starch residues. **Cereal Chem**, v. 68, n. 1, p. 86–91, 1991.

SINGH, N.; KAUR, S.; RANA, J. C.; NAKAURA, Y.; INOUCHI, N. Isoamylase debranched fractions and granule size in starches from kidney bean germplasm: Distribution and relationship with functional properties. **Food Research International**, v. 47, n. 2, p. 174–181, 2012.

SOEST, J. J. G. Van; VLIEGENTHART, J. F. G. Crystallinity in starch plastics: consequences for material properties. **Trends in biotechnology**, v. 15, n. 6, p. 208–213, 1997.

SUTTER, S. C.; BUERA, P.; ELIZALDE, B. E. Beta-Carotene encapsulation in a mannitol matrix as affected by divalent cations and phosphate anion. **International journal of pharmaceutics**, v. 332, n. 1–2, p. 45–54, 2007.

TAPANAPUNNITIKUL, O.; CHAISERI, S.; PETERSON, D. G.; THOMPSON, D. B. Water solubility of flavor compounds influences formation of flavor inclusion complexes from dispersed high-amylose maize starch. **Journal of Agricultural and Food Chemistry**, v. 56, n. 1, p. 220–226, 2008.

TESTER, R. F.; KARKALAS, J.; QI, X. Starch composition, fine structure and architecture. **Journal of Cereal Science**, v. 39, n. 2, p. 151–165, mar. 2004.

TIAN, Y.; ZHU, Y.; BASHARI, M.; HU, X.; XU, X.; JIN, Z. Identification and releasing characteristics of high-amylose corn starch-cinnamaldehyde inclusion complex prepared using ultrasound treatment. **Carbohydrate polymers**, v. 91, n. 2, p. 586–9, 16 jan. 2013.

WINTER, H. H.; CHAMBON, F. Analysis of Linear Viscoelasticity of a Crosslinking Polymer at the Gel Point. **J. Rheol.**, v. 30, n. 2, p. 367–382, 1986.

WU, Y.; CHEN, Z.; LI, X.; LI, M. Effect of tea polyphenols on the retrogradation of rice starch. **Food Research International**, v. 42, n. 2, p. 221–225, 2009.

WULFF, G.; AVGENAKI, G.; GUZMANN, M. S. P. Molecular encapsulation of flavours as helical inclusion complexes of amylose. **Journal of Cereal Science**, v. 41, n. 3, p. 239–249, 2005.

XIAO, H.; LIN, Q.; LIU, G.; WU, Y. Inhibitory Effects of Green Tea Polyphenols on the Retrogradation of Starches from Different Botanical Sources. **Food Bioprocess Technol**, v. 6, p. 2177–2181, 2013.

ZABAR, S.; LESMES, U.; KATZ, I.; SHIMONI, E.; BIANCO-PELED, H. Structural characterization of amylose-long chain fatty acid complexes produced via the acidification method. **Food Hydrocolloids**, v. 24, n. 4, p. 347–357, jun. 2010.

ZHENG, J.; LI, Q.; HU, A.; YANG, L.; LU, J.; ZHANG, X.; LIN, Q. Dual-frequency ultrasound effect on structure and properties of sweet potato starch. **Starch/Starke**, v. 65, n. 7–8, p. 621–627, 2013.

ZHU., F. Encapsulation and delivery of food ingredients using starch based systems. **Food Chemistry**, v. 229, p. 542–552, 2017.

ZHU, F. Interactions between starch and phenolic compound. **Trends in Food Science & Technology**, v. 43, n. 2, p. 129–143, 2015.

ZHU, J.; LI, L.; CHEN, L.; LI, X. Study on supramolecular structural changes of ultrasonic treated potato starch granules. **Food Hydrocolloids**, v. 29, n. 1, p. 116–122, 2012.

CAPÍTULO 3. ENCAPSULAÇÃO DE BIXINA COM AMIDO DE ALTO CONTEÚDO DE AMILOSE, EFEITO DA TEMPERATURA E ADIÇÃO DE PROTEÍNA

ENCAPSULATION OF BIXIN WITH HIGH AMYLOSE STARCH AS AFFECTED BY TEMPERATURE AND ADDITION OF WHEY PROTEIN

Ezequiel José Pérez-Monterroza, Célia Maria Landi Franco, Vânia Regina Nicoletti

Department of Food Engineering and Technology; São Paulo State University (Unesp), Institute of Biosciences, Humanities and Exact Sciences (Ibilce), Campus São José do Rio Preto; Rua Cristovão Colombo 2265, Zip Code 15054-000 São José do Rio Preto, SP, Brazil.

*Correspondence:

Ezequiel José Pérez-Monterroza

Email: eperez494@gmail.com, ejperezm@unalmed.edu.co

Abstract

Microencapsulation of bixin using high-amylose corn starch was carried out by the acidification method. Bixin powders were characterized by differential scanning calorimetry (DSC), X-ray diffractometry (XRD), FT-IR spectrometry, color parameters, encapsulated bixin content, bixin release profile. In addition, the effect of whey protein (WP) on the microencapsulation process was investigated. The results obtained from DSC, X-ray diffraction and FT-IR spectrometry indicated that only in the samples prepared at 90 °C (B0WP90°C, B10WP90°C, and B20WP90°C) there was formation of crystalline structures, with melting temperatures at 117.2, 105 and 104 °C, respectively. The possible interactions between bixin, WP and amylose starch are also discussed.

3.1 Introduction

The seeds of the tropical plant *Bixa Orellana*, which grows in Central and South America, are the source of Annatto, a natural dye that has been used as a yellow to orange food colorant and has widespread usage in dairy and fat-based products such as butter, cheese, margarine, meat and snacks. Annatto extracts are prepared by solvent extraction of the seeds and contains bixin as the major pigment. Bixin is an oil-soluble apocarotenoid that

has the characteristic isoprenoid structure of the carotenoid pigments, but with a much shorter chain length of 26 carbons, presenting a carboxylic acid group at one end, and a methyl ester at the opposite end (PRESTON; RICKARD, 1980; WROLSTAD; CULVER, 2012; GIRIDHAR; VENUGOPALAN; PARIMALAN, 2014). Bixin can be oxidized by light and can be affected by elevated temperatures, but their major cause of instability is the contact with atmospheric oxygen (BALASWAMY et al., 2006). It is known that the amylose present in starch granules can form inclusion complexes with hydrophobic molecules such as alcohols, flavors, aromas, fatty acids and nutraceutical compounds (NUESSLI et al., 1997; LALUSH et al., 2005a; WULFF; AVGENAKI; GUZMANN, 2005b; ITTHISOPONKUL et al., 2007; PUTAUX et al., 2008; ZABAR et al., 2010). These are called V-type inclusion complexes, which are formed when a hydrophobic molecule is entrapped inside of an amylose helix cavity. Diffraction patterns of amylose complexes suggest that V-type complexes might be formed by six (V_6), seven (V_7) or eight (V_8) glycosyl residues per helical turn, and their diameters depend on the structure and size of the guest molecule (BILIADERIS; GALLOWAY, 1989; OBIRO; SINHA RAY; EMMAMBUX, 2012b). Microencapsulation may be a feasible alternative to improve the stability of annatto colorants. The microencapsulation of bixin can be carried out using chitosan, gum Arabic, or maltodextrin by spray drying (BARBOSA; BORSARELLI; MERCADANTE, 2005; PARIZE et al., 2008). Also, as it was reported by De Sousa Lobato et al. (2013), bixin can be microencapsulated by interfacial deposition on preformed poly(ε-caprolactone). Encapsulation by complexation with amylose is an alternative that could be applied to protecting bixin against oxidation, as well as for developing controlled delivery systems. Bixin can form inclusion complexes with α-cyclodextrin and β-cyclodextrin (LYNG; PASSOS; FONTANA, 2005b; MARCOLINO et al., 2011) and, due to the similarity between the hydrophobic helical cavity of amylose with that of cyclodextrin , it is reasonable to consider the possibility of producing amylose-bixin complexes. .On the other hand, the encapsulation process based on starch can be affected by the presence of proteins, which could affect the release characteristics of the system. In fact, whey protein can compete for a guest molecule by forming a three-in-one complex, affecting the amount of complex formed (ZHANG; MALADEN; HAMAKER, 2003), i.e., in the complex formed with bixin, whey protein can increase the percentage of unordered structures, indicating that the secondary structure of whey protein can be changed (ZHANG; ZHONG, 2012a). Notwithstanding, these observations have been tackled by a limited number of researchers. Hence, this work

presents the results of bixin encapsulation with high-amylose corn starch, including the characterization of the produced bixin powder, as well as the effect of whey protein addition on the microencapsulation.

3.2 Material and Methods

High-amylose (72 % of amylose, according to manufacturer) corn starch (Hylon VII) was obtained from Ingredion Brasil Ing. Ind. Ltda (Mogi Guaçu, SP, Brazil). Bixin was obtained from BKG (Adicon, Brazil). Whey protein concentrate (WP) was obtained from Alibra ingredients Ltda (SP, Brazil). Sodium hydroxide (NaOH) was supplied by Synth (Diadema, Brazil), hydrochloric acid was provided by Quimis (Diadema, Brazil), and pancreatin was provided by Sigma-Aldrich (St. Louis, MO). Starch suspensions were prepared using deionized water. All chemicals were of analytical grade.

3.2.1 Microencapsulation

Ninety grams of high-amylose corn starch (Hylon VII) in 2350 g of water were gelatinized at 130 °C for 45 min. One hundred and fifty grams of the gelatinized starch suspension (GS) was mixed with bixin (0.3 g) in 0.01 M KOH solution (50 g) at temperatures of 60, 70, and 90 °C for 60 min, followed by precipitation at pH 4.5 using 0.01M HCl. The precipitate was separated by centrifugation at 9000×g for 10 min, cooled at -18 °C for 12 hours and lyophilized. When the use of protein (WP) was necessary, it was added to the gelatinized starch (based on starch concentration) suspension according to Table 3.1. The samples were coded with the letter B followed by whey protein ratio and temperature of treatment. A control sample (GS-B), consisting of GS (150 g) and bixin (0.3 g) in 0.01 M KOH solution (50 g), was prepared at 45 °C for 1 min. Also, a control sample (GS-WP), consisting of GS (150 g) and WP (1.24 g), was prepared at 60, 70 and 90 °C for 60 min.

Table 3.1 Sample codification and respective protein content and temperature treatment

Temperature treatment (°C)	Samples	WP (%)	WP (g)
60	B0WP60°C	0	0
	B10WP60°C	10	0.6
	B20WP60°C	20	1.24
70	B0WP70°C	0	0
	B10WP70°C	10	0.6
	B20WP70°C	20	1.24
90	B0WP90°C	0	0
	B10WP90°C	10	0.6
	B20WP90°C	20	1.24

3.2.2 Differential scanning calorimetry (DSC)

The thermal characterization of the inclusion complex was carried out by analyzing the thermograms obtained in a PerkinElmer DSC 8000 (PerkinElmer Corp, Shelton, CT, USA). The equipment was calibrated with indium before analysis. Nitrogen was used as a purge gas for the system. For the analysis, 4-5 mg of the samples were weighed in aluminum pans. An empty aluminum pan was used as the reference. The samples were heated at 10 °C/min from 80 to 140 °C, then subsequently cooled at 10 °C/min from 140 to 80 °C. The results of the thermal analyses were processed using PerkinElmer Pyris software, version 10.0 (PerkinElmer Inc, Shelton, CT, USA).

3.2.3 X-ray diffraction (XRD)

X-ray diffraction was carried out with a diffractometer RINT 2000 wide angle Goniometer unit (Rigaku, Tokyo, Japan). The diffractometer was operated at a voltage of 45 kV and a current of 40 mA. The samples were scanned from 5º to 40° in 2θ, at a rate of $1°\cdot min^{-1}$ and a step size of 0.1°. The relative crystallinity was calculated based on the relationship between the peak area and total area of the X-ray diffractograms, according to Itthisoponkul et al. (2007), by using Origin software (Microcal Inc, Northampton, USA). Diffractograms were smoothed and the baseline was corrected. The analyses were carried out in duplicate.

3.2.4 FT-IR spectroscopy

Infrared spectra were recorded on a Spectrum One spectrophotometer (PerkinElmer Corp, Shelton, CT, USA) with an attenuated total reflectance accessory and a ZnSe crystal. Samples were analyzed directly after pressing them on the crystal (80 psi), and FT-IR scanning was conducted at ambient conditions. The resolution was set to 4 cm^{-1}, and the operating range was set to 400 to 4000 cm^{-1}. In all cases, 20 scans per sample were recorded. The data were processed using Origin Pro 8 Software (Microcal Inc, Northampton, USA). The analyses were carried out in duplicate.

3.2.5 Content of bixin on surface and inside of matrix.

The surface and encapsulated bixin content in the amylose complexes was determined according to Lalush et al. (2005a) and Sutter, Buera, and Elizalde (2007), with modifications. Surface bixin was determined by washing 0.010 g of the complex with 4 mL of acetone in a test tube and shaking the mixture in a vortex for 2 min. After sedimentation, the powder was separated and the concentration of bixin in the acetone was measured spectrophotometrically at 457 nm. Encapsulated bixin in the remaining powder was determined by degradation of the complex with pancreatin. The powder was incubated in 4 mL of pancreatin solution at 37 °C for 36 hours. Then, bixin was extracted with 7 mL of acetone, centrifuged, filtered and quantified spectrophotometrically at 457 nm. This wavelength was found to correspond to the maximum absorbance of the used bixin, in the spectrum range of 200 to 600 nm. For preparing the pancreatin solution, 0.18 g of pancreatin was dissolved in 20 mL of phosphate buffer 20 mM (pH 7.0) containing NaCl (0.04% w/w). This solution was centrifuged (9000×g, 10 min), and the supernatant was filtered and used for the test. Bixin content (BC) in the complex was calculated for each formulation as μg of bixin per g of total complex (RODRIGUEZ-AMAYA, 2001; RAHMALIA et al., 2014). The analyses were carried out in duplicate.

3.2.6 Release profile of bixin in simulated intestinal fluid

Determination of the release profile was carried out according to Lesmes et al. (2008) with modification. The complexes (0.010 g) were dispersed in 15 mL of simulated intestine fluid (SIF), which was prepared by dissolving 0.18 g of pancreatin in a phosphate buffer solution (20 mM, pH 7.0) containing NaCl (0.04% w/w). This dispersion was centrifuged (9000×g, 10 min), and the supernatant was filtered and used to incubate the complexes at 37 °C. At intervals of time (30, 60, 90, 150, 210 and 270 min), aliquots of

1 mL of this dispersion were separated and immediately subjected to bixin extraction with 4 mL of acetone, which was centrifuged and measured spectrophotometrically at 457 nm. The volume taken was replaced with fresh SIF. The analyses were carried out in duplicate.

3.2.7 Color analysis

The color of the inclusion complexes was determined using a ColorFlex model 45/0 spectrophotometer (Hunterlab, USA) with the D65 illuminant and observer at 10º. The 4.10 version of Universal software was used to determine the absolute values of L*, a*, and b*. The system used for specification of color was CIELAB. Values of L* (lightness) range between zero (black) and one hundred (white), a* between -a* (green) and +a* (red), and b* between -b* (blue) and +b* (yellow). The chroma (C*), which expresses the degree of intensity or saturation of the color (Eq. 1), and the hue angle (°hue), which represents the tonality of the color (Eq. 2), were calculated. The analyses were carried out in triplicate.

$$C^* = \sqrt{(a^*)^2 + (b^*)^2} \quad (1)$$

$$°hue = arctg\left(\frac{b^*}{a^*}\right) \quad (2)$$

3.3 Results and discussion

3.3.1 Differential scanning calorimetry (DSC)

DSC analysis was performed on encapsulated bixin (Fig 3.1a). Samples B0WP90°C, B10WP90°C, B20WP90°C, which were prepared at 90 °C, showed an endothermic peak at 117.2, 105, and 104 °C respectively, which were similar to V-type amylose complexes. The melting was not thermally reversible since the endothermal transitions in the second scan were not observed. The crystalline structures do not return to its initial state after the cooling stage because the rate of heating and cooling used in DSC analysis are higher than those used during of preparation of samples. The necessary time to form these structures at 90 °C seems to be higher than that used in the heating and cooling stages, which makes difficult the recrystallization after them have melted during DSC analysis.

This behavior was observed in other systems as these formed by b-carotene and starch dextrin, the cooling and heating used during DSC analysis migth not be a ideal kinetical process to regenerate crysline structures (KIM; SEO; LIM, 2013). The melting temperatures of samples are similar to the type-II V-amylose complexes, which are characterized by forming partially-ordered structures, with different amorphous and crystalline regions. These complexes have melting temperatures above 100 °C and are excellent matrices with great resistance to heat (KARKALAS et al., 1995; PUTAUX et al., 2008). Although the formation of amylose bixin complex was not confirmed by X-ray diffration. The crystalline structure formed are highly thermical resistent, melting above 100 °C. It is notable that the samples prepared at 60º and 70 °C did not display endothermic transitions (Figure 3.1b). WP may have interfered in the interaction between starch and bixin, competing with the amylose chains by binding to bixin. The increase in protein content led to a decrease in the melting enthalpy ($\Delta H_{melting}$), which had values of 3334.4 J/g for B0WP90°C (0% WP), 1550.4 J/g for B10WP90°C (10% WP) and 1383.8 J/g for S3 B20WP90°C (20% WP). Proteins have a high availability to interact with bixin and this behavior is due, as it was suggested by Zhang & Zhong (2012a), to an increase in the hydrophobicity of protein in alkaline conditions, which leads to increase the active sites that can binding bixin. The hydrophobicity increases due to higher exposure of tryptophan residues on the surface of protein, after unfolding of the WP chains, as a result of denaturation process and the alkaline pH (close to 11) (MONAHAN; GERMAN; KINSELLAT, 1995; ZHANG; ZHONG, 2012b). The increase in the hydrophobicity of the samples with 10% and 20% of WP was probably a factor that avoided the formation of crystallites with higher size, resulting in a lower energy for their melting, thus leading to a decrease in their melting temperature and melting enthalpy. In other starchy systems, the proteins can reduce the binding between amylose and lipids, avoiding the formation of amylose-lipid complexes (Zhang et al., 2003).

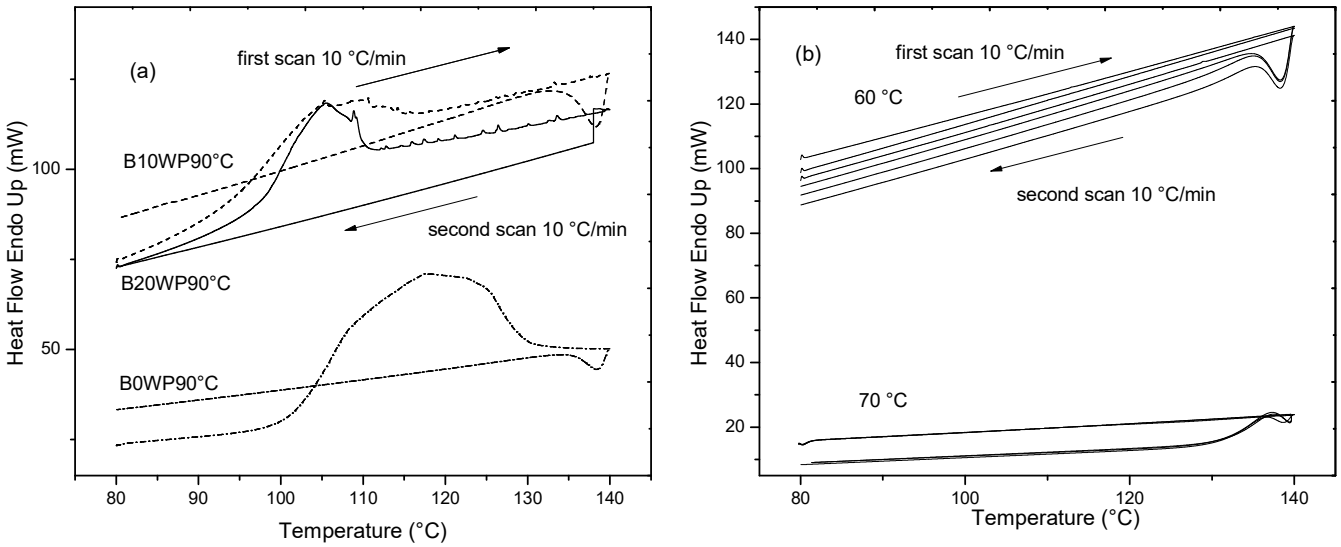

Figure 3.1 Thermograms obtained by differential scanning calorimetry of samples prepared at 90 °C (a). Samples prepared at 60 and 70 °C (b). First and second scan at 10 °C/min.

3.3.2 X-ray diffraction

X-ray diffraction patterns of the treated samples and the control are shown in Figure 3.2. The samples B0WP90°C, B10WP90°C, B20WP90°C (90 °C) showed slight reflections in the Bragg angles, close to 20° (2θ). The samples also displayed a strong diffraction pattern of retrograded amylose, which is suggested by the reflection in the Bragg angle close to 17° and for peaks close to 23° (2θ) similar to those reported by Felker et al. (2013) and Czuchajowska et al. (1991). The samples prepared at 60 and 70 °C showed similar diffraction patterns to those prepared at 90 °C. The thermograms do not show endothermic transitions in the temperature range studied, suggesting no formation of crystalline structure type V-amylose in the treated samples.

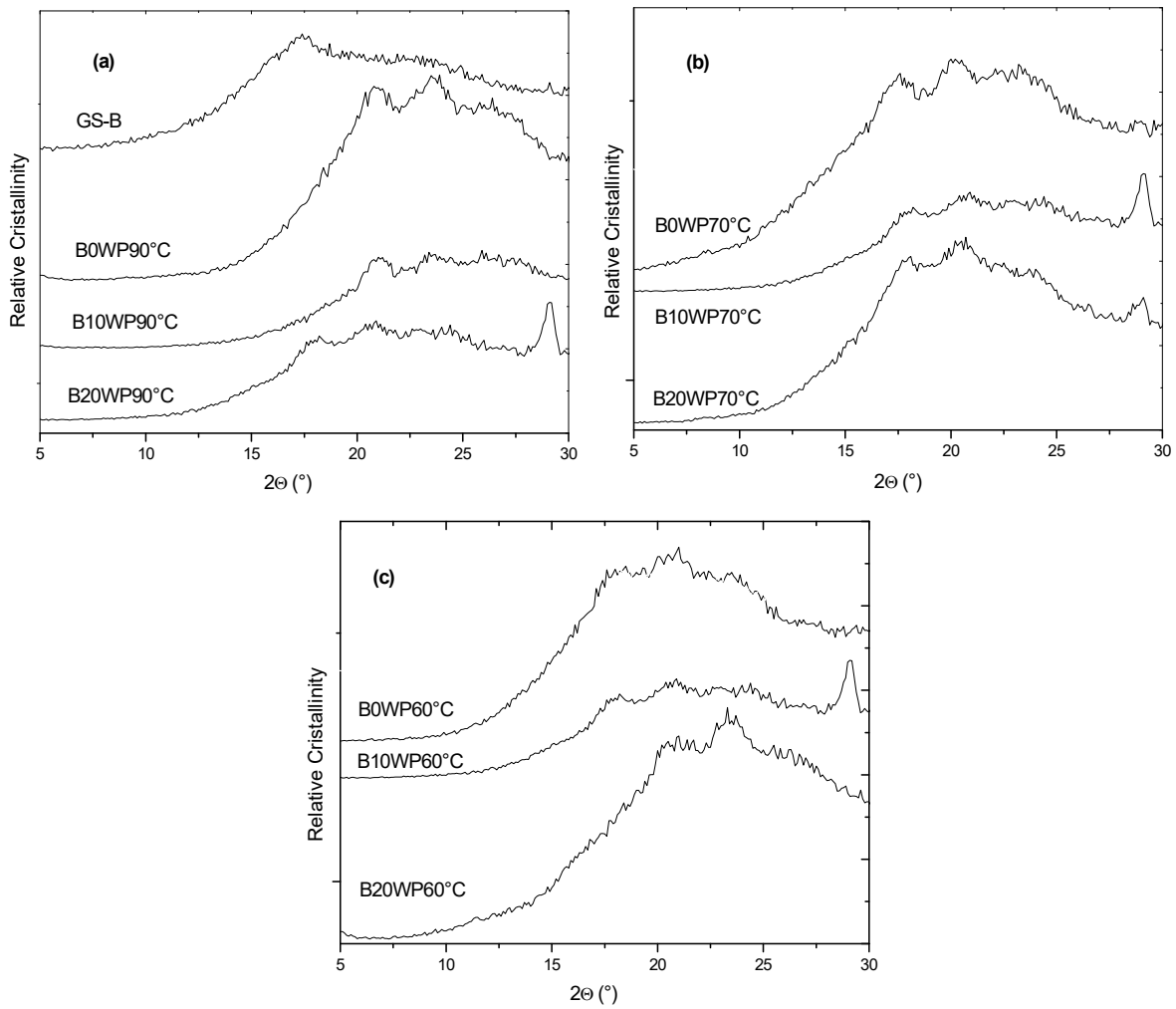

Figure 3.2 X-ray diffraction patterns of samples prepared at 90°C and control sample (GS-B) (a), 70°C (b) and 60 °C (c).

The treatments used to prepare the samples resulted in a tendency for decreasing relative crystallinity (Figure 3.3) with the increase in WP content. This was probably caused by the interaction between WP and bixin, which can reduce the crystalline order (ZHANG; ZHONG, 2012a). Samples prepared without WP showed significant differences ($p < 0.05$) in their relative crystallinity. Similarly, the samples at 60 °C and 90 °C, had significant differences in their relative crystallinity compared to the GS-B. These results seem to affect the release of bixin as it will be discussed in the next sections. Both DSC and XRD analyses confirmed the no formation of V-amylose bixin complexes. Nevertheless, at 90

°C a structure possibly formed by WP-Bixin-Starch is formed, which has a crystalline structure with a melting temperature similar to a V-amylose complex type-II.

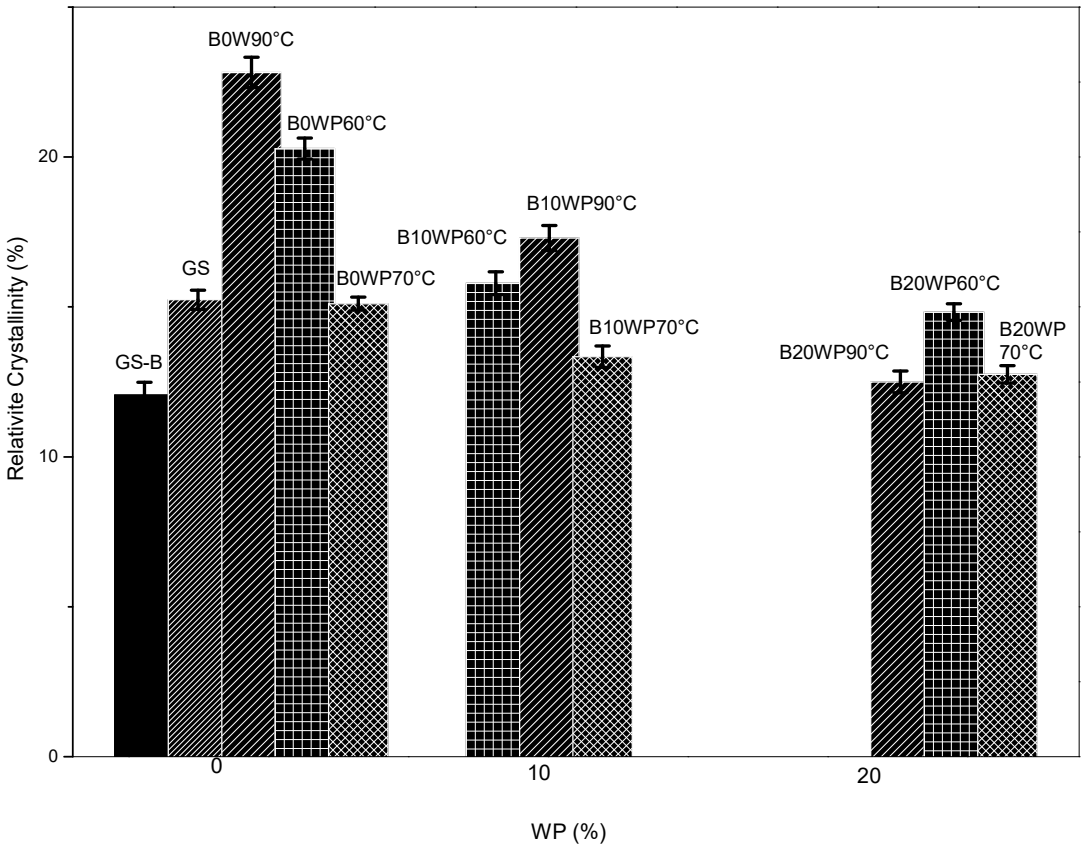

Figure 3.3. Relative crystallinity for samples prepared at 90, 70 and 60 °C, GS-B and GS.

3.3.2 FT-IR spectroscopy.

Figure 3.4 shows the FT-IR spectra of bixin, GS-WP and GS-B, as well as samples of WP and GS with no treatment. The spectra of bixin showed a band at 1744 cm^{-1} which was associated with stretching vibrations of the –C=O group from aliphatic carboxylic acid, and bands associated with stretching vibrations of conjugated C=C groups at 1613 cm^{-1} (Figure 3.4a). Sample GS showed bands between 1200 and 1800 that were correlated with minor components, such as proteins and native lipids present in the starch (Figure 3.4b). On the other hand, characteristic bands of proteins called Amide I, II and III display absorption in the regions between 1600-1700, 1500-1600 and 1200-1350 cm^{-1}, respectively (SINGH, 2000). In this region, WP displayed bands at 1628 cm^{-1} (Amide I)

and 1526 cm^{-1} (Amide II), associated with -C=O and C-N weak stretching and strongly coupled with N-H bending, respectively, as well as a band close to 1231 cm^{-1} (Amide III), which corresponds to twisting of N-H in the plane, coupled with N-N stretching and C-H and N-H deformation vibrations (Figure 3.4b). As it is shown in detail (Figure 3.4c), the bands at 1310 and 1280 cm^{-1} correspond to α-helix and unordered structure, and the band at 1240 cm^{-1} corresponds to the β-sheet conformation of protein (SINGH, 2000). The low intensity of the band at 1280 cm^{-1} indicates that WP has a lower unordered structure content in comparison to α-helix and β-sheet. GS-WP displayed a combination of bands associated with WP and GS, although the band of Amide III was seen to increase in bandwidth (Figure 3.4b). When comparing FT-IR spectra of GS-B, GS-WP and the B0WP90°C, B10WP90°C and B20WP90°C samples, in which a endothermal transition was observed (Figure 3.1a), a band at 1744 cm^{-1} associated with the vibration of the –C=O group of bixin was observed. However, a band at 1613 cm^{-1} of conjugated -C=C- groups of bixin disappeared, indicating that vibration of this group was restricted. On the other hand, the FT-IR spectra of B0WP90, B10WP90 and B20WP90 samples showed narrow bands at the region between 1300 to 1500 cm^{-1} (Figure 3.4d) compared to those of GS-WP and GS-B, which were similar to those observed in the GS sample (Figure 3.4b). Nevertheless, the spectra of B10WP90°C and B20WP90°C showed a broadband (at the Amide I and Amide II regions) compared to B0WP90°C sample. Widening in the bands was associated with the higher WP content. This result indicates that there was an increase in WP availability to interact with bixin. Notwithstanding, these interactions seem to be fewer at a higher temperature of treatment, but enough to affect the thermal stability of the crystalline structures as it was observed in DSC results. On the other hand, after microencapsulation process, the α-helix and β-sheet structures were not observed. This result suggests that the heat treatment and pH affect the secondary structure of WP significantly. The pH can also induce a negative charge on the WP, increasing the repulsion and led to unfolding and loss of the secondary structure of proteins (MONAHAN; GERMAN; KINSELLAT, 1995). In other systems such as that formed by casein and bixin, no effects of thermal treatment on casein-bixin binding were observed, due to the higher thermal stability of casein (ZHANG; ZHONG, 2013). In contrast, Zhang & Zhong (2012b) reported that after the thermal process, the hydrophobicity of the β-Lactoglobulin, which is the major component in whey proteins, increases its availability to interact with bixin. In this study, the results suggest that protein and the temperature treatment reduced the interaction between bixin and amylose chains at 60 and 70 °C,

probably due to the higher facility of WP to bind to bixin. This is in agreement with Zhang and Zhong (2012b), who reported that protein-bixin binding is favored at lower temperatures.

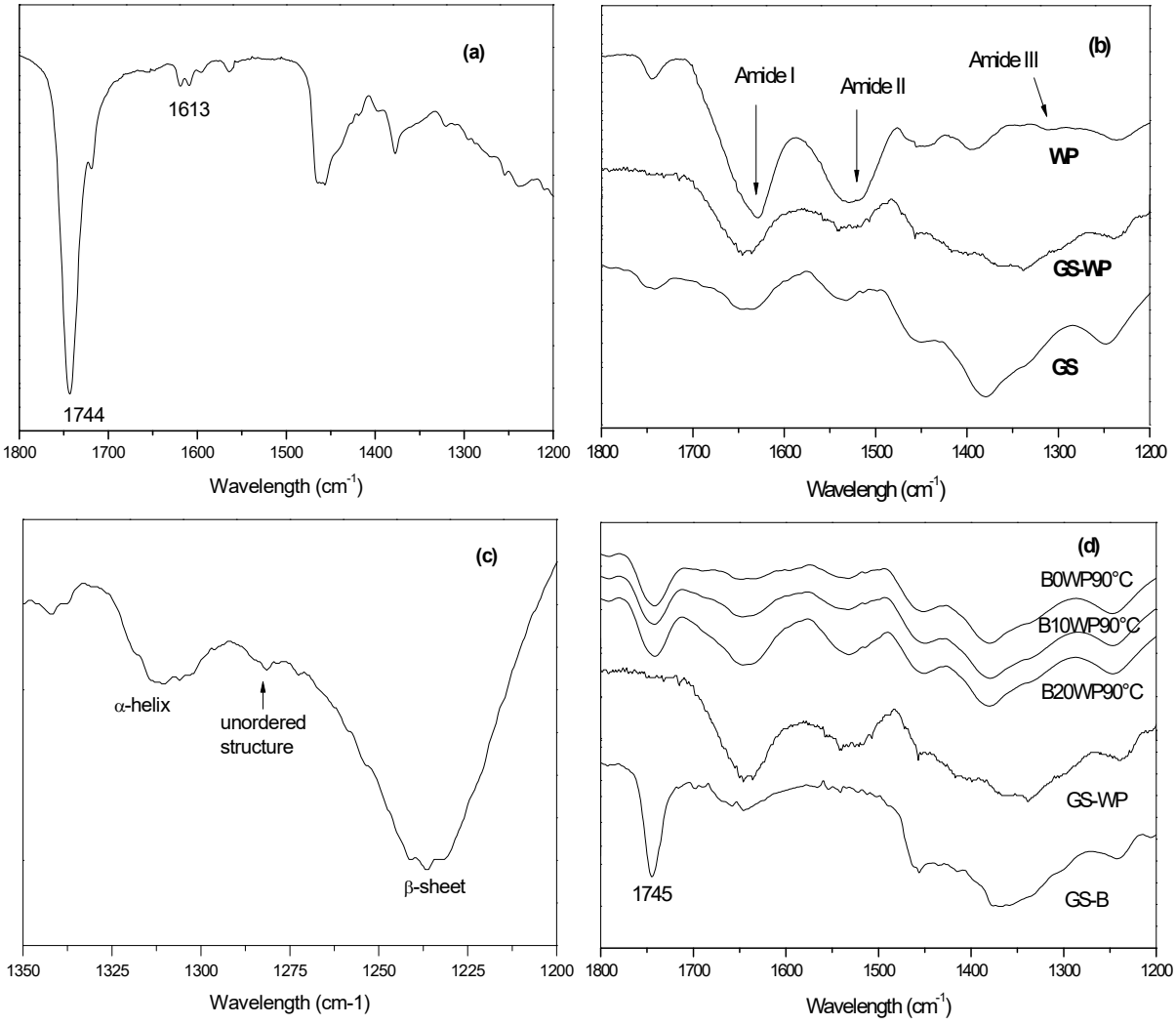

Figure 3.4 FT-IR spectra of Bixin (a), WP, GS-WP, GS (b), α-helix and the β-sheet conformation of WP (c), samples at 90°C (d).

3.3.3 Content of bixin on surface and inside of matrix.

The results of surface and bixin encapsulation are shown in Table 3.2. Bixin content is divided into a fraction that remains on the surface, while the encapsulated fraction is included in the starch/WP matrix. It is probable that only the encapsulated fraction be protected against heat action. In the first set of samples which were prepared without WP, B0WP70 (70 °C) showed a bixin content, both on the surface and encapsulated, higher than B0WP90°C (90 °C) and B0WP60°C (60 °C), even though, as it was previously discussed, only in B0WP90°C it was possible to identify the crystalline structure using DSC. This suggests that only 76 μg of bixin·g^{-1} of total matter corresponds to encapsulated bixin, and that this portion is thermally protected, resulting in an structure highly resistant to heat, as demonstrated by its high melting temperature. Moreover, in the group of samples prepared with 10% w/w WP, B10WP60°C (60 °C) showed higher bixin contents than B10WP90°C (90 °C) and B10WP70°C (70 °C) on the surface (121 μg bixin·g^{-1} of total matter) and encapsulated (568 μg bixin·g^{-1} of total matter), respectively. In this set of samples, the crystalline structure was only identified in B10WP90°C, which had an encapsulated bixin content of about 93 μg bixin·g^{-1} of total matter. Regarding samples with 20% w/w WP, the crystalline structure was identified in B20WP90°C sample (90 °C), which showed encapsulated bixin content higher than in samples B20WP70°C (70 °C) and B20WP60°C (60 °C). In summary, the samples B0WP70°C, B10WP60°C and B20WP90 °C with 0, 10 and 20% w/w WP respectively, showed higher bixin contents. The results of the treatment suggest that, regardless of WP content, at 60 °C the capacity of bixin binding by protein is higher than at 90 °C, which probably is a factor that prevent the microencapsulation of bixin with a crystalline form. In the set of samples prepared at 90 °C, the increase of protein content resulted in a tendency to raise the encapsulated bixin content, indicating that, at this temperature level, the interaction bixin and starch was favored in detriment of WP-bixin interaction. On the other hand, it is also known that upon heating, cis-bixin can polymerize to trans-bixin (MONTENEGRO et al., 2004; RIOS; BORSARELLI; ADRIANA, 2005), and the trans configuration is less polar than the cis isomer; this transition apparently allows the bixin chains to be partially trapped more easily inside the apolar cavity of amylose.

Table 3.2 Values of bixin content on the surface and encapsulated.

Sample	Bixin on Surface µg bixin· g^{-1} of total matter	Encapsulated bixin µg bixin· g^{-1} of total matter
B0WP60°C	72.35 ± 4.98 ^{fg}	126.61 ± 7.78 ^{b}
B10WP60°C	121.02 ± 7.48 ^{de}	568.91 ± 15.7 ^{a}
B20WP60°C	148.36 ± 10.82 ^{d}	58.55 ± 4.61 ^{cd}
B0WP70°C	418.06 ± 9.22 ^{a}	134.19 ± 8.51 ^{b}
B10WP70°C	56.27 ± 12.18 ^{g}	74.75 ± 3.54 ^{cd}
B20WP70°C	94.88 ± 5.83 ^{ef}	51.58 ± 2.32 ^{d}
B0WP90°C	252.52 ± 12.66 ^{b}	76.70 ± 6.89 ^{cd}
B10WP90°C	16.00 ± 6.99 ^{h}	77.64 ± 3.41 ^{cd}
B20WP90°C	78.55 ± 8.17 ^{fg}	128.55 ± 12.7 ^{b}
GS-B	197.57 ± 10.89 ^{c}	98.61 ± 2.35 ^{bc}

Mean value ± Standard deviation. Means with the same letter in the same column indicate no significant difference by the Tukey test ($p < 0.05$).

3.3.4 The release profile of bixin

The release profile of samples in simulated intestinal fluid (SIF) is shown in Figure 3.5. Samples prepared at 60 °C presented a slightly lower release percent compared to WP-B sample after two hours. Meanwhile, samples prepared at 70 °C with WP had a higher release percent. Samples prepared at 90 °C presented a release percent similar to the control in the first two hours, followed by a stabilization until a nearly constant value was reached, becoming more stable against the action of the SIF. The release pattern is seen to be associated with relative crystallinity percent and treatment temperature.

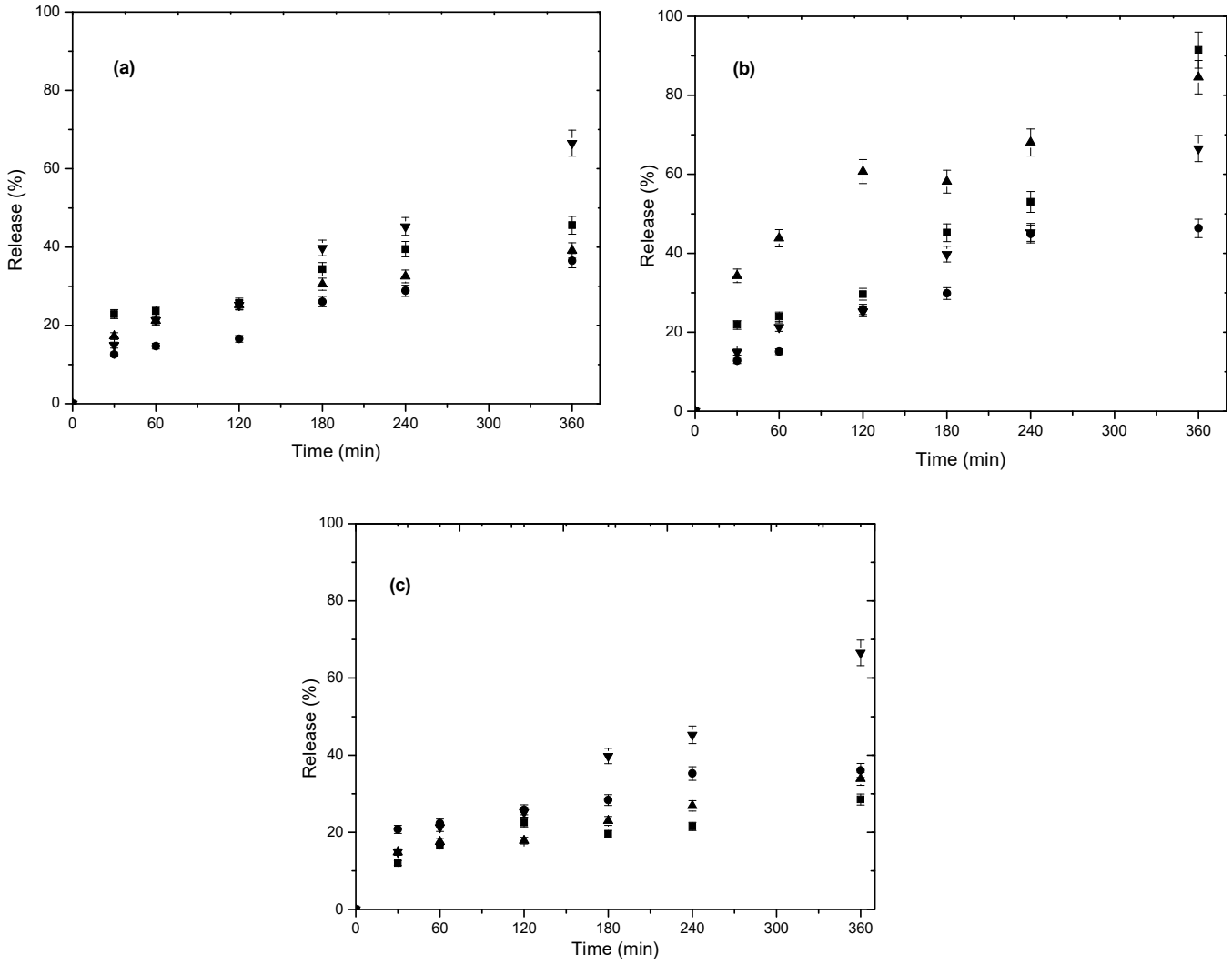

Figure 3.5. Bixin-release profiles of samples prepared at 60 °C (a), 70 °C (b) and 90°C (c). 0% WP (-●-), 10% WP (-■-), 20% WP (-▲-) and GS-B (-▼-).

The sample without protein and with a lower crystallinity percent had a trend to show a higher release percent. Probably, the low crystallinity percent led to a greater effect of the enzymatic action, allowing a higher release percent. This is due to the preference of enzymatic action by amorphous regions (PUTSEYS; LAMBERTS; DELCOUR, 2010). Samples prepared at 60 °C had a release percent of bixin lower than WP-B. Nevertheless, the increase in protein content decreased the release percent. As it was previously discussed, the affinity of the WP for bixin is increased at lower temperature, hindering the SIF action. In samples prepared at 90 °C, an increase in the WP content does not seem to decrease the release percent of bixin. Nevertheless, the release percent of bixin was lower than WP-B. At 70 °C, the WP seems does not have the affinity to binding with

bixin. Also, this condition is not appropriate for forming of crystalline structures, resulting in a higher release percent.

Color analysis

Table 3 shows the color parameters L*, a*, b*, C*, and °hue of the treated and WP-B samples in addition to pure bixin. The parameter L* had higher values in the encapsulated samples than pure bixin, with a trend of being lower than in samples treated at 60 and 70 °C, which can be attributed to the presence of WP and starch. The parameter L* was not affected by the WP content. Regarding parameter a*, in all of the treated samples, a decreasing redness compared to pure bixin was observed. Parameter a* had a tendency to be higher at 70 and 90 °C and lower at 60 °C than the control; this suggests that the redness grows along with the temperature. However, the a* values seem not to rise with the protein content. The treated samples had b* values higher than pure bixin and a pattern of being lower than the control, indicating a higher yellowness compared to pure bixin. Furthermore, there was a disposition for parameter b* to increase along with a rise in temperature. Concerning chroma C*, the treatment samples presented values in the range between 54.09 and 65.05, which were greater than pure bixin, indicating a higher saturation and consequently a higher intense color. In contrast, parameter C* had values lower than the control, indicating a less intense color, which was probably caused by the thermal treatment. The °hue, which represents the color tonality, varied between 51.73 and 62.3 in the second quadrant of the chromaticity diagram, between red (°hue = 0) and yellow (°hue = 90). In all treatment samples, these parameters had values greater than pure bixin, with the trend of being lower than WP-B. The values of the color parameters suggest that the treatment samples are less red, but with a higher intense color and a tendency to be more red orange than the original color of pure bixin. The color parameters a* and b* of the bixin complex, were higher than those reported by De Sousa Lobato et al. (2013), for nanocapsules of bixin (a*=13.54 and b*=25.50) in a suspension prepared by interfacial deposition. Moreover, L* had a lower value in comparison to those observed in the treatment samples at 60, 70 and 90 °C.

Table 3.3 Color parameters for amylose-bixin complexes and the control.

Sample	*L**	*a**	*b**	*C**	*°hue*
B0WP60°C	50.72 ± 0.25 ^{c}	36.86 ± 0.11 ^{c}	48.52 ± 0.26 ^{ef}	60.93 ± 0.20 ^{def}	52.77 ± 0.19 ^{f}
B10WP60°C	45.69 ± 0.59 ^{e}	39.36 ± 0.13 ^{b}	49.89 ± 0.35 ^{de}	63.55 ± 0.35 ^{bc}	51.73 ± 0.10 ^{f}
B20WP60°C	53.22 ± 0.54 ^{b}	34.29 ± 0.11 ^{e}	52.03 ± 0.29 ^{c}	62.31 ± 0.20 ^{cd}	56.61 ± 0.22 ^{cd}
B0WP70°C	51.09 ± 0.28 ^{c}	34.77 ± 0.20 ^{e}	49.45 ± 0.17 ^{de}	60.45 ± 0.13 ^{ef}	54.89 ± 0.11 ^{e}
B10WP70°C	49.50 ± 0.83 ^{d}	29.36 ± 0.40 ^{j}	45.45 ± 0.50 ^{gh}	54.09 ± 0.45 ^{g}	57.15 ± 0.48 ^{c}
B20WP70°C	49.69 ± 0.12 ^{d}	35.40 ± 0.04 ^{d}	50.69 ± 0.20 ^{cd}	61.84 ± 0.15 ^{de}	55.05 ± 0.13 ^{e}
B0WP90°C	53.61 ± 0.14 ^{b}	31.01 ± 0.12 ^{h}	48.56 ± 0.23 ^{ef}	57.64 ± 0.26 ^{g}	57.40 ± 0.04 ^{c}
B10WP90°C	56.28 ± 0.20 ^{a}	30.23 ± 0.10 ^{i}	57.59 ± 0.49 ^{a}	65.05 ± 0.44 ^{a}	62.30 ± 0.21 ^{a}
B20WP90°C	48.85 ± 0.70 ^{d}	31.76 ± 0.16 ^{g}	47.06 ± 0.95 ^{fg}	56.78 ± 0.86 ^{g}	55.98 ± 0.45 ^{de}
GS-B	53.32 ± 0.98 ^{b}	33.48 ± 0.14 ^{f}	55.45 ± 1.16 ^{b}	64.78 ± 0.92 ^{ab}	58.87 ± 0.62 ^{b}
Bixin	30.59 ± 0.79 ^{f}	40.15 ± 0.2 ^{a}	44.98 ± 0.96 ^{h}	59.86 ± 0.62 ^{f}	48.41 ± 0.85 ^{g}

Mean value ± Standard deviation. Means with the same letter in the same column indicate no significant difference by the Tukey test ($p < 0.05$).

3.4 Conclusion

The current study carried out the microencapsulation of bixin using high-amylose corn starch and whey protein. Whey protein and microencapsulation process affected the profile and total amount of bixin released under simulated gastrointestinal fluid conditions. The crystalline structure was favored at higher temperature. Amylose is a good wall material, protecting bixin against heat; this was confirmed by the high melting temperature of the crystalline structure. Future studies are desirable to select the best proportions of starch and whey protein, in order to improve the controlled release system.

3.5 Acknowledgements

The authors thank Coordenação de Aperfeiçoamento de Pessoal de Nível Superior (CAPES) for financial support.

3.6 References

BALASWAMY, K.; PRABHAKARA RAO, P. G.; SATYANARAYANA, A.; RAO, D. G. Stability of bixin in annatto oleoresin and dye powder during storage. **LWT - Food Science and Technology**, v. 39, n. 8, p. 952–956, 2006.

BARBOSA, M. I. M; BORSARELLI, C. .; MERCADANTE, A. . Light stability of spray-dried bixin encapsulated with different edible polysaccharide preparations. **Food Research International**, v. 38, n. 8–9, p. 989–994, 2005.

BILIADERIS, C. G.; GALLOWAY, G. Crystallization behavior of amylose-v complexes: structure-property relationships. **Carbahydrate Research**, v. 189, p. 31–48, 1989.

DE SOUSA LOBATO, K. B.; PAESE, K.; CASANOVA, J.; STANISÇUASKI, S.;

JABLONSKI, A.; DE OLIVEIRA, A. Characterisation and stability evaluation of bixin nanocapsules. **Food Chemistry**, v. 141, n. 4, p. 3906–3912, 2013.

GIRIDHAR, P.; VENUGOPALAN, A.; PARIMALAN, R. A Review on Annatto Dye Extraction, Analysis and Processing – A Food Technology Perspective. **Journal of Scientific Research & Reports**, v. 3, n. 2, p. 327–348, 2014.

ITTHISOPONKUL, T.; MITCHELL, J. R.; TAYLOR, A. J.; FARHAT, I. a. Inclusion complexes of tapioca starch with flavour compounds. **Carbohydrate Polymers**, v. 69, n. 1, p. 106–115, 1 maio 2007.

KARKALAS, J.; MA, S.; MORRISON, W. R.; PETHRICK, R. a. Some factors determining the thermal properties of amylose inclusion complexes with fatty acids. **Carbohydrate Research**, v. 268, n. 2, p. 233–247, 1995.

KIM, J.; SEO, T.; LIM, S. Preparation of aqueous dispersion of b-carotene nano-composites through complex formation with starch dextrin. **Food hydrocolloids**, v. 33, n. 2, p. 256–263, 2013.

LALUSH, I.; BAR, H.; ZAKARIA, I.; EICHLER, S.; SHIMONI, E. Utilization of amylose-lipid complexes as molecular nanocapsules for conjugated linoleic acid. **Biomacromolecules**, v. 6, n. 1, p. 121–130, 2005.

LESMES, U.; BARCHECHATH, J.; SHIMONI, E. Continuous dual feed homogenization for the production of starch inclusion complexes for controlled release of nutrients. **Innovative Food Science & Emerging Technologies**, v. 9, n. 4, p. 507–515, out. 2008.

LYNG, S. M.; PASSOS, M.; FONTANA, J. D. Bixin and α-cyclodextrin inclusion complex and stability tests. **Process Biochemestry**, v. 40, n. 2, p. 865–872, 2005.

MARCOLINO, V. A.; ZANIN, G. M.; DURRANT, L. R.; BENASSI, M. D. T.; MATIOLI, G. Interaction of curcumin and bixin with β-cyclodextrin: Complexation methods, stability, and applications in food. **Journal of Agricultural and Food Chemistry**, v. 59, n. 7, p. 3348–3357, 2011.

MONAHAN, F. J.; GERMAN, J. B.; KINSELLAT, J. E. Effect of pH and Temperature on Protein Unfolding and Thiol/ Disulfide Interchange Reactions during Heat-Induced Gelation of Whey Proteins. **J. Agric. Food Chem**, v. 43, n. 1, p. 46–52, 1995.

MONTENEGRO, M. A.; RIOS, A. D. O.; MERCADANTE, A. Z.; NAZARENO, M. A.; BORSARELLI, C. D. Model Studies on the Photosensitized Isomerization of Bixin. **Journal of Agricultural and Food Chemistry**, v. 52, n. 2, p. 367–373, 2004.

NUESSLI, J.; SIGG, B.; CONDE-PETIT, B.; ESCHER, F. Characterization of amylose—flavour complexes by DSC and X-ray diffraction. **Food Hydrocolloids**, v. 11, n. 1, p. 27–34, jan. 1997.

OBIRO, W. C.; SINHA RAY, S.; EMMAMBUX, M. N. V-amylose Structural Characteristics, Methods of Preparation, Significance, and Potential Applications. **Food Reviews International**, v. 28, n. 4, p. 412–438, out. 2012.

PARIZE, A. L.; CRISTINA, T.; SOUZA, R. De; MARIA, I.; BRIGHENTE, C.; FÁVERE, V. T. De; LARANJEIRA, M. C. M.; SPINELLI, A.; LONGO, E. Microencapsulation of the natural urucum pigment with chitosan by spray drying in different solvents. **African Journal of Biotechnology**, v. 7, n. 17, p. 3107–3114, 2008.

PRESTON, H. D.; RICKARD, M. D. Extraction and chemistry of annatto. **Food Chemistry**, v. 5, n. 1, p. 91–107, 1980.

PUTAUX, J.-L.; CARDOSO, M. B.; DUPEYRE, D.; MORIN, M.; NULAC, A.; HU, Y. Single Crystals of V-Amylose Inclusion Complexes. **Macromolecular Symposia**, v. 273, n. 1, p. 1–8, nov. 2008.

PUTSEYS, J. a; LAMBERTS, L.; DELCOUR, J. a. Amylose-inclusion complexes: Formation, identity and physico-chemical properties. **Journal of Cereal Science**, v. 51, n. 3, p. 238–247, 2010.

RAHMALIA, W.; FABRE, J.-F.; USMAN, T.; MOULOUNGUI, Z. Aprotic solvents effect on the UV-visible absortion spectra of bixin. **Spectrochimica Acta Part A: Molecular and Biomolecular Spectroscopy**, v. 131, p. 455–460, 2014.

RIOS, A. de O.; BORSARELLI, C.; ADRIANA, M. Thermal Degradation Kinetics of Bixin in an Aqueous Model System. **Journal of Agricultural and Food Chemistry**, v. 53, n. 6, p. 2307–2311, 2005.

RODRIGUEZ-AMAYA, D. B. **A Guide to carotenoide analysis in foods**. Washington, D.C: ILSI PRESS, 2001.

SINGH, B. R. Basic Aspects of the Technique and Applications of Infrared Spectroscopy of Peptides and Proteins. In: SING, B. R. (Ed.). **Infrared Analysis of Peptides and proteins: principles and aplication**. Washington, D.C: ACS symposium serie, 2000. p. 190.

SUTTER, S. C.; BUERA, P.; ELIZALDE, B. E. Beta-Carotene encapsulation in a mannitol matrix as affected by divalent cations and phosphate anion. **International journal of pharmaceutics**, v. 332, n. 1–2, p. 45–54, 2007.

WROLSTAD, R. E.; CULVER, C. A. Alternatives to Those Artificial FD&C Food Colorants. **Annual Review of Food Science and Technology**, v. 3, p. 59–77, 2012.

WULFF, G.; AVGENAKI, G.; GUZMANN, M. S. P. Molecular encapsulation of flavours as helical inclusion complexes of amylose. **Journal of Cereal Science**, v. 41, n. 3, p. 239–249, maio 2005.

ZABAR, S.; LESMES, U.; KATZ, I.; SHIMONI, E.; BIANCO-PELED, H. Structural characterization of amylose-long chain fatty acid complexes produced via the acidification method. **Food Hydrocolloids**, v. 24, n. 4, p. 347–357, jun. 2010.

ZHANG, G.; MALADEN, M. D.; HAMAKER, B. R. Detection of a novel three component complex consisting of starch, protein, and free fatty acids. **Journal of Agricultural and Food Chemistry**, v. 51, n. 9, p. 2801–2805, 2003.

ZHANG, Y.; ZHONG, Q. Effects of Thermal Denaturation on Binding between Bixin and Whey Protein. **Journal of Agricultural and Food Chemistry**, v. 60, n. 30, p. 7526–7531, 2012a.

ZHANG, Y.; ZHONG, Q. Binding between bixin and whey protein at pH 7.4 studied by spectroscopy and isothermal titration calorimetry. **Journal of Agricultural and Food Chemistry**, v. 60, n. 7, p. 1880–1886, 2012b.

ZHANG, Y.; ZHONG, Q. Encapsulation of bixin in sodium caseinate to deliver the colorant in transparent dispersions. **Food hydrocolloids**, v. 33, n. 1, p. 1–9, 2013.

CAPÍTULO 4. OPTIMIZATION OF ENCAPSULATE BIXIN CONTENT IN STARCH MATRIX

OPTIMIZATION OF ENCAPSULATE BIXIN CONTENT IN STARCH MATRIX

Ezequiel José Pérez-Monterroza[1]*, Vânia Regina Nicoletti [1]

1 Department of Food Engineering and Technology; São Paulo State University (Unesp), Institute of Biosciences, Humanities and Exact Sciences (Ibilce), Campus São José do Rio Preto; Rua Cristovão Colombo 2265, Zip Code 15054-000 São José do Rio Preto, SP, Brazil.

Abstract

Encapsulation of bixin was carried out by ultrasound treatment and alkaline method, using amylose extracted from cassava starch and high-amylose corn starch (Hylon VII). The effect of process conditions on encapsulated bixin content was determined by employing UV-vis spectroscopy and modeled using the response surface methodology. In addition, optimum process conditions were determined by using desirability functions. Bixin content obtained using the alkaline method ranged from 910 µg/g to 6475 µg/g for encapsulated bixin inside of matrix and from 96 to 10330 µg/g for bixin on surface of matrix. Encapsulated bixin by using ultrasound treatment ranged between 1234 to 3788 µg/g for bixin inside of matrix, and between 267 to 6210 µg/g for bixin on the surface. Encapsulation efficiency ranged between 13.1% to 62.1% and 17.3% to 94.5% using ultrasound and the alkaline method respectively. The optimum conditions were found as 2% amylose, 150 W and 20 min for ultrasound treatment. In case of the alkaline method the best conditions were 2% amylose from cassava with protein at 68 °C. Finally, there were no differences between encapsulated bixin content under optimum and experimental conditions in the model validation.

Keywords: Whey protein, RSM, optimization, carotenoid, cassava.

4.1 Introducction

Bixin represents about 80% of carotenoids content in the annatto (*Bixa Orellana*) seeds. Its structure contains a system of double bonds, which affect their stability and makes them susceptible to physical and oxidative degradation induced during the processing and storage (MONTENEGRO et al., 2004; RIOS; BORSARELLI; ADRIANA, 2005). Microencapsulation is a technology by which bioactive molecules are packed inside of carrier or wall material, improving their stability or solubility (FATHI; MARTÍN; MCCLEMENTS, 2014). Generally, drying methodologies are used for development of microencapsulation systems, turning the bioactive compound into powder. These types of technologies commonly use carbohydrates or proteins as wall materials, which include starch, cellulose, pectin, guar gum, chitosan, alginate, dextrin, cyclodextrin, gums and their combinations (MARCOLINO et al., 2011; RODEA-GONZÁLEZ et al., 2012; FATHI; MARTÍN; MCCLEMENTS, 2014; JANISZEWSKA-TURAK, 2017). In the case of carotenoids as bixin, the microencapsulation improve their stability against light and enhance their solubility (LYNG; PASSOS; FONTANA, 2005a). In the last few years, preference of consumers by oral comsumption of bioactive compounds has notably increased, which motive the continuous search of technologies and delivery systems that improve the bioavailability of bioactive agents (MCCLEMENTS; LI, 2010; BRAITHWAITE et al., 2014; GIRIDHAR; VENUGOPALAN; PARIMALAN, 2014).

In our previous studies about bixin microencapsulation, we explored the possibility of preparation of V-amylose complex by ultrasound treatment and using the alkaline method. The results indicated that there was no formation of V-amylose complexes. Nevertheless, the results obtained with both methods suggested that it is possible to obtain a good encapsulation matrix, resulting in a system with several delivery patterns. For this reason, this study aimed to choose the best condition and to compare these two encapsulation methodologies. The best condition was selected using the response surface methodology (RSM). The RSM is a statistical tool based on in the fitting of experimental data to a polynomial equation. The model provides by RSM describe and predict the statistical behavior of experimental data (GILMOUR, 2006; BEZERRA et al., 2008). The RSM is one of the most common optimization methods applicable to design, improvement, and formulation of new products and also development of existing products properties (BAS; BOYACI, 2007). It is useful in the resolve of optimization problems in

the engineering of food. The RSM has advantage over methodologies such as the optimization of one-variable-at-a-time, due it is possible to determine the effects and interactions of the parameters in the study (BEZERRA et al., 2008). For this reason, The RSM was used to determine the best conditions in the microencapsulation of bixin.

4.2 Material and Methods

High-amylose (72 % of amylose, according to manufacturer) corn starch (Hylon VII) was obtained from Ingredion Brasil Ing. Ind. Ltda (Mogi Guaçu, SP, Brazil). Bixin was obtained from BKG (Adicon, Brazil). Whey protein concentrate (WP) was obtained from Alibra ingredients Ltda (SP, Brazil). Sodium hydroxide (NaOH) was supplied by Synth (Diadema, Brazil), hydrochloric acid was provided by Quimis (Diadema, Brazil), and pancreatin was provided by Sigma-Aldrich (St. Louis, MO). Starch suspensions were prepared using deionized water. All chemicals were of analytical grade.

4.2.1 Fractionation of cassava starch.

Amylose was isolated from cassava starch by precipitation with ethanol according to methodology proposed by Mua and Jackson (1995). A dispersion of cassava starch (2% w/w) was heated at 70 °C for 20 min. The obtained solution was cooled to 40 °C and centrifuged at 3500×g for 10 min. The supernatant was separated and the amylose was precipitated using ethanol (95% v/v). This precipitate was separated by centrifugation at 1500×g for 3 min and stored at 8 °C until used.

4.2.2 Encapsulation using the alkaline method

One hundred and fifty grams of the suspension of Hylon VII starch or of amylose fractionated from cassava starch were mixed with bixin (0.1 g) in 0.01 M KOH solution (50 g) at temperatures and concentration according to the experimental design shown in Table 4.1, followed by precipitation at pH 4.5 using 0.01M HCl. The precipitate was separated by centrifugation at 3500×g for 10 min, was cooled at -18 °C for 12 hours and lyophilized. When the use of whey protein (WP) was necessary, it was added to the starch suspension according to Table 4.1.

4.2.3 Encapsulation by ultrasound treatment

Ninety grams of high-amylose corn starch suspension (GS) were mixed with bixin (0.2 g) in 0.01 M KOH solution (50 g) at 60 °C for 1 min. This mixture was subjected to ultrasound treatment according to the experimental design shown in Table 3 at 78 °C in an ultrasonic homogenizer (Omni Ruptor 4000, Omni International, Marietta, USA) equipped with a standard probe 1.9 mm in diameter. The pH was adjusted to 4.7 using 0.01 M HCL solution and the samples were stored at 47 °C for 12 h. After that, the gels formed were frozen at -18 °C and lyophilized.

4.2.4 Surface and bixin encapsulation

The surface and encapsulated bixin contents were determined according to Lalush et al. (2005a) and Sutter et al. (2007), with modifications. Surface bixin was determined by washing 0.010 g of the complex with 4 mL of acetone in a test tube and shaking in a vortex for 2 min. After sedimentation, the powder was separated and the concentration of bixin in the acetone was measured spectrophotometrically at 457 nm. Encapsulated bixin in the remaining powder was determined by degradation of the complex with pancreatin. The powder was incubated in 4 mL of pancreatin solution at 37 °C for 36 h. Then, bixin was extracted with 7 mL of acetone, centrifuged, filtered and quantified spectrophotometrically at 457 nm. This wavelength was found to correspond to the maximum absorbance of the used bixin, in the spectrum range of 200 to 800 nm. For preparing the pancreatin solution, 0.18 g of pancreatin was dissolved in 20 mL of phosphate buffer 20 mM (pH 7.0) containing NaCl (0.04 % w/w). This solution was centrifuged (9000×g, 10 min), the supernatant was filtered and used for the test. Bixin content in the complex (BC) was calculated for each formulation as μg of bixin per g (RODRIGUEZ-AMAYA, 2001; RAHMALIA et al., 2014). The analyses were carried out in duplicate.

4.2.5 Color analysis

The color parameters of the freeze-dried samples was determined using a ColorFlex model 45/0 spectrophotometer (Hunterlab, USA) with the D65 illuminant and observer at 10^{o}. The 4.10 version of Universal software was used to determine the absolute values of L^*, a^*, and b^*. The system used for specification of color was CIELAB. Values of L^* (lightness) range between zero (black) and one hundred (white),

a^* between -a^* (green) and +a^* (red), and b^* between -b^* (blue) and +b^* (yellow). The chroma (C*), which expresses the degree of intensity or saturation of the color (Eq. 1), and the hue angle (°*hue*), which represents the tonality of the color (Eq. 2), were calculated. The analyses were carried out in triplicate.

$$C^* = \sqrt{(a^*)^2 + (b^*)^2} \quad (1)$$

$$°hue = arctg\left(\frac{b^*}{a^*}\right) \quad (2)$$

4.2.6 Experimental design

Response surface methodology was used for modelling response (encapsulated bixin inside of matrix, encapsulated bixin outside of matrix and color parameters). Determination of the effects of each factor on the microencapsulation of bixin was performed using d-optimal design. In the microencapsulation by alkaline method two numerical factors were used: the concentration of amylose between 2 to 8%, heating temperature between 60 to 90 °C, and two categorical factors: type of starch (Hylon VII or cassava amylose), and presence of whey protein. In the microencapsulation by ultrasound three numerical factors were used: concentration of amylose between 2% to 8%, ultrasound power between 50% (150 W) to 100% (300 W) of the maximum, time of ultrasound treatment between 20 to 40 min. The experimental design consisted of 13 and 10 points for the model in the encapsulation by precipitation from acid solution and by ultrasound, respectively, 5 points to determine lack of fit, and 5 replicates. Statistical analysis of the experimental design was defined for a significance level of 5%, The optimum levels of independent values were analyzed by using the desirability function method. Design-Expert Software 8.0.5 (Statease Inc., Minneapolis, USA) was used for regression, analysis of variance (ANOVA) and optimization. The behavior of factors for predicting the response variables was explained by Equation 3.

$$Y = \beta_0 + \beta_A A + \beta_B B + \beta_C C + \beta_D D + \beta_{A^2} A^2 + \beta_{B^2} B^2 + \beta_{C^2} C^2 + \beta_{D^2} D^2$$
$$+\beta_{AB} AB + \beta_{AC} AC + \beta_{AD} AD + \beta_{BC} BC + \beta_{BD} BD + \beta_{CD} CD \quad (3)$$

In which Y is the response, β_0 is the intercept, β_A, $\beta_B, \beta_C, \beta_D$ are the coefficients of the linear terms, $\beta_{A^2}, \beta_{B^2}, \beta_{C^2}, \beta_{D^2}$ are the coefficients of the quadratic terms, and β_{AB}, $\beta_{AC}, \beta_{AD}, \beta_{BC}, \beta_{BD}, \beta_{CD}$ are the coefficients of interaction terms. The optimum processing conditions were determined for responses by using the desirability function $(d_i(Y_i))$. Desirability function for each response is a function ranging between zero (undesirable $(d_i(Y_i)) = 0$) and unity (desirable or ideal value $(d_i(Y_i)) = 1$) and the optimization finds a point that maximixe this function; for several factors, the desirability function is combinated into one desirability function called D.

$$D = ((d_1(Y_1)d_2(Y_2) \dots d_k(Y_k))^{\frac{1}{k}} \quad (4)$$

D is the geometrical mean of individual desaribilities or overral desirability, $d_1(Y_1)$, $d_2(Y_2), d_k(Y_k)$ are the individual desirability for each response, k is the number of response.

$$d_i(Y_i) = \begin{cases} 0 \; if \; Y_i(x) < L_i \\ \left(\frac{Y_i(x) - L_i}{T_i - L_i}\right) \; if \; L_i \leq Y_i(x) \leq L_i \\ 1 \quad if \; Y_i(x) > T_i \end{cases}$$

Li, Ui and Ti are the lower, upper, and target values that are desired for response Yi, with Li ≤ Ti ≤ Ui.

4.3 Results and discussion

4.3.1 Efficiency of bixin encapsulation

Table 4.1 shows the values of bixin content on the surface, inside the starch matrix, and encapsulation efficiency obtained using the alkaline method. Table 4.2 shows the coefficients of the model according to Equation 3. An analysis of variance (ANOVA) indicated that the factors amylose concentration, heating temperature, type of starch used, presence of whey protein and interaction terms were all significant ($p < 0.05$). Presence of protein was not significant on L^* parameter. The encapsulated bixin is represented by two fractions. The first one is located on the surface and the other remains inside of the

wall material. The last of them probably is protected against heat and gastrointestinal action. Response values (minimum and maximum) from the experimental design ranged from 910 µg/g to 6475µg /g for encapsulated bixin inside of matrix, and from 96 µg/g to 10330 µg/g for bixin on the surface. The higher encapsulated bixin content inside of matrix was obtained under the following conditions: 90 °C with cassava amylose and protein. The encapsulation efficiency (E*e*) was obtained from the Equation 4.

$$Ee\ (\%) = \frac{C_i}{C_T} x\ 100 \qquad (4)$$

In which C_i represents the encapsulated bixin content inside starch matrix and C_T the total bixin content in the starch matrix.

The determination coefficient R^2_{adj} is reasonably close to R^2_{pred}, with a difference lower than 0.2. The determination coefficient R^2_{adj} of models was higher than 0.83 in both methods. This indicates that the models explain more than 83% of data of experimental design. The model has non-significant lack of fit, for this reason, can be used for predictive proposes.

Table 4.1 Surface and encapsulated bixin, and encapsulation efficiency obtained using the alkaline method.

Run	Factors				Bixin content outside of matrix (µg/g)	Bixin content inside of matrix (µg/g)	Total bixin content (µg/g)	Encapsulation efficiency (%)
	A Amylose (%)	**B** Temperature (°C)	**C** Type of starch	**D** Whey protein				
1	2.5	63	Hylon VII	Presence	1736.3	2693.5	4429.8	60.8
2	5.5	78	Hylon VII	Absence	2859.7	967.2	3826.9	25.3
3	2.1	78	Cassava	Absence	10330.1	5685.4	16015.5	35.5
4	5.6	60	Hylon VII	Presence	1890.9	2133.9	4024.8	53.0
5	4.4	73	Cassava	Presence	1156.2	5140.9	6297.1	81.6
6	8.0	60	Hylon VII	Absence	2488.1	1037.3	3525.4	29.4
7	5.0	84	Hylon VII	Presence	1226.5	2374.0	3600.5	65.9
8	6.9	75	Cassava	Absence	2180.0	3252.9	5432.9	59.9
9	2.1	78	Cassava	Absence	9177.7	5445.7	14623.3	37.2
10	2.0	90	Hylon VII	Absence	4266.8	1135.1	5401.8	21.0
11	5.6	60	Cassava	Absence	96.00	1644.0	1740.0	94.5
12	7.9	72	Cassava	Presence	612.8	2471.5	3084.2	80.3
13	7.9	72	Cassava	Presence	551.7	2648.3	3200.0	82.8
14	5.6	60	Hylon VII	Presence	2768.8	2289.4	5058.2	45.7
15	7.4	90	Hylon VII	Absence	584.5	1621.0	2205.5	73.5
16	8.0	90	Hylon VII	Presence	712.4	2106.6	2818.9	74.8
17	2.0	60	Cassava	Presence	3190.7	5338.2	8528.9	62.6
18	2.1	78	Hylon VII	Presence	3402.6	2280.6	5683.2	40.1
19	5.5	78	Hylon VII	Absence	3076.6	910.0	3986.6	22.8
20	4.4	90	Cassava	Presence	5098.0	6100.9	11198.9	54.5
21	2.0	60	Hylon VII	Absence	4589.1	958.1	5547.3	17.3
22	8.0	90	Cassava	Absence	1165.0	5054.6	6219.6	81.3
23	4.4	90	Cassava	Presence	5980.2	6475.2	12455.4	51.9

Table 4.2 Coefficients of the linear, quadratic and interaction terms for the model in the encapsulation using the alkaline method.

	Bixin content inside of matrix	Bixin content outside of matrix	*L**	*a**	*b**	*°hue*
β_0	2895.7	3023.2	44.7	32.3	38.2	48.5
β_A	-783.1	-2216.3	4.2	0.1	4.0	3.7
β_B	871.1	930.4	-6.0	0.8	-2.9	-3.5
β_C	-1353.4	-431.8	10.0	-0.3	6.8	5.7
β_D	455.7	-578.7	n.s	0.4	3.4	2.4
β_{AB}	209.2	-648.1	n.s	1.2	1.0	n.s
β_{AC}	753.5	1462.7	n.s	-3.2	-4.9	-2.1
β_{AD}	-260.3	734.6	n.s	-2.4	-1.0	0.9
β_{BC}	-800.1	-1546.4	n.s	0.8	4.2	3.3
β_{BD}	-210.1	25.5	n.s	n.s	n.s	n.s
β_{CD}	126.2	115.0	n.s	-1.9	n.s	n.s
β_A^2	131.5	844.2	n.s	n.s	-2.1	n.s
β_B^2	65.3	-787.5	n.s	n.s	2.1	n.s
β_C^2	n.s	n.s	n.s	n.s	-2.7	n.s
β_D^2	n.s	n.s	n.s	n.s	n.s	n.s
R^{2pred}	0.83	0.83	0.85	0.92	0.99	0.95
R^{2adj}	0.98	0.89	0.82	0.97	0.98	0.98
C.V. %	8.35	28.20	12.0	1.82	2.63	2.52
Press	1.07e7'	1.07e8'	838.40	23.06	60.02	57.13
Model (p-value)	< 0.0001	< 0.0001	<0.0001	< 0.0001	< 0.0001	< 0.0001

n.s: non-significant term

In general, the encapsulation of bixin using alkaline method and amylose from cassava starch presented a higher encapsulated bixin content than obtained with Hylon VII (Figure 4.1). This was probably because isolated amylose from cassava starch may have a greater film-forming ability, which entrapped the bixin and gave more protection during processing. Barbosa et al. (2005) reported that bixin encapsulated with maltodextrin had lower encapsulation efficiency probably due to low film-forming ability of maltodextrin when compared to gum Arabic. It is known that the quantity of a guest molecule inside of delivery systems is affected by the type of formulation and technique used (DE SOUSA LOBATO et al., 2013). In the present study, the differences in the composition of each formulation and the types of starch used also resulted in a bixin content outside of matrix different from these obtained inside of matrix. Indeed, starches from different botanical sources differ in their structural characteristics, resulting in differences in their gelatinization, pasting and retrogradation properties (SRICHUWONG; JANE, 2007). Spada et al (2012) suggested that carotene on surface degrade more easily during drying process and this increase the losses of carotene. The influence of type of starch on the carotenoid surface content was also reported by Loksuwan (2007). These authors used acid-modified tapioca starch, native tapioca starch, and maltodextrin as wall material in the encapsulation of β-carotene by spray drying, obtaining a lower surface carotene content using modified tapioca starch than obtained with native tapioca starch. In microencapsulation of β-carotene by freeze-drying using native pinhão starch, hydrolyzed pinhão starch and their mixtures with gelatin as coating material, the hydrolyzed pinhão starch showed lower carotenoid content than observed with native pinhão starch (SPADA et al., 2012).

The encapsulated bixin using 2% of amylose was higher than obtained with 8% of amylose, suggesting that probably an increase in the viscosity of starch dispersion during encapsulation process affects the diffusivity of bixin, resulting in a decrease in the encapsulated bixin content.

Figure. 4.1 shows a three-dimensional response plots in function of two factors and keeping the other constant for the encapsulated bixin inside of matrix. In the microencapsulation by alkaline method, the encapsulate bixin content inside of matrix

increase with the presence of proteins, regardless of the type of amylose used. Also increases with the increase in the temperature (at 8% of amylose) (Figure 1, a-1 e a-2).

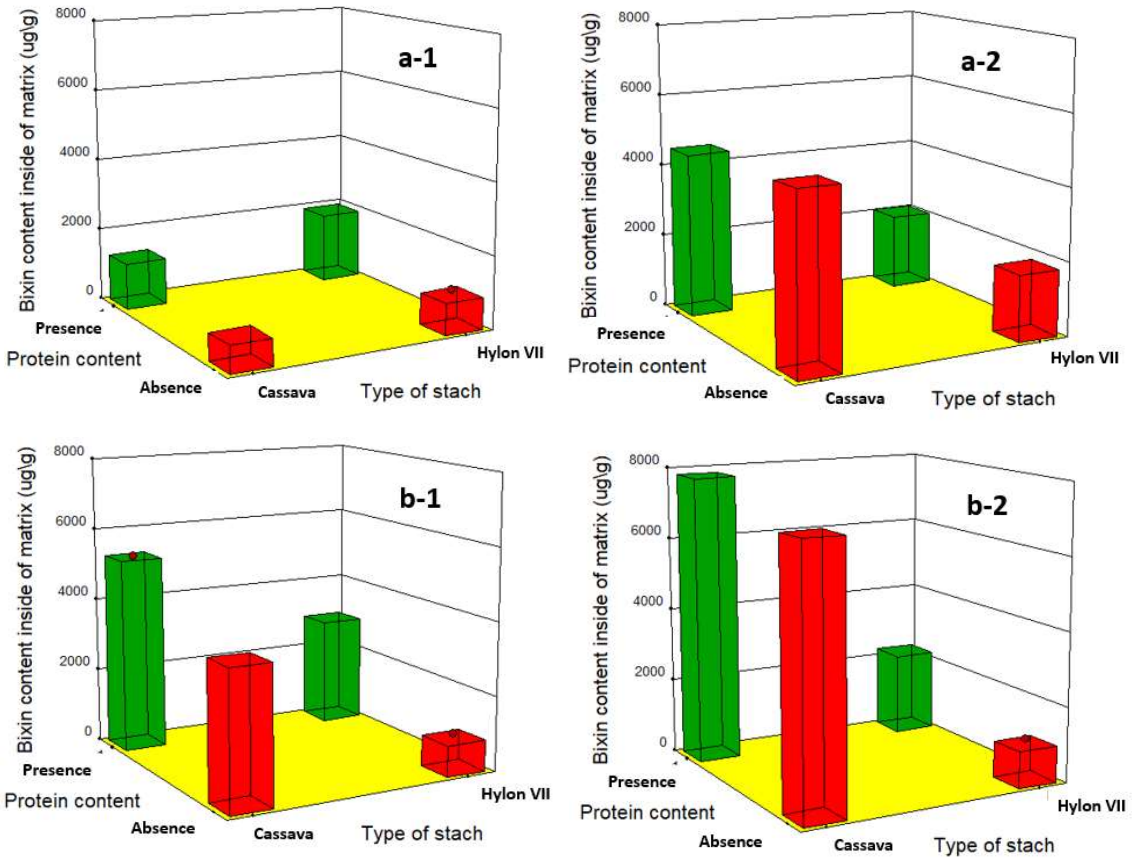

Figure 14.1 Response plot for the effect of whey protein presence and type of starch. 8 % (a) and 2 % (b), at 60 °C (1) and 90 °C (2).

Regarding the encapsulation process by ultrasound, Table 4.3 shows the surface and bixin encapsulated obtained by the alkaline method. Table 4.4 shows the coefficients of the model according to Equation 3. The analysis of variance (ANOVA) indicated that the factors were all significant (amylose, power level and time) ($p < 0.05$). Interaction terms were not significant on L^* parameter. Encapsulated bixin ranged between 1234 µg /g to 3788µg/g for bixin inside of matrix, and between 267µg/g to 6210 µg/g for bixin on the surface. There was a tendency to increase the encapsulated bixin inside of matrix with an increase in the ultrasound power level when using 8% of amylose, regardless of treatment time (Figure 4.2).

It should be noted that the maximum values achieved for this method were higher than those obtained with Hylon VII without protein in the alkaline method. The sonication is a method that causes degradation of retrograded molecules and chemical modification of starch, leading to the reduction in particle size, molar mass and formation of shorter chains (BAXTER; ZIVANOVIC; WEISS, 2005; MONTALBO-LOMBOY et al., 2010; ZHU et al., 2012). It is probably that short chains allow more easily the accommodation of the bixin molecules, increasing the encapsulated bixin content. Spada et al. (2012) suggested that in the case of encapsulation of β-carotene using hydrolyzed starch, the small molecules of the hydrolysates may facilitate the packing of the carotene in the matrix. On the other hand, the encapsulated bixin was higher at low concentration of Hylon VII and treatment time of 20 min (Figure 4.2a). It seems that an increase in the material content might lead to a decrease in the encapsulated material. Rocha et al. (2012) encapsulated lycopene by spray drying using modified starch and obtaining efficiency between 21% to 29 %. Shu et al. (2006) encapsulated lycopene in gelatin and sucrose by spray dryer as well, and both authors reported that a higher wall material content induced to lower encapsulation efficiency.

Table 4.3. Surface and encapsulated bixin, and encapsulation efficiency obtained by ultrasound treatment.

Run	Factors			Bixin content inside of matrix (µg/g)	Bixin content outside of matrix (µg/g)	Total bixin content (µg/g)	Encapsulation efficiency (%)
	A Amylose (%)	**B** Power level (%)	**C** Time (min)				
1	2.0	100	40	2627.0	3913.5	6540.5	59.8
2	4.4	70	40	2623.4	655.2	3278.6	19.9
3	2.0	82	20	3467.9	5020.2	8488.1	59.2
4	2.0	50	20	3787.7	6210.4	9998.1	62.1
5	8.0	70	28	1676.0	430.3	2106.3	20.4
6	2.0	50	33	3147.2	3147.2	6294.3	50.0
7	5.5	79	20	2100.0	722.03	2822.0	25.6
8	2.0	50	33	2900.4	2900.4	5800.9	50.0
9	2.0	82	20	3460.0	4996.4	8456.4	59.1
10	5.9	50	20	2283.0	1632.2	3915.3	41.7
11	4.4	100	28	2232.1	615.9	2847.9	21.6
12	7.4	75	38	1773.0	267.3	2040.3	13.1
13	8.0	50	40	1349.0	427.0	1776.0	24.0
14	4.4	70	40	2550.0	1501.6	4051.6	37.1
15	8.0	100	20	1234.0	426.0	1660.0	25.6
16	8.0	100	40	2361.6	582.1	2943.7	19.8
17	4.4	100	28	2228.0	580.2	2808.2	20.7
18	8.0	70	28	1632.5	365.8	1998.3	18.3
19	7.4	95	30	1729.1	299.8	2028.9	14.8
20	5.5	51	31	2007.9	1128.3	3136.3	35.9

Table 4.4 Coefficients of the linear, quadratic and interaction terms for the model in the encapsulation by ultrasound.

	Bixin content inside of matrix (μg/g)	Bixin content outside of matrix (μg/g)	*L**	*a**	*b**	°*hue*
β_0	2378.08	578.44	44.72	32.32	38.2	48.45
β_A	-742.08	-1677.56	4.25	0.09	4.01	3.72
β_B	-33.30	-227.14	-5.96	0.77	-2.88	-3.49
β_C	-30.37	-523.05	10.01	-0.26	6.76	5.67
β_{AB}	224.48	-118.54	n.s	1.2	1.05	n.s
β_{AC}	288.90	369.10	n.s	-3.22	-4.9	-2.08
β_{BC}	251.22	510.35	n.s	0.83	4.16	3.32
β_A^2	23.66	1377.12	n.s	n.s	-2.1	n.s
β_B^2	-208.16	n.s	n.s	n.s	2.12	n.s
β_C^2	100.15	606.51	n.s	n.s	-2.67	n.s
R^{2pred}	0.82	0.80	0.82	0.96	0.88	0.94
R^{2adj}	0.96	0.94	0.94	0.98	0.97	0.99
C.V. %	5.96	25.20	3.38	1.35	1.25	0.44
Press	2.06E'6	1.34E´7	140.7	13.35	25.06	5.38
Modelo (p-valor)	< 0.0001	< 0.0001	< 0.0001	< 0.0001	< 0.0001	< 0.0001

n.s: non-significant term.

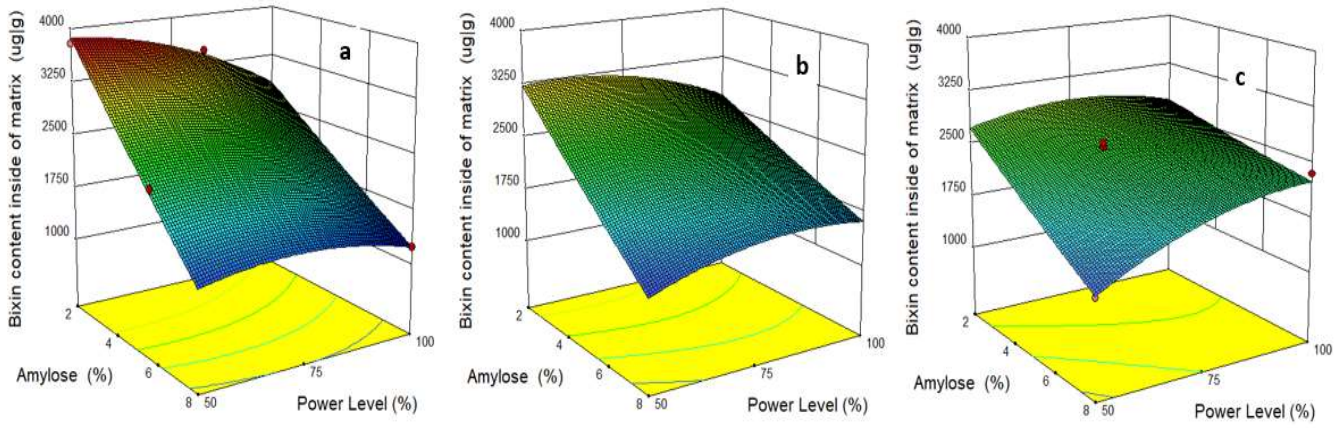

Figure 4.2 Encapsulated bixin inside of starch matrix by ultrasound method: 20 min (a), 30 min (b) and 40 min (c).

Encapsulation efficiency ranged between 13.10% to 62.12% and 17.27% to 94.48% by ultrasound treatment and alkaline method, respectively. The results are according to those obtained by other authors. De Sousa Lobato (2013) reported encapsulation efficiency of bixin of about 98% in a system prepared by the interfacial deposition of preformed poly-ε-caprolactone. The authors associated the high encapsulation efficiency with the presence of triglycerides in the system, which improved bixin solubility. Encapsulation efficiency of bixin using gum Arabic and maltodextrin by spray drying ranged between 75% to 86% (BARBOSA; BORSARELLI; MERCADANTE, 2005). De Marco et al. (2013) encapsulated annatto extract by spray drying using a combination of maltodextrin and gum Arabic. They reported efficiency about 75.69%. The encapsulation of bixin with poly(3-hydroxybutirate-co-hydroxyvalerate) and dichloromethane as organic solvent using the technology of supercritical carbon dioxide achieved values between 6.36% to 92.02% (BOSCHETTO et al., 2014). Molecules similar to bixin have been encapsulated by spray drying of multiple emulsions with encapsulating efficiency of 87% using gellan and mesquite gum (RODRÍGUEZ-HUEZO et al., 2004). Shen e Quek (2014) reported encapsulation efficiency of astaxanthin emulsions ranging between 63% to de 95 %, using proteins as wall material by spray drying. Sharif et al. (2017) reported encapsulation efficiency

higher than 90% in the preparation of microcapsules of β-carotene and eugenol by spray drying using modified starch.

Regarding color of samples prepared using ultrasound and alkaline method, Tables 4.2 and 4.4 show the model coefficients for color parameters according to Equation 3. The parameter *a** that represents intensity of redness varied between 24.6 to 36.7, and between 25.2 to 39.0, whereas the parameter *b** ranged between 16.0 to 50.0 and between 31.5 to 44.8 for samples prepared using precipitation from acid solution and ultrasound treatment, respectively. The °hue parameter, which represents the color tonality, varied between 32.93 and 59.32, and from 44.92 to 52.6, standing between red (°hue = 0) and yellow (°hue = 90). The °hue is an important parameter since it allows establishing the redness of samples treated and the effect of two methods on the original bixin color. Results indicated that there is a tendency of samples prepared with Hylon VII to have an orange color closer to those obtained with cassava amylose. Whilst microencapsulate bixin by ultrasound are slightly less reddish than the original color of pure bixin.

4.3.3 Optimization of bixin encapsulation by RSM

Ultrasound treatment and alkaline method conditions were optimized for determining the maximum bixin encapsulated content inside of starch matrix. Jafari et al. (2008) suggested that in the encapsulation, the wall material should be a powder with minimum surface compound content and maximum retention inside of the matrix. In this sense, for both methods, the encapsulated bixin inside of starch matrix was maximized keeping the parameter °*hue* between 42 to 52, which represents a color tonality similar to bixin. The optimized conditions for encapsulated bixin by ultrasound were: 2% of amylose, 150 W and 20 min of treatment, with an encapsulated bixin content predicted by the model of 3864 µg/g. In the case of encapsulation using alkaline method, the optimized conditions were: 2 % amylose from cassava with protein, temperature of 68 °C, with an encapsulated bixin content predicted by the model of 5714 µg/g.

4.3.4 Verification of model

Encapsulation process using the two methods was carried out with the optimized conditions, with the goal of verifying the encapsulated bixin content predicted by the models. Encapsulated bixin content achieved by ultrasound treatment (2% amylose, 150 W, 20 min) was 3872.2± 3.2 µg/g, whereas regarding the method of precipitation from

acid solution, the encapsulated bixin content (2% cassava amylose with protein, 68 °C) was 5722± 4.3 μg/g. There were no significant differences observed between encapsulated bixin predicted and experimental. The models may be used for predicting purpose.

4.4 Conclusion

Encapsulation of bixin was carried out by ultrasound treatment and alkaline method. Encapsulated bixin content obtained using both methods were analysed using a response surface methodology. RSM results showed that the bixin encapsulated contents were influenced by all the studied factors in both methods. Encapsulation using the alkaline method and ultrasound could be used successfully to encapsulate bixin with good encapsulation efficiency, in spite of the encapsulation efficiency achieved by alkaline method was higher than that obtained by ultrasound. The optimization of conditions showed that in order to improve the encapsulated bixin content inside of matrix it is recommended to use cassava amylose with protein. Future studies are desirable to study the effect of the increase of protein concentration on microencapsulation by both methods.

4.5 References

BARBOSA, M. I. M..; BORSARELLI, C..; MERCADANTE, A. . Light stability of spray-dried bixin encapsulated with different edible polysaccharide preparations. **Food Research International**, v. 38, n. 8–9, p. 989–994, 2005.

BAS, D.; BOYACI, I. Modeling and optimization II : Comparison of estimation capabilities of response surface methodology with artificial neural networks in a biochemical reaction. **Journal of Food Engineering**, v. 78, p. 846–854, 2007.

BAXTER, S.; ZIVANOVIC, S.; WEISS, J. Molecular weight and degree of acetylation of high-intensity ultrasonicated chitosan. **Food Hydrocolloids**, v. 19, n. 5, p. 821–830, 2005.

BEZERRA, M. A.; SANTELLI, R. E.; OLIVEIRA, E. P.; VILLAR, L. S.; ESCALEIRA, L. A. Response surface methodology (RSM) as a tool for optimization in analytical chemistry. **Talanta**, v. 76, n. 5, p. 965–977, 2008.

BOSCHETTO, D. L.; LOSS, R. A.; PEREIRA, G. N.; AGUIAR, G. S. P.; MACHADO, J. R.; CHAVES, L. M. P. C.; SILVA, M. J. A.; OLIVEIRA, D.; OLIVEIRA, J. V. Encapsulation of eugenyl acetate in PHBV using SEDS technique and in vitro release evaluation. **Journal of Food Science and Technology**, v. 53, n. 10, p. 3859–3864, 2014.

BRAITHWAITE, M. C.; TYAGI, C.; TOMAR, L. K.; KUMAR, P.; CHOONARA, Y. E.; PILLAY, V. Nutraceutical-based therapeutics and formulation strategies augmenting their efficiency to complement modern medicine: An overview. **Journal of Functional Foods**, v. 6, p. 82–99, jan. 2014.

DE MARCO, R.; VIEIRA, A. M. S.; UGRI, M. C. A.; MONTEIRO, A. R. G.; BERGAMASCO, R. D. C. Microencapsulation of annatto seed extract: Stability and application. **Chemical Engineering Transactions**, v. 32, p. 1777–1782, 2013.

DE SOUSA LOBATO, K. B.; PAESE, K.; CASANOVA, J.; STANISÇUASKI, S.; JABLONSKI, A.; DE OLIVEIRA, A. Characterisation and stability evaluation of bixin nanocapsules. **Food Chemistry**, v. 141, n. 4, p. 3906–3912, 2013.

FATHI, M.; MARTÍN, Á.; MCCLEMENTS, D. J. Nanoencapsulation of food ingredients using carbohydrate based delivery systems. **Trends in Food Science and Technology**, v. 39, n. 1, p. 18–39, 2014.

GILMOUR, S. G. Response surface designs for experiments in bioprocessing. **Biometrics**, v. 62, n. 2, p. 323–331, 2006.

GIRIDHAR, P.; VENUGOPALAN, A.; PARIMALAN, R. A Review on Annatto Dye Extraction , Analysis and Processing – A Food Technology Perspective. **Journal of Scientific Research & Reports**, v. 3, n. 2, p. 327–348, 2014.

JAFARI, S. M.; ASSADPOOR, E.; HE, Y.; BHANDARI, B. Encapsulation efficiency of food flavours and oils during spray drying. **Drying Technology**, v. 26, n. 7, p. 816–835, 2008.

JANISZEWSKA-TURAK, E. Carotenoids microencapsulation by spray drying method and supercritical micronization. **Food Research International**, v. 99, p. 891–901, 2017.

LALUSH, I.; BAR, H.; ZAKARIA, I.; EICHLER, S.; SHIMONI, E. Utilization of amylose-lipid complexes as molecular nanocapsules for conjugated linoleic acid. **Biomacromolecules**, v. 6, n. 1, p. 121–130, 2005.

LOKSUWAN, J. Characteristics of microencapsulated β-carotene formed by spray drying with modified tapioca starch, native tapioca starch and maltodextrin. **Food Hydrocolloids**, v. 21, n. 5–6, p. 928–935, 2007.

LYNG, S. M. O.; PASSOS, M.; FONTANA, J. D. Bixin and α-cyclodextrin inclusion complex and stability tests. **Process Biochemistry**, v. 40, n. 2, p. 865–872, 2005.

MARCOLINO, V. A.; ZANIN, G. M.; DURRANT, L. R.; BENASSI, M. D. T.; MATIOLI, G. Interaction of curcumin and bixin with β-cyclodextrin: Complexation methods, stability, and applications in food. **Journal of Agricultural and Food Chemistry**, v. 59, n. 7, p. 3348–3357, 2011.

MCCLEMENTS, D. J.; LI, Y. Structured emulsion-based delivery systems: controlling the digestion and release of lipophilic food components. **Advances in colloid and interface science**, v. 159, n. 2, p. 213–28, 15 set. 2010.

MONTALBO-LOMBOY, M.; KHANAL, S. K.; VAN LEEUWEN, J. (Hans); RAJ RAMAN, D.; DUNN, L.; GREWELL, D. Ultrasonic pretreatment of corn slurry for saccharification: A comparison of batch and continuous systems. **Ultrasonics Sonochemistry**, v. 17, n. 5, p. 939–946, 2010.

MONTENEGRO, M. A.; RIOS, A. D. O.; MERCADANTE, A. Z.; NAZARENO, M. A.; BORSARELLI, C. D. Model Studies on the Photosensitized Isomerization of Bixin. **Journal of Agricultural and Food Chemistry**, v. 52, n. 2, p. 367–373, 2004.

MUA, J. P.; JACKSON, D. S. Fractionation of Regular Corn Starch : A Comparison of

Aqueous Leaching and Aqueous Dispersion Methods ’. **Carbohydrate.**, v. 72, n. 5, p. 508–511, 1995.

RAHMALIA, W.; FABRE, J.-F.; USMAN, T.; MOULOUNGUI, Z. Aprotic solvents effect on the UV-visible absortion spectra of bixin. **Spectrochimica Acta Part A: Molecular and Biomolecular Spectroscopy**, v. 131, p. 455–460, 2014.

RIOS, A. de O.; BORSARELLI, C.; ADRIANA, M. Thermal Degradation Kinetics of Bixin in an Aqueous Model System. **Journal of Agricultural and Food Chemistry**, v. 53, n. 6, p. 2307–2311, 2005.

ROCHA, G. A.; FÁVARO-TRINDADE, C. S.; GROSSO, C. R. F. Microencapsulation of lycopene by spray drying: Characterization, stability and application of microcapsules. **Food and Bioproducts Processing**, v. 90, n. 1, p. 37–42, 2012.

RODEA-GONZÁLEZ, D. A.; CRUZ-OLIVARES, J.; ROMÁN-GUERRERO, A.; RODRÍGUEZ-HUEZO, M. E.; VERNON-CARTER, E. J.; PÉREZ-ALONSO, C. Spray-dried encapsulation of chia essential oil (Salvia hispanica L.) in whey protein concentrate-polysaccharide matrices. **Journal of Food Engineering**, v. 111, n. 1, p. 102–109, 2012.

RODRIGUEZ-AMAYA, D. B. **A Guide to carotenoide analysis in foods**. Washington, D.C: ILSI PRESS, 2001.

RODRÍGUEZ-HUEZO, M. .; PEDROZA-ISLAS, R.; PRADO-BARRAGÁN, L. .; BERISTAIN, C. .; VERNON-CARTER, E. . Microencapsulation by Spray Drying of Multiple Emulsions Containing Carotenoids. **Food Engineering and Physical Properties**, v. 69, n. 7, p. 351–359, 2004.

SHARIF, H. R.; GOFF, H. D.; MAJEED, H.; SHAMOON, M.; LIU, F.; NSOR-ATINDANA, J.; HAIDER, J.; LIANG, R.; ZHONG, F. Physicochemical properties of β-carotene and eugenol co-encapsulated flax seed oil powders using OSA starches as wall material. **Food Hydrocolloids**, v. 73, p. 274–283, 2017.

SHEN, Q.; QUEK, S. Y. Microencapsulation of astaxanthin with blends of milk protein and fiber by spray drying. **Journal of Food Engineering**, v. 123, p. 165–171, 2014.

SHU, B.; YU, W.; ZHAO, Y.; LIU, X. Study on microencapsulation of lycopene by spray-drying. **Journal of Food Engineering**, v. 76, n. 4, p. 664–669, 2006.

SPADA, J. C.; MARCZAK, L. D. F.; TESSARO, I. C.; NOREÑA, C. P. Z. Microencapsulation of β-carotene using native pinhão starch, modified pinhão starch and gelatin by freeze-drying. **International Journal of Food Science and Technology**, v. 47, n. 1, p. 186–194, 2012.

SRICHUWONG, S.; JANE, J. Physicochemical Properties of Starch Affected by Molecular Composition and Structures: A Review. **Food Sci. Biotechnol.**, v. 16, n. 5, p. 663–674, 2007.

SUTTER, S. C.; BUERA, P.; ELIZALDE, B. E. Beta-Carotene encapsulation in a mannitol matrix as affected by divalent cations and phosphate anion. **International journal of pharmaceutics**, v. 332, n. 1–2, p. 45–54, 2007.

ZHU, J.; LI, L.; CHEN, L.; LI, X. Study on supramolecular structural changes of ultrasonic treated potato starch granules. **Food Hydrocolloids**, v. 29, n. 1, p. 116–122, 2012.

CAPÍTULO 5. EMCAPSULAÇÃO DE ÓLEO DE ABACATE EM SOLUÇÃO DE AMILOSE DE MANDIOCA

Os resultados desse capítulo foram aceitos para publicação no periódico

Journal of Food Processing and Preservation

DOI: 10.1111/jfpp.13594

ENCAPSULATION OF AVOCADO OIL IN AMYLOSE SOLUTION FROM CASSAVA STARCH.

Ezequiel José Pérez-Monterroza[1]*, Ana María Chaux-Gutiérrez[1], Vânia Regina Nicoletti Telis [1]

[1] *Department of Food Engineering and Technology; São Paulo State University (Unesp), Institute of Biosciences, Humanities and Exact Sciences (Ibilce), Campus São José do Rio Preto; Rua Cristovão Colombo 2265, Zip Code 15054-000 São José do Rio Preto, SP, Brazil.*

*Correspondence: Ezequiel José Pérez Monterroza
Email address: eperez494@gmail.com, ejperezm@unalmed.edu.co

Abstract

Encapsulation of avocado oil was carried out mixing it with amylose extracted from cassava starch. Then, the oleogel formed was retrograded at 8 and -18 °C for 24 h and later dried by freeze-drying or vacuum at 3.3 kPa at 60 °C. Samples were characterized by X-ray diffractometry, FT-IR spectrometry and differential scanning calorimetry (DSC). The lutein and neoxanthin content was also determined. Results obtained from DSC and FT-IR spectroscopy indicated no formation of inclusion complexes V-type of amylose. Nevertheless, the results from X-ray diffractometry showed that samples had a diffraction pattern characteristics from V-type amylose complex. The samples that retrograded at -18 °C and dried using freeze-drying had a slight higher encapsulation degree than the samples retrograded at 8°C.

Keywords: Lutein, neoxanthin, xerogels, cryogels, avocado oil, amylose.

Practical Application

Xerogels and cryogels from amylose of cassava can be considered an interesting tool for encapsulation of edible oil rich in bioactive compounds such as lutein and neoxanthin. Xerogels and cryogels are a potential biodegradable matrix for loading biocompounds, as well as an alternative for formulating controlled delivery systems of nutrients.

5.1 Introduction

Xerogels, cryogels and aerogels have gained interest as tool for microencapsulation of bioactive compounds in the food industry due to their properties of low density and high porosity (GAUTHIER et al., 2004; COMIN; TEMELLI; SALDAÑA, 2012). The porous structure is produced during the drying process, which may be carried out by freeze-drying, forming the called cryogels, by hot-air drying, resulting in the xerogels, or by using supercritical CO_2 ($scCO_2$) forming the aerogels (GLENN; IRVING, 1995; JOB et al., 2006; HOEPFNER; RATKE; MILOW, 2008; COMIN; TEMELLI; SALDAÑA, 2012; DE MARCO et al., 2015). The use of silica aerogels as delivery systems has been demonstrated with success (SMIRNOVA; MAMIC; ARLT, 2003), nevertheless, these delivery systems have the drawback of lower biodegradability when compared to matrices such as polysaccharides. For this reason the biopolymers have been attracting much attention as potential matrices for loading of bioactive compounds (HUANG; YUAN; CHEN, 2008; MEHLING et al., 2009; GARCÍA-GONZÁLEZ; ALNAIEF; SMIRNOVA, 2011). Spheres of alginate have been used as carrier for the microencapsulation of drugs as ibuprofen, paracetamol, ketoprofen and benzoic acid. The amount of the material load within the matrix depends on the structure and composition of the aerogel (MEHLING et al., 2009; GARCÍA-GONZÁLEZ et al., 2015). Characteristics of the aerogels with possibility of being used in the food industry, prepared from marine and plant-derivatives polysaccharides were reviewed by Mikkonen et al. (2013) showing the potential advantages of these materials. Starches are other biodegradable raw material that are considered as safe to be used in the development of matrices and coating of bioactive compounds (LALUSH et al., 2005b). It is known that the amylose present in the granule of starch forms inclusion complexes with hydrophobic compounds, and this characteristic has been used to prepare amylose-guest complexes with lipids, fatty acids as palmitic, oleic and linoleic, as well as some flavors (SZCZODRAK; POMERANZ, 1992; ZHANG; MALADEN; HAMAKER, 2003; WULFF; AVGENAKI; GUZMANN, 2005b; ABU-HARDAN; HILL; FARHAT, 2007; ITTHISOPONKUL et al., 2007; RADHIKA; SHANAVAS; MOORTHY, 2008). Studies on aerogels, xerogels and cryogels prepared from starches have been reported (Chang et al. 2010; García-González et al. 2012; Mehling et al. 2009; De Marco et al. 2015; Svagan et al. 2008; Salam et al. 2011). Specifically, starch with higher amylose content was used to prepared porous microspheres in controlling parasitic mites in honey bee colonies

(GLENN et al., 2010b). The final properties of the xerogel depend on the biopolymer used and on the preparation process. Xerogels, cryogels and aerogels have been prepared from pure amylose, and from potato starch with higher amylose content, which has been used in the most studies on inclusion complexation. According to Kapuśniak & Tomasik (2006b), on the preparation of microcapsules from waxy corn and tapioca starches with lipid, the guest molecule does not react with starch, but the structure formed may be potentially used for their encapsulation. In the present work, we report preparation of xerogels and cryogels from amylose gels with avocado oil and their ability for carotenoid retention.

5.2 Materials and Methods

Cassava starch (16% of amylose) and avocado fruit (*Persea americana Mill cv. Hass*) were obtained from local market. Ethanol (95% v/v) was supplied by Synth (Diadema, Brazil). Pancreatin was provided by Sigma-Aldrich (St. Louis, MO). Deionized water was used in the preparation of the starch suspensions. All chemicals were of analytical grade.

5.2.1 Avocado oil extraction

Ripe fruits purchased from the local market were washed, peeled, and depulped. The avocado pulp was liquefied with water to prepare a 15 g/100 g avocado dispersion, and the oil was then extracted using a centrifuge at 3500×g for 15 min. The lipid fraction was separated from the water-soluble fraction. The oil obtained was stored at 5 °C until it was used in the preparation of beads.

5.2.2 Lipid profile of the avocado oil

The fatty acids in the avocado oil were determined by gas chromatography. The equipment used was an Agilent Model 6890N equipped with a split/splitless injector and an Agilent 123_5536 capillary column (nominal length 30 m, nominal diameter 0.32 mm, film thickness 0.5 m). The oven temperature was programmed to increase from 150 to 250 °C at a speed of 10 °C/min and then from 250 to 300 °C at a speed of 15 °C/min. The carrier gas was helium at 1.79 kPa. The sample size was 0.2 mL, and the split ratio was 15:1 (HAIYAN et al., 2007; BERASATEGI et al., 2012).

5.2.3 Fractionation of cassava starch.

Amylose was isolated from cassava starch by precipitation with ethanol according to methodology proposed by MUA JACKSON (1995). A dispersion of cassava starch (2% w/w) was heated at 70 °C for 20 min. The solution obtained was cooled to 40 °C and centrifuged to 3500×g for 10 min. The supernatant was separated and the amylose was precipitated using ethanol (95% v/v). This precipitate was separated by centrifugation to 1500×g for 3 min and stored at 8 °C until used.

5.2.4 Preparation of beads from amylose and avocado oil

Fifty-four grams of a solution from amylose isolate of cassava starch was mixed with avocado oil (11 g) in deionized water (35 g) in an ultraturrax at 2500 rpm at 25 °C for 1 min. The dispersion obtained was heated in a microwave oven (Electrolux, Brazil) set at 900 W for 1 min. The oleogel formed was injected through syringe (0.55 Ø mm) and the beads were collected in ethanol (95% v/v). Then, they were washed three times using a 50% ethanol/water mixture (v/v). The beads were retrograded at 8 and -18 °C for 24 h and later dried by freeze-drying or vacuum at 3.3 kPa at 60 °C.

5.2.5 Content of lutein and neoxanthin in the avocado oil

The carotenoids (lutein and neoxanthin) in 2 g the avocado oil were extracted using 50 mL of petroleum ether, and after phase transfer the absorbance was read, at wavelength of maximum absorbance of the lutein and neoxanthin (421 and 413 nm, respectively), using an UV-vis spectrophotometer (Model SP-220, Biospectro, Brasil) (Rodriguez-Amaya & Kimura 2004; Minguez-Mosquera & Hornero-Méndez 1993).

5.2.6 Encapsulation degree of the lutein and neoxanthin

The encapsulation degree after drying process was calculated as the amount of lutein and neoxanthin per gram of the dryed beads. The beads (0.1 g) were incubated in 3 mL of pancreatin solution (0.8 g of pancreatin was dissolved in 20 mL of phosphate buffer 20 mM (pH 6.9, 0.04% NaCl) at 37 °C, for 24 h. Finally, the carotenoids were extracted with petroleum ether (8 mL) and quantified by spectrophotometry at 421 and 413 nm according to Lalush et al. (2005b) with modifications.

5.2.7 Differential scanning calorimetry

The thermal characterization of the beads was conducted by analyzing the thermograms obtained in a PerkinElmer DSC 8000 (PerkinElmer Corp, Shelton, CT USA). The equipment was calibrated with indium before analysis. Nitrogen was used as a purge gas for the system. For the analysis, 4-5 mg of beads were weighed in aluminum pans. An empty aluminum pan was used as reference. The samples were cooled and kept at -50 °C for one minute, then heated at 10, 35 and 50 °C/min from -50 to 300 °C. The results of thermal analyze were processed using the Perkin Elmer Pyris software, version 10.0 (Perkin Elmer Inc, Shelton, CT, USA). Each sample was analyzed in duplicate.

5.2.8 X-Ray Diffraction.

The X-ray diffraction was carried out with a diffractometer RINT 2000 wide angle Goniometer unit (Rigaku, Tokio, Japan). The diffractometer was operated with a voltage of 45 kV and current of 40 mA. The sample was scanned from 5 to 40° in 2θ, with a step size of 0.1°. The relative crystallinity was calculated based on the relationship between the peak area and total area of the X-ray diffractograms, according to Itthisoponkul et al. (2007), by using the Origin software (Microcal Inc, Northampton, USA). Diffractograms were smoothed and the baseline was corrected. The analyses were carried out in duplicate.

5.2.9 FT-IR spectroscopy

Infrared spectra were recorded on spectrophotometer Spectrum One (Perkin-Elmer Corp, Shelton, CT, USA) with attenuated total reflectance accessory with a ZnSe crystal. Samples were analyzed directly after pressing them on the crystal (551.6 kPa) and FT-IR scanning was conducted at ambient conditions. The resolution was set to 4 cm^{-1} and the operating range was 400 to 4000 cm^{-1}. In all cases, 20 scans per sample were recorded. The data were processed using Origin Pro 8 Software (Microcal Inc, Northampton, USA). The analyses were carried out in duplicate.

5.2.10 Scanning Electron Microscopy (SEM)

SEM was used to visualize the morphology of the beads, which were coated with gold in a sputter under vacuum for 3 min. The images were made using a scanning electron microscope (JSM7500F, FEG-MEV JEOL, Germany).

5.3 Results and discussion

Table 5.1 shows the fatty acid composition of the virgin avocado oil. The extracted oil contained 80.21% of unsaturated fatty acids (UFAs), both mono and polyunsaturated. Oleic acid contributed with 53.8% of total UFAs. Another common UFA found was linoleic acid at 12.5%. HAIYAN ET AL. (2007) found 62.7% and 11.4% of oleic and linoleic acid of the total fatty acids, respectively. BERASATEGI et al. (2012) reported lower values for Hass avocado oil with 54.4% g and 10.87% of oleic and linoleic acid, respectively. RODRÍGUEZ-CARPENA et al. (2012) reported 57.4% of oleic acid and 18.7% of linoleic acid. Among the saturated fatty acids, palmitic acid was most prevalent at 20.51%. Carotenoid content in the avocado oil was of 136 µg (lutein + neoxanthin/g avocado oil), which was lower than reported by ASHTON et al. (2006), but the pigment content may vary with the cultivar. The encapsulation degrees for beads retrograded at 8 or -18 °C were of the same order with an encapsulation degree of the carotenoids of 115 ± 1.2 and 127.7 ± 2.3 µg (lutein + neoxanthin)/g of beads respectively, showing that most carotenoids expressed as lutein and neoxanthin remained entrapped in the beads after the drying processes. Nevertheless, the beats retrograded at -18 °C presented slight encapsulation degrees higher than those stored at 8 °C. Probably, the amylose chains retrograded at lower temperature were arranged in ordered structures, allowing a better accommodation of avocado oil and avoiding a greater exposure to oxygen during the drying process.

Table 5.1. Lipid profile of avocado oil (Persea americana Mill, cv. Hass).

Fatty acids	Content (%)
C14:0 (Myristic)	0.09 ± 0.00
C16:0 (Palmitic)	20.51 ± 0.08
C16:1 (n-7) (Palmitoleic)	12.89 ± 0.01
C18:0 (Stearic)	0.52 ± 0.01
C18:1 (n-9) (Oleic)	53.8 ± 0.03
C18:2 (n-6) (Linoleic)	12.5 ± 0.01
C18:3 (n-3) (Linolenic)	0.80 ± 0.00
C20:0 (Arachidic)	0.15 ± 0.04
C20:1 (n-9) (Eicosanoic)	0.22 ± 0.00
C22:0 (Behenic)	0.16 ± 0.00
C24:0 (Lignoceric)	0.12 ± 0.00
Polyunsaturated fatty acids	13.3 ± 0.01
Monounsaturated fatty acids	66.9 ± 0.03
Saturated fatty acids	21.5± 0.01

5.3.1 Differential scanning calorimetry

The thermal behavior of the beads prepared from avocado oil and cassava amylose is shown Figure 5.1. The sample retrograded at 8°C showed an endotherm at 207 °C with a shoulder at 205 °C, which were caused likely by melting and partial recrystallization of the structures. Regarding second-order transitions, this sample showed two glass transition temperature (T_g), at 143 and 260 °C. Futhermore, the amylose without avocado oil displayed one endotherm with melting temperature (T_m) at 195 and T_g at 242 °C. As it has been previously reported, the V-amylose complexes and their polymorphs of the type IIa have dissociation temperatures above 100 °C, whereas for type IIb dissociation occurs above 121 °C, these complex are characterized for having distinct amorphous and crystalline regions (KARKALAS et al., 1995). The dissociation temperature observed for the sample subjected to vacuum drying, are far from the T_m values previously reported for V-type complexes, suggesting that there was no formation of inclusion complexes of cassava amylose with the avocado oil, due to the absence of endotherms around the T_m of the V-amylose complexes. The thermogram for the freeze-dried samples (retrograded at -18) is shown in Figure 5.1B. It revealed the presence of several endotherms in the range 150 to 190 °C. Differently from beads retrograded at 8 °C, only a T_g was observed at 123 °C. Similarly as with beads retrograded at 8 °C, this samples does not form inclusion complexes. On the other hand, T_m at 153 °C was associated to chains of retrograded amylose. When amylose is heated in presence of lipid, a T_m nearly to this temperature is observed, which corresponds to retrograded amylose (RAPHAELIDES; KARKALAS, 1988; BILIADERIS; GALLOWAY, 1989; SIEVERT; POMERANZ, 1989). It is also known that the retrograded amylose has a double helix conformation which does not form inclusion complexes (KARKALAS et al., 1995). Fatty acids such as oleic, linoleic or their alkyl esters encapsulated in potato starch may exhibit T_m above 200 °C. KAPUSNIAK & TOMASIK (2006b) reported that oleic acid embedded in potato starch showed an endotherm at 240 °C, which is higher than the dissociation temperature observed in this study. The results could be due to the avocado oil containing a high amount of unsaturated fatty acids, which could decrease the dissociation temperature.

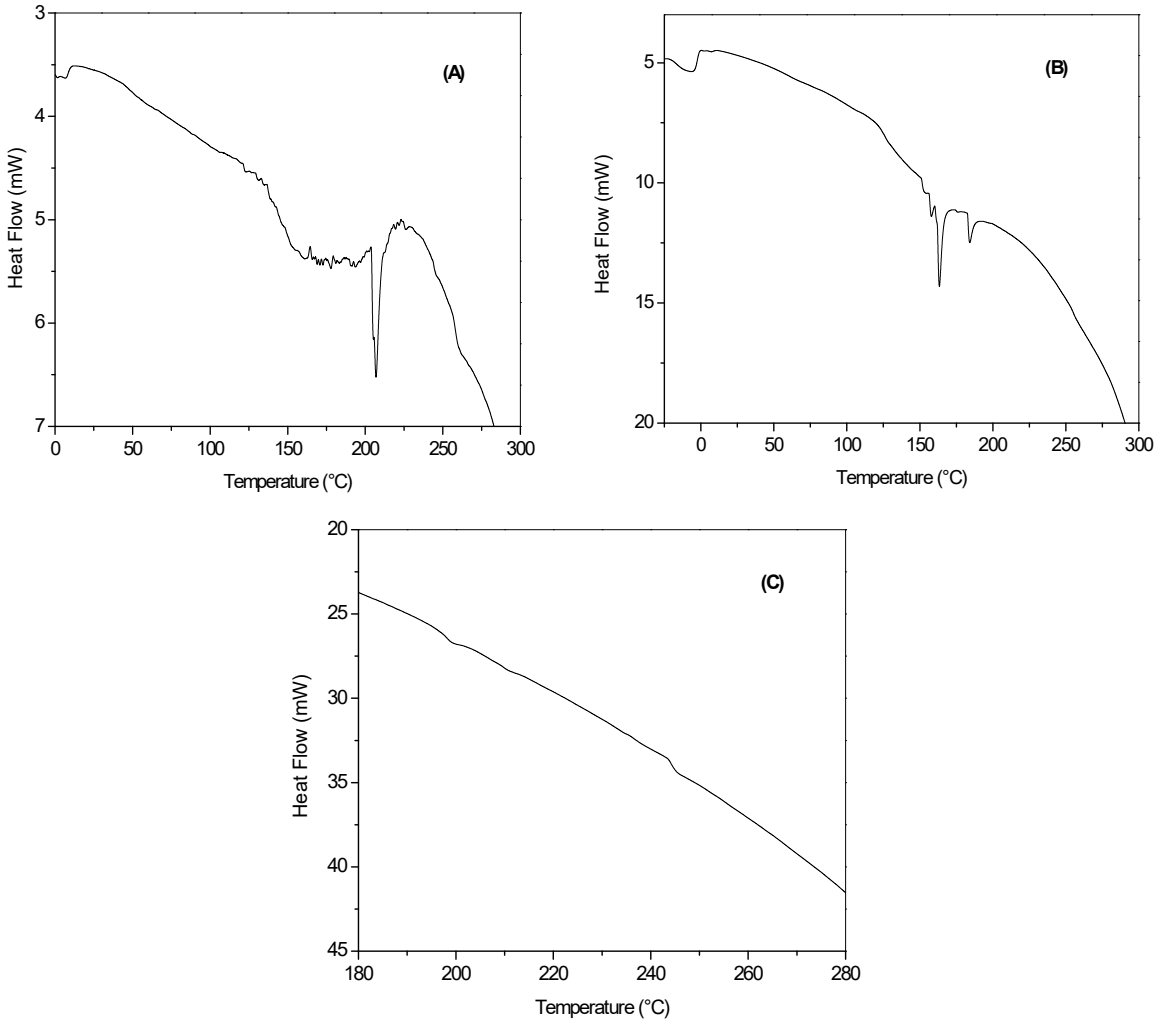

Figure 5.1 DSC scans for the beads retrograded at 8 °C (A) and -18 °C (B), and amylose (C).

5.3.2 X-ray diffraction

X-ray diffraction analysis was carried out with the purpose to evaluate the identity of the structures formed by the avocado oil and the amylose gel. The diffraction pattern of the amylose without avocado oil was used as reference (Figure 5.2). Amylose displayed one weak peaks with reflections in the Bragg angle at 13.5° °, and a peak with greater intensity at 21.6 °. The reflection at 22.2° belong to retrograded amylose. The reflections at 13.5°-13.6°, 20.4°-21.6° are characteristics of the helical inclusion complexes of the V_h-type of the amylose.

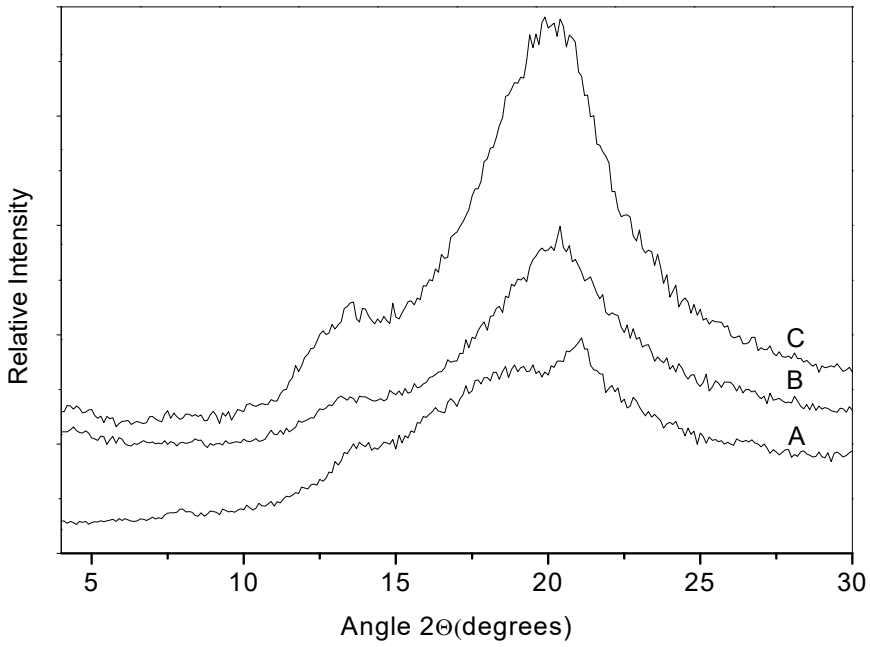

Figure 5.2 X-ray scattering diagrams of amylose (A), beads retrograded at -18 °C (B) and 8 °C (C).

Similar patterns but of a greater intensity were observed in the complexes formed by corn starch and native lipids present in the granule, after that they were heated by microwave, as well as the inclusion complexes formed using conjugated linoleic acid prepared from diluted solution of corn starch with higher amylose content in H2O/DMSO and KOH/HCL (BULÉON et al., 1990; LALUSH et al., 2005b; ITTHISOPONKUL et al., 2007; FELKER et al., 2013). Beads retrograded at -18 °C displayed a peak with low intensity at 7.7°, 13.6° and a sharp peak at 19.9°. These reflections were considered as corresponding to amylose V_H complexes (HEINEMANN et al., 2001; LE BAIL; RONDEAU; BULÉON, 2005). Which also suggests the presence of a diffraction pattern typical of the V_H amylose complexes. In general, the beads had diffraction patterns to V_H-amylose complexes specifically to the type V_6 and retrograded amylose. Amylose showed a relative crystallinity of 41%, whilst retrograded sample at -8 and -18 °C had percent of 49.6 and 52.73 respectively. The increase in relative crystallinity was independent on the

retrograded conditions or the drying process. The results observed are higher than reported by Itthisoponkul et al. (2007) for complexes of cassava starch with flavors, which showed values between 0.17 to 7.85 %.

5.3.3 FT-IR spectra analysis

Figure 5.3 shows FT-IR spectra of avocado oil, the amylose solution and treatment samples. Spectra of the avocado oil showed characteristic bands in 2857, 2918, 1464 and 715 cm^{-1} for stretching and bending vibrations from aliphatic hydrocarbons (=CH_2 group). Band in 1743 cm^{-1} was associated to C=O stretching from esters group (GURDENIZ; OZEN, 2009; MAHBOUBIFAR et al., 2017). Amylose showed bands between 2837 to 3010 cm^{-1} associated with stretching vibrations from –C-H, and bands between 920 to 1180 cm^{-1} associated with stretching from C-O, C-C and -C-O-H respectively.

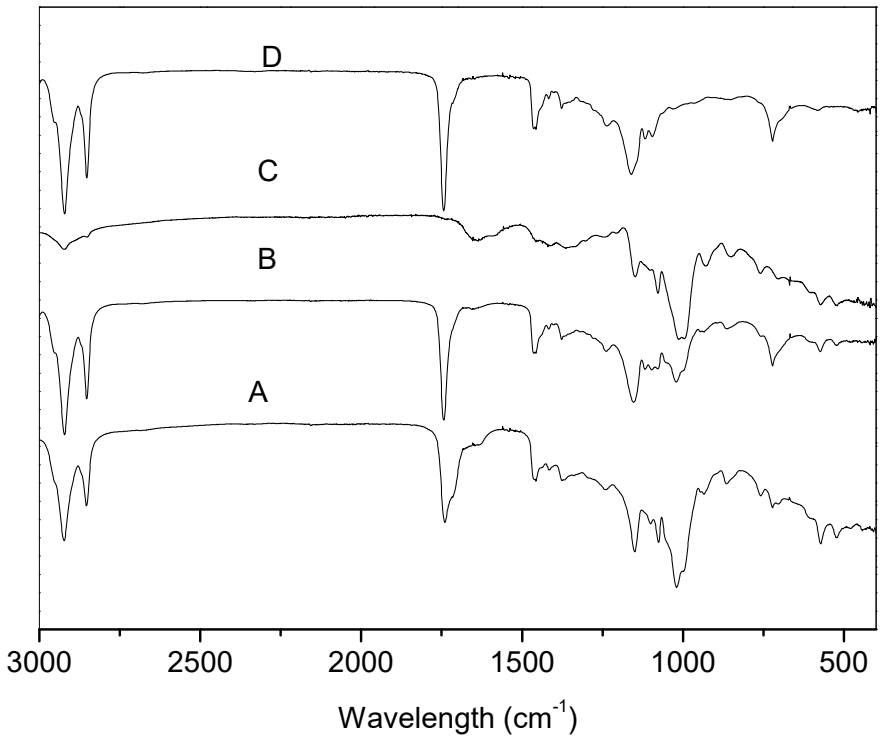

Figure 5.3 FT-IR spectra of samples retrograded at -18 °C (A), 8 °C (B), amylose (C) and avocado oil (D).

When comparing FT-IR spectra, it is possible to see that the bands of the FT-IR spectra had no change in treatment samples. The band at 1744 cm^{-1}, which is typical of the –C=O esters group of avocado oil, indicated that stretching vibrations from -C=O were not

restricted after the treatment and freeze-drying process. This group was not entrapped inside of the helical cavity of amylose and did not restrict their vibrations.

5.3.4 Scanning Electron Microscopy (SEM)

Figure 5.4 shows the surfaces of the beads retrograded at 8 and -18 °C. In general, the beads presented a corrugated surface, most likely due to the contraction produced during the drying process. Microscopy SEM also shows solid beads with a round shape forming aggregates. Beads retrograded at -18 °C showed protrusions and a rougher surface than those retrograded at 8 °C. These protrusions could be caused by aggregation of amylose molecules. Results suggest that the drying process affects the morphological aspect of beads. Indeed, air-dried aerogels of β-glucan had more continuous and uniform surfaces than aerogels dried using supercritical CO_2 (COMIN; TEMELLI; SALDAÑA, 2012). Although potato starch aerogels obtained by supercritical drying showed uniform and porous surface, an increase in the time for solvent exchange resulted in a more fibrous nanostructure (DE MARCO et al., 2015). Avocado oil loading into beads retrograded at 8 and -18 °C probably occupied most cavities, resulting in a less porous surface. Ahmadi-Abhari et al. (2015) similarly observed a less porous surface for wheat protein aerogels loaded with fish oil. In addition, the capillary stress during the drying process can produce the collapse of the structure. Nevertheless, a surfactant can be used in order to decrease capillary stress and improve the mechanical properties (GARCÍA-GONZÁLEZ; ALNAIEF; SMIRNOVA, 2011; CHENG et al., 2012). The freeze-drying process produced a notably rough surface on beads retrograded at -18 °C.

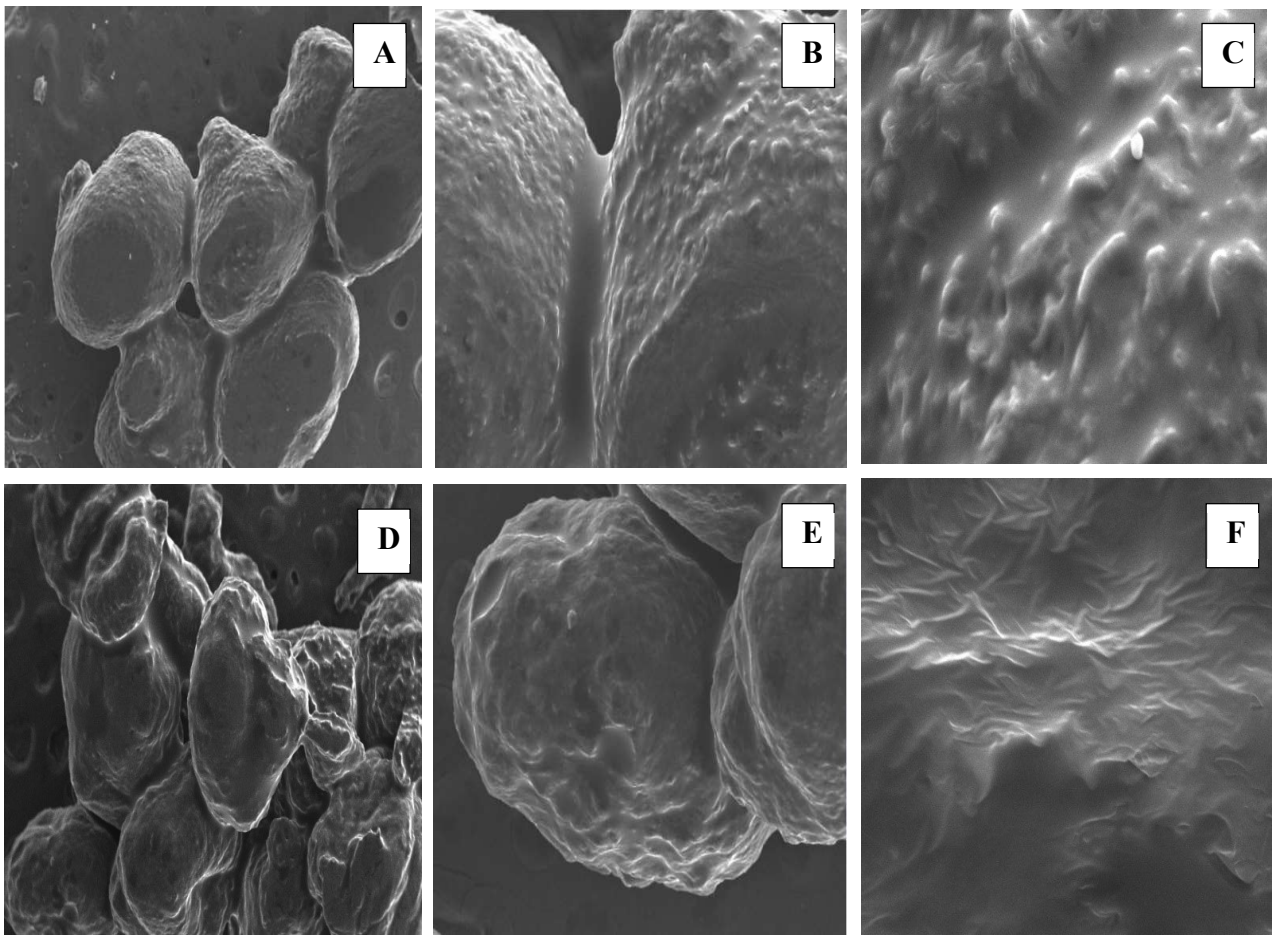

Figure 5.4 SEM micrographs of the samples retrograded at -18 °C (A, B, C) and 8 °C (D, E, F). Magnification 30× (A, D), 70× (E), 100× (B) and 300× (C, F).

5.4 Conclusion

Amylose gels can host avocado oil within their structure. Beads retrograded at -18 °C had a higher encapsulation degree than those prepared at 8 °C. All beads retain the diffraction patterns characteristic of V-Amylose complex, although formation of amylose complexes was not verified. The amylose solution from cassava starch can be considered for the encapsulation of bioactive compounds. Nevertheless, future studies are necessary to determine the delivery profile of the avocado oils under simulating gastrointestinal conditions.

5.5 Acknowledgements

The authors thank Conselho Nacional para o Desenvolvimento Científico e Tecnológico (CNPq, Grant 476927/2012-9) for financial support.

5.6 Reference

ABU-HARDAN, M. O.; HILL, S. E.; FARHAT, I. a. A Calorimetric Study of the Interaction between Waxy Maize Starch and Lipid. **Starch - Stärke**, v. 59, n. 5, p. 217–223, maio 2007.

AHMADI-ABHARI, S.; WOORTMAN, A. J; HAMER, R; LOOS, K. Rheological Properties of wheat starch influenced by amylose-lysophosphatidylcholine complexation at different gelation phases. **Carbohydrate Polymers**, v. 122, p. 197–201, 2015.

ASHTON, O.; WONG, M.; MCGHIE, T.; VATHER, R.; WANG, Y.; REQUEJO-JACKMAN, C.; RAMANKUTTY, P.; WOOLF, A. Pigments in Avocado Tissue and Oil. **Journal of Agricultural and Food Chemistry**, v. 54, n. 26, p. 10151–10158, 2006.

BERASATEGI, I.; BARRIUSO, B.; ANSORENA, D.; ASTIASARÁN, I. Stability of avocado oil during heating: Comparative study to olive oil. **Food Chemistry**, v. 132, n. 1, p. 439–446, 2012.

BILIADERIS, C. G.; GALLOWAY, G. Crystallization behavior of amylose-v complexes: structure-property relationships. **Carbahydrate Research**, v. 189, p. 31–48, 1989.

BULÉON, A.; DELAGE, M.; BRISSON, J.; CHANZY, H. Single crystals of V amylose complexed with isopropanol and acetone. **Int. J. Biol. Macromol**, v. 12, p. 25–33, 1990.

CHANG, X.; CHEN, D.; JIAO, X. Starch-derived carbon aerogels with high-performance for sorption of cationic dyes. **Polymer**, v. 51, n. 16, p. 3801–3807, 2010.

CHENG, Y.; LU, L.; ZHANG, W.; SHI, J.; CAO, Y. Reinforced low density alginate-based aerogels: Preparation, hydrophobic modification and characterization. **Carbohydrate Polymers**, v. 88, n. 3, p. 1093–1099, 2012.

COMIN, L. M.; TEMELLI, F.; SALDAÑA, M. D. a. Barley beta-glucan aerogels via supercritical CO2 drying. **Food Research International**, v. 48, n. 2, p. 442–448, 2012.

DE MARCO, I.; BALDINO, L.; CARDEA, S.; REVERCHON, E. Supercritical Gel Drying for the Production of Starch Aerogels for Delivery Systems. **Chemical Engineering Transactions**, v. 43, p. 307–312, 2015.

FELKER, F. C.; KENAR, J. A.; FANTA, G. F.; BISWAS, A. Comparison of microwave processing and excess steam jet cooking for spherulite production from amylose-fatty acid inclusion complexes. **Starch/Starke**, v. 65, n. 9–10, p. 864–874, 2013.

GARCÍA-GONZÁLEZ, C. a.; ALNAIEF, M.; SMIRNOVA, I. Polysaccharide-based aerogels - Promising biodegradable carriers for drug delivery systems. **Carbohydrate Polymers**, v. 86, n. 4, p. 1425–1438, 2011.

GARCÍA-GONZÁLEZ, C. A.; CAMINO-REY, M. C.; ALNAIEF, M.; ZETZL, C.; SMIRNOVA, I. The Journal of Supercritical Fluids Supercritical drying of aerogels using CO2: Effect of extraction time on the end material textural properties. **The Journal of Supercritical Fluids**, v. 66, p. 297–306, 2012.

GARCÍA-GONZÁLEZ, C. a.; JIN, M.; GERTH, J.; ALVAREZ-LORENZO, C.; SMIRNOVA, I. Polysaccharide-based aerogel microspheres for oral drug delivery. **Carbohydrate Polymers**, v. 117, p. 797–806, 2015.

GAUTHIER, B. M.; BAKRANIA, S. D.; ANDERSON, A. M.; CARROLL, M. K. A fast supercritical extraction technique for aerogel fabrication. **Journal of Non-Crystalline Solids**, v. 350, p. 238–243, 2004.

GLENN, G. M.; IRVING, D. W. Starch-Based Microcellular Foams. **American Association of Cereal Chemists**, v. 72, n. 2, p. 155–161, 1995.

GLENN, G. M.; KLAMCZYNSKI, A. P.; WOODS, D. F.; CHIOU, B.; ORTS, W. J.; IMAM, S. H. Encapsulation of plant oils in porous starch microspheres. **Journal of Agricultural and Food Chemistry**, v. 58, n. 7, p. 4180–4184, 2010.

GURDENIZ, G.; OZEN, B. Detection of adulteration of extra-virgin olive oil by chemometric analysis of mid-infrared spectral data. **Food Chemistry**, v. 116, n. 2, p. 519–525, 2009.

HAIYAN, Z.; BEDGOOD, D. R.; BISHOP, A. G.; PRENZLER, P. D.; ROBARDS, K. Endogenous biophenol, fatty acid and volatile profiles of selected oils. **Food Chemistry**, v. 100, n. 4, p. 1544–1551, jan. 2007. Disponível em: <http://linkinghub.elsevier.com/retrieve/pii/S030881460501109X>. Acesso em: 24 out. 2013.

HEINEMANN, C.; CONDE-PETIT, B.; NUESSLI, J.; ESCHER, F. Evidence of starch inclusion complexation with lactones. **Journal of Agricultural and Food Chemistry**, v. 49, n. 3, p. 1370–1376, 2001.

HOEPFNER, S.; RATKE, L.; MILOW, B. Synthesis and characterisation of nanofibrillar cellulose aerogels. **Cellulose**, v. 15, n. 1, p. 121–129, 2008.

HUANG, H.-J.; YUAN, W.-K.; CHEN, X. D. Microencapsulation Based on Emulsification for Producing Pharmaceutical Products: A Literature Review. **Developments in Chemical Engineering and Mineral Processing**, v. 14, n. 3–4, p. 515–544, 2008.

ITTHISOPONKUL, T.; MITCHELL, J. R.; TAYLOR, A. J.; FARHAT, I. a. Inclusion complexes of tapioca starch with flavour compounds. **Carbohydrate Polymers**, v. 69, n. 1, p. 106–115, 1 maio 2007.

JOB, N.; PANARIELLO, F.; MARIEN, J.; CRINE, M.; PIRARD, J. P.; LÉONARD, A. Synthesis optimization of organic xerogels produced from convective air-drying of resorcinol-formaldehyde gels. **Journal of Non-Crystalline Solids**, v. 352, n. 1, p. 24–34, 2006.

KAPUŚNIAK, J.; TOMASIK, P. Lipid microencapsulation in starch. **Journal of Microencapsulation**, v. 23, n. 3, p. 341–348, 2006.

KARKALAS, J.; MA, S.; MORRISON, W. R.; PETHRICK, R. a. Some factors determining the thermal properties of amylose inclusion complexes with fatty acids. **Carbohydrate Research**, v. 268, n. 2, p. 233–247, 1995.

LALUSH, I.; BAR, H.; ZAKARIA, I.; EICHLER, S.; SHIMONI, E. Utilization of amylose-lipid complexes as molecular nanocapsules for conjugated linoleic Acid. **Biomacromolecules**, v. 6, n. 1, p. 121–30, 2005.

LE BAIL, P.; RONDEAU, C.; BULÉON, A. Structural investigation of amylose complexes with small ligands: Helical conformation, crystalline structure and thermostability. **International Journal of Biological Macromolecules**, v. 35, n. 1–2, p. 1–7, 2005.

MAHBOUBIFAR, M.; HEMMATEENEJAD, B.; JAVIDNIA, K.; YOUSEFINEJAD, S. Evaluation of long-heating kinetic process of edible oils using ATR–FTIR and chemometrics tools. **Journal of Food Science and Technology**, v. 54, n. 3, p. 659–668, 2017.

MEHLING, T.; SMIRNOVA, I.; GUENTHER, U.; NEUBERT, R. H. H. Polysaccharide-based aerogels as drug carriers. **Journal of Non-Crystalline Solids**, v. 355, n. 50–51, p. 2472–2479, 2009.

MIKKONEN, K. S.; PARIKKA, K.; GHAFAR, A.; TENKANEN, M. Prospects of polysaccharide aerogels as modern advanced food materials. **Trends in Food Science and Technology**, v. 34, n. 2, p. 124–136, 2013.

MINGUEZ-MOSQUERA, M. I.; HORNERO-MBNDEZ, D. Separation and Quantification of the Carotenoid Pigments in Red Peppers (Capsicum annuum L.), Paprika, and Oleoresin by Reversed-Phase HPLC. **J. Agric. Food Chem**, v. 41, p. 1616–1620, 1993.

MUA, J. P.; JACKSON, D. S. Fractionation of Regular Corn Starch : A Comparison of Aqueous Leaching and Aqueous Dispersion Methods ’. **Carbohydrate.**, v. 72, n. 5, p. 508–511, 1995.

RADHIKA, G. S.; SHANAVAS, S.; MOORTHY, S. N. Influence of lipids isolated from soybean seed on different properties of cassava starch. **Starch/Starke**, v. 60, n. 9, p. 485–492, 2008.

RAPHAELIDES, S.; KARKALAS, J. Thermal dissociation of Amylose-Fatty acid complexes. **Carbohydrate Polymers**, v. 172, p. 65–82, 1988.

RODRIGUEZ-AMAYA, D. .; KIMURA, M. **HarvestPlus Handbook for Carotenoid Analysis**. [s.l: s.n.]

RODRÍGUEZ-CARPENA, J.; MORCUENDE, D.; ESTÉVEZ, M. Avocado , sunflower and olive oils as replacers of pork back-fat in burger patties : Effect on lipid composition , oxidative stability and quality traits. **Meat Science**, v. 90, n. 1, p. 106–115, 2012.

SALAM, A.; VENDITTI, R. a.; PAWLAK, J. J.; EL-TAHLAWY, K. Crosslinked hemicellulose citrate-chitosan aerogel foams. **Carbohydrate Polymers**, v. 84, n. 4, p. 1221–1229, 2011.

SIEVERT, D.; POMERANZ, Y. Enzyme-Resistant Starch. I. Characterization and

Evaluation by Enzymatic, Thermoanalytical, and Microscopic Methods. **Cereal Chem**, v. 66, n. 4, p. 342–347, 1989.

SMIRNOVA, I.; MAMIC, J.; ARLT, W. Adsorption of drugs on silica aerogels. **Langmuir**, v. 19, n. 20, p. 8521–8525, 2003.

SVAGAN, A. J.; SAMIR, M. a S. a; BERGLUND, L. a. Biomimetic foams of high mechanical performance based on nanostructured cell walls reinforced by native cellulose nanofibrils. **Advanced Materials**, v. 20, n. 7, p. 1263–1269, 2008.

SZCZODRAK, J.; POMERANZ, Y. Starch-Lipid Interactions and Formation of Resistant Starch in High-Amylose Barley. **Cereal Chemistry**, v. 69, n. 6, p. 626–632, 1992.

WULFF, G.; AVGENAKI, G.; GUZMANN, M. S. P. Molecular encapsulation of flavours as helical inclusion complexes of amylose. **Journal of Cereal Science**, v. 41, n. 3, p. 239–249, maio 2005.

ZHANG, G.; MALADEN, M. D.; HAMAKER, B. R. Detection of a novel three component complex consisting of starch, protein, and free fatty acids. **Journal of Agricultural and Food Chemistry**, v. 51, n. 9, p. 2801–2805, 2003.

CONCLUSÕES GERAIS

Os géis formados durante a aplicação de ultrassom são fracos, com uma leve dependência em relação à frequência. Os três níveis de potência aplicados afetaram as interações entre a bixina e as cadeias de amilose, permitindo a formação de arranjos com capacidade de encapsular a bixina em diferentes graus, levando à formação de estruturas com maior ou menor estabilidade. Embora, o processo de encapsulação tenha ocorrido, não foi evidenciada a formação de complexos de inclusão. De forma geral, a aplicação de ultrassom foi capaz de prover proteção e estabilidade à bixina contra a ação do fluido gastrointestinal modelo, além de conferir diferentes padrões de liberação, convertendo essa metodologia, juntamente com o uso de amido de alto conteúdo de amilose, em um bom sistema de liberação controlada.

Em relação à encapsulação usando a precipitação em meio ácido, a presença de proteína aumentou a capacidade de encapsulação da matriz e afetou o perfil de liberação da bixina no sistema de acordo com a temperatura do processo. A 90 °C evidencia-se a formação de estruturas com pontos de fusão maiores que 100 °C, o que provê à bixina boa proteção à ação do calor. Porém, não houve evidência da formação de complexos de inclusão tipo V da amilose. A encapsulação de bixina por este método apresenta-se como um bom sistema de liberação controlada, com a possibilidade de gerar diferentes perfis de liberação usando diferentes concentrações de proteína.

A otimização das condições para a encapsulação de bixina usando ultrassom e precipitação em meio ácido foram selecionadas usando a metodologia de superfície de resposta. A encapsulação por tratamento com ultrassom resultou ser um processo que leva a um maior grau de encapsulação no interior da matriz, quando é comparado com o método por precipitação ácida usando Hylon VII. No entanto, este é menor que o obtido quando é usada a amilose de mandioca. O modelo que descreve as variáveis de resposta em função de condições de preparação conseguiu explicar satisfatoriamente o comportamento do sistema e a validação das condições otimizadas não apresentou diferenças estatisticamente significativas, o que confirmou o bom ajuste do modelo.

A estrutura das cápsulas preparadas a partir de amilose de mandioca e retrogradadas a menor temperatura constitui um melhor arranjo para a inclusão de um maior conteúdo de carotenoides, o que aumenta a capacidade de encapsulação. No entanto, esse sistema de liberação não evidenciou formação de complexos do tipo V da amilose. Esse sistema de liberação é uma alternativa para a encapsulação de óleos, porém, é necessário o estudo dos padrões de liberação e sua resistência às condições simuladas do sistema gastrointestinal.

De forma geral foi realizada a encapsulação de bixina, luteína e neoxantina usando tratamento com ultrassom, precipitação em meio ácido e através do uso de xerogéis e criogéis a partir de amilose de mandioca e amido com alto conteúdo de amilose; foram avaliadas as condições de preparação e efeito da proteína na capacidade de encapsulação, visando apresentar alternativas às já existentes metodologias de encapsulação de bixina e de óleos com alto valor nutricional.

SUGESTÕES PARA TRABALHOS FUTUROS

São sugestões para trabalhos futuros:

Avaliar a estabilidade oxidativa da bixina encapsulada pelo tratamento com ultrassom e encapsulação usando precipitação de uma solução ácida.

Fazer um estudo adicional sobre a encapsulação de bixina e óleo de abacate usando amilose fracionada da mandioca através de tratamento com ultrassom.

Fazer um estudo adicional sobre o efeito do uso de emulsificantes no aumento da capacidade de encapsulação e verificar a formação de complexos V-amilose.

Avaliar a estabilidade dos xerogéis e criogéis de óleo de abacate no fluido gástrico simulado.

Avaliar a formação e a viabilidade de formação de bigéis amido-proteína como sistema de liberação usando tratamento com ultrassom.

APÊNDICE A.

Figura 2S. Freeze-dried control (a) and sonicated samples BC1 150 W(b), BC2 210 W (c), BC3 300 W(d).